SIMULATION AND DESIGN OF PASSIVE MODERATOR COOLING SYSTEM FOR ADVANCED HEAVY WATER REACTOR

By
Eshita Pal
ENGG01201104016

Homi Bhabha National Institute, Mumbai

A thesis submitted to the

Board of Studies in Engineering Sciences

In partial fulfillment of requirements

for the Degree of

DOCTOR OF PHILOSOPHY

of

HOMI BHABHA NATIONAL INSTITUTE

August, 2016

Homi Bhabha National Institute

Recommendations of the Viva Voce Committee

As members of the Viva Voce Committee, we certify that we have read the dissertation prepared by Eshita Pal entitled "Simulation and Design of Passive Moderator Cooling System for Advanced Heavy Water Reactor" and recommend that it may be accepted as fulfilling the thesis requirement for the award of Degree of Doctor of Philosophy.

Chairman – Dr. P. K. Vijayan — **Date:** 23/7/16

Guide / Convener – Prof. J. B. Joshi — **Date:** 23/7/16

Co-guide - Dr. A. K. Nayak — **Date:** 23/7/16

Examiner – Prof. Giridhar Madras — **Date:**

Member 1- Dr. K. Velusamy — **Date:** 23/7/2016

Member 2- Prof. J. C. Mandal — **Date:**

Final approval and acceptance of this thesis is contingent upon the candidate's submission of the final copies of the thesis to HBNI.

I/We hereby certify that I/we have read this thesis prepared under my/our direction and recommend that it may be accepted as fulfilling the thesis requirement.

Date:

Place:

Co-guide **Guide**

STATEMENT BY AUTHOR

This dissertation has been submitted in partial fulfillment of requirements for an advanced degree at Homi Bhabha National Institute (HBNI) and is deposited in the Library to be made available to borrowers under rules of the HBNI.

Brief quotations from this dissertation are allowable without special permission, provided that accurate acknowledgement of source is made. Requests for permission for extended quotation from or reproduction of this manuscript in whole or in part may be granted by the Competent Authority of HBNI when in his or her judgment the proposed use of the material is in the interests of scholarship. In all other instances, however, permission must be obtained from the author.

Eshita Pal

DECLARATION

I, hereby declare that the investigation presented in the thesis has been carried out by me. The work is original and has not been submitted earlier as a whole or in part for a degree / diploma at this or any other Institution / University.

Eshita Pal

I dedicate this thesis to my family

ACKNOWLEDGEMENTS

I wish to express my sincere gratitude to my research guide Prof. J. B. Joshi, Emeritus Professor, Homi Bhabha National Institute, Mumbai and my co-guide Dr. A. K. Nayak, Head-Thermal hydraulic section, Reactor Engineering Divison, Bhabha Atomic Research Centre, Mumbai for their invaluable guidance and continuous encouragement throughout the course of this work.

I sincerely thank my Doctoral Committee chairman Dr. P. K. Vijayan and members Dr. K. Velusamy, Dr. J. C. Mandal for time-to-time evaluation of the research work and useful suggestions.

My sincere thanks to Shri. Inder Kumar for his technical and moral guidance throughout my research work. I would also like to take the opportunity to thank with great pleasure the guidance and technical inputs provided by Shri. Mukesh Kumar. Finally, I would like to thank Shri Purnendra Verma, who had provided much required aid in setting up the experimental facility.

I wish to acknowledge my Ma, Baba, Dada and Boudi for their blessings and for have always supported me through high and low times. I would also like to thank my colleague Nitin for his constant moral support, extremely helping attitude and his regular discussions on turbulence. Finally, I would like to thank my PhD friends, Ruchi, Ankur, Sapna and Vishal, who had been a good company.

Eshita Pal

CONTENTS

Homi Bhabha National Institute

SYNOPSIS REPORT

1. **Name of the Student:** Eshita Pal
2. **Name of the Constituent Institution:** Homi Bhabha National Institute, BARC
3. **Enrollment No.:** ENGG01201104016
4. **Title of the Thesis:** Simulation and Design of Passive Moderator Cooling System for Advanced Heavy Water Reactor
5. **Board of Studies:** Engineering Science

The Fukushima station blackout scenario has enforced the reactor designers to have a relook on the safety features of the newly designed and existing nuclear reactors. The accident has raised a question on the reliability of conventional safety systems, which are dependent on active components or systems. In view of this, new reactor designs propose passive systems extensively. The Advanced Heavy Water Reactor (AHWR) is one of the advanced designs of nuclear reactor, which is a vertical pressure tube type boiling water cooled natural circulation nuclear reactor with heavy water moderator (Sinha and Kakodkar, 2006). In this reactor, the coolant channels (Calandria tubes) are housed inside a vertical cylindrical tank called the Calandria vessel. The heavy water moderator is filled inside the Calandria vessel surrounding these Calandria tubes.

During normal operation of the reactor at full power, the heat generated in moderator is removed by dedicated heat exchangers using pumps. However, in the event of a prolonged station blackout (SBO), the radiation heat transfer from the main heat transport system to the moderator may lead to boiling of the moderator and pressurization in the Calandria in long term.

In this case, to prevent the moderator temperature and pressure to rise above permissible safe limits for at least 7 days without operator intervention, a passive moderator cooling system (PMCS) is conceptualized.

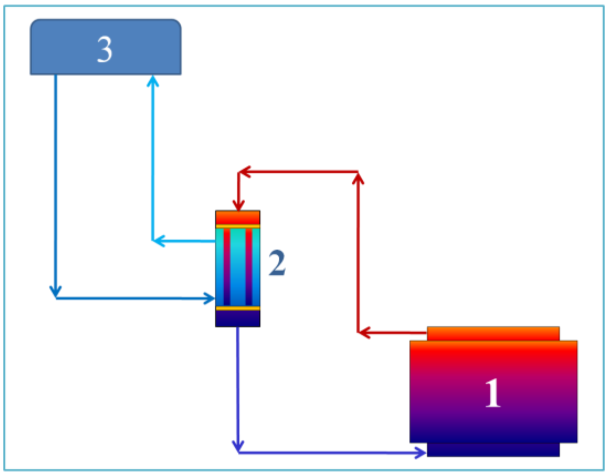

Figure 1: Schematic of Passive Moderator Cooling System (1) Calandria vessel, (2) Heat Exchanger and (3) Gravity Driven Water Pool (GDWP).

The main objective of this thesis is to evaluate and establish capability of the Passive Moderator Cooling System to remove the decay heat under a prolonged Station BlackOut (SBO) condition for the advanced reactor under consideration. In previous literature, a passive moderator cooling system is reported to be developed for the Canadian heavy water reactor CANDU-6 (Baek and Spinks, 1994). This system is a two phase, flashing driven natural circulation system, which was found to be susceptible to flow instabilities. However, in AHWR, the PMCS is a single phase system, which is designed to operate under normal operation (operates along with active pumped cooling system) as well as accidental scenario (only PMCS operates). The PMCS is designed to remove 2MW heat from the moderator by means of a shell and tube type heat exchanger. The heat generated in Calandria will increase the temperature of the moderator. This hot and less dense moderator fluid rises due to buoyancy and enters the tube side of the shell and tube type heat exchanger. After heat transfer to the shell side the cooled moderator returns to Calandria forming a natural circulation loop. The moderator in tube side is cooled by the water in the shell side, which is coming from the Gravity Driven Water Pool (GDWP), forming another natural circulation loop between the shell side and the GDWP. Thus, two interdependent natural circulation loops (coupled natural circulation loops) are formed, one between the Calandria and the tube side of the heat exchanger, and the second one between the shell side of the heat exchanger and the GDWP.

An extensive literature survey related to this field has brought forth the following unresolved issues:

1. Complex multidimensional flow inside a 3D structures- heat exchanger and Calandria.
2. Flow initiation from rest phenomena in natural circulation system, when the pumps are unavailable due to SBO.
3. Thermal hydraulic behavior of a coupled natural circulation loop.

Insights taken from the literature are used to further accentuate the motivation for the present work. From the literature it was understood that, an efficient heat transfer depends on flow field inside the PMCS and the flow velocities in the loops. Furthermore, the flow field inside the Calandria is highly multidimensional because of its large size and tube bank, which can result in local hotspots and dead zones. Thus it is important to study the thermal hydraulics of the PMCS using a CFD tool, in order to obtain the detailed temperature and velocity distribution inside the system. Thus the objectives of the current research work are:

1. Establishment of the CFD code to simulate the flow field inside large geometry of Calandria.
2. Establishment of heat removal capability for Calandria tubes for PMCS.

To meet these objectives, the following strategy is undertaken:

1. Building of a scaled experimental facility to simulate the natural convection in the PMCS of AHWR and conduction of various experiments.

2. Validating the CFD model using experimental data and its application to PMCS.
3. Study of the thermal hydraulics of PMCS under long term transient behavior of SBO.

First, a RELAP simulation of the PMCS for the reactor is performed considering a prolonged Station Blackout Scenario. The analysis led to the conclusion that the concept of PMCS works, as the system is able to maintain the moderator temperature below boiling conditions for a time period of 7 days without any operator intervention.

Table 1. Geometrical details of the scaled model.

Component	Dimensions	AHWR PMCS	Scaled Model
Calandria	Diameter of shell, Ds (m)	6.9	0.6
	Outer diameter of fuel channel, dt (m)	0.168	0.09
	Length, L (m)	5.3	0.6
	Total no. of tubes, Nt	513	19
Heat Exchange	Diameter of shell, Ds' (m)	1.35	0.0525
	Outer diameter of tube, dt' (mm)	12.7	6
	Length, L' (m)	3.5	0.6
	Total no. of tubes, Nt'	3431	40
	Thickness of tube, t (mm)	2.5	0.7

A scaled facility of the PMCS in AHWR was built, in order to validate various numerical codes and to understand the overall thermal hydraulic behavior of the PMCS during a prolonged SBO (Table 1). There are 57 thermocouples located at various axial and radial locations inside the Calandria and two each at the inlet and outlets of the Calandria, and tube side as well as shell side of the heat exchanger. Two types of experiments were performed: (1) step wise power rise and fall; and (2) steady operation at constant power for a long duration. The thermal hydraulics of the coupled natural circulation system was captured (Fig. 2), which shows a delay in development of flow inside the primary loop and also in the secondary loop due to occurrences of 3D flow phenomena. The temperature contours inside the Calandria show that initially the hot fluid is present near the heated tubes, but as time progresses, the temperature inside Calandria becomes progressively more stratified.

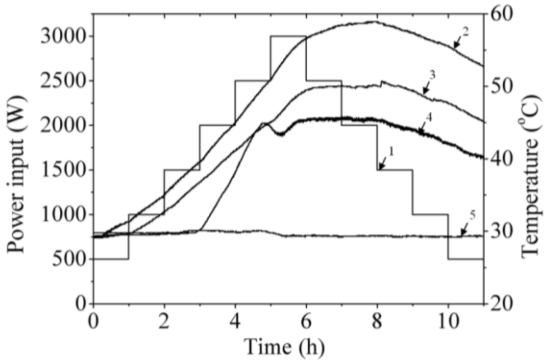

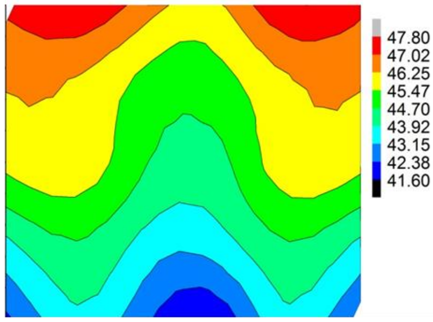

(A) **(B)**

Figure 2: (A) Power and Temperature plot with time for "*one hour stepwise power input*" experiment (1) power input, (2) Calandria outlet temperature, (3) Calandria inlet temperature (4) Heat exchanger shell side outlet temperature and (5) Heat exchanger shell side inlet temperature (B) Temperature contour on a plane passing through centre of Calandria at (4h).

The experiments in the scaled PMCS test facility were then simulated using RELAP5/Mod3.2 1D system code, which was done for the code validation purpose. For t>6 h, the RELAP code shows good agreement with the experimental data of temperature difference across the Calandria and that across the heat exchanger shell side (Figure 3).

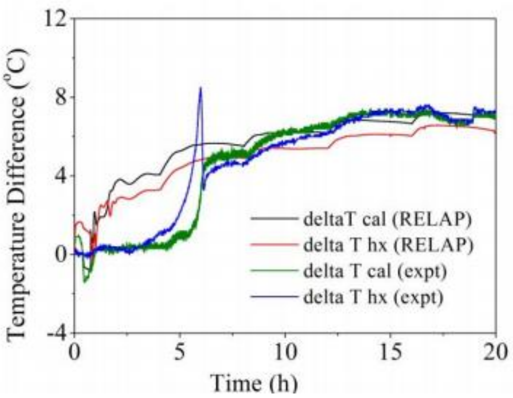

Figure 3: Comparison of RELAP analysis with experimental data for temperature difference across the Calandria and across the shell side of heat exchanger with time (for "*four hours stepwise power input*" experiment).

The RELAP being a 1D code is not able to capture the initial period (time t<6 h) in which there are 3D recirculatory flows within the Calandria. It is known that, during an SBO, the heat flux is high in the initial phase. Therefore, to capture accurately the initial high flux phase, it is desirable to undertake a 3D CFD simulations. Also, further details of flow and temperature distribution inside the Calandria can be better understood.

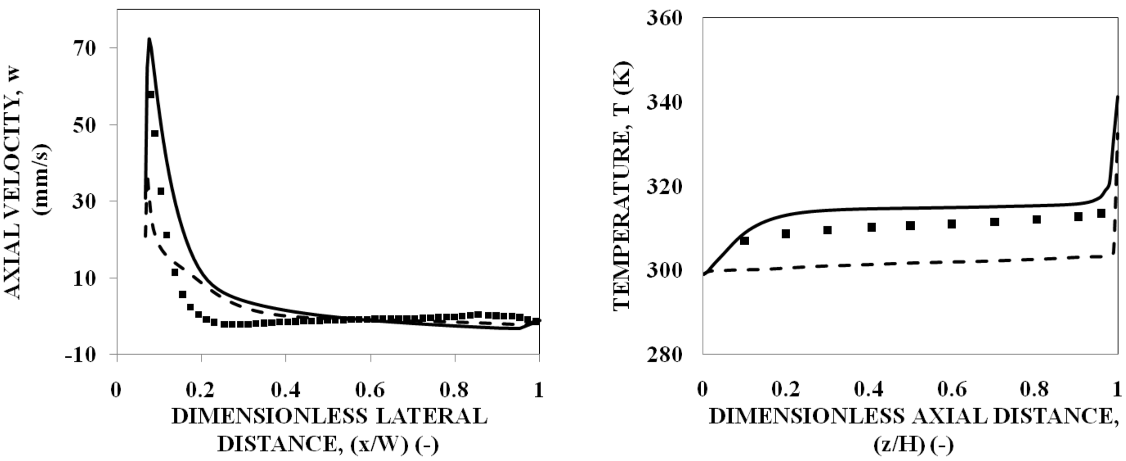

(A) **(B)**

Figure 4: Code validation for natural convection from reported literature (Ganguli et al, 2010) (A) Axial velocity plot along the radial distance at mid level of the tank, and (B) Temperature plot along axial height at a distance 3mm from the central heated tube, (—): SST k-ω model, (- - -): standard k-ε model.

The CFD code (OpenFoam-2.2.0) is first validated against experimental data reported in literature, in order to assess the capability to simulate a complex natural circulation system such as the PMCS. It was observed that the SST k-omega turbulence model is able to capture the temperature and velocity for the natural circulation phenomena as compared to the experimental results.

To further test the validity of the 3D CFD code, the PMCS test facility is simulated. For the current work, only the primary loop in the PMCS was simulated (Fig. 5), i.e. the Calandria connected to the tube side of the heat exchanger. It was observed that, at steady state, the temperature inside the Calandria is stratified, despite the gross flow in the loop.

A transient simulation for the primary loop at an input heater power of 500W was carried out for a physical time of 3000s. It is observed that with system at condition of rest, when power is switched on, temperature in the Calandria vessel close to the tubes rises. This causes the hot fluid to rise due to buoyancy. Slowly, the hot fluid starts leaking out of the Calandria vessel through the two horizontal outlets, and the velocity of fluid inside Calandria also increases. With time as temperature inside the Calandria rises, the buoyancy forces also rise and the driving force is large enough to initiate flow in the entire loop. The comparison between the CFD predictions and the experimental measurements of the temperatures at the inlet and outlet of the Calandria for the different heater input shows a fairly close agreement (within ±6%).

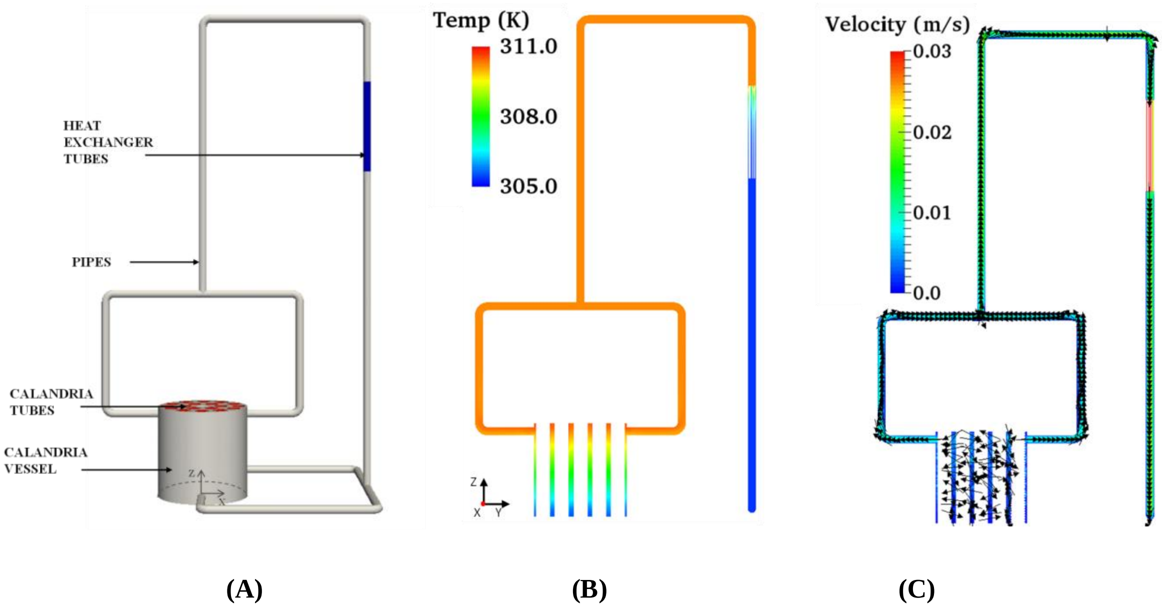

Figure 5: (A) Geometry of PMCS loop in CFD Steady state; (B) contours of temperature and (C) velocity vectors on a vertical plane passing through the center of Calandria and the heat exchanger tube section for 500W power.

Since the code is validated for simulation of a scaled down facility of the PMCS, a 3D CFD simulation of the Calandria was performed inside the PMCS for a SBO condition. A reactor scale CFD simulation of the PMCS, for a SBO transient scenario, is quite challenging and immensely computationally expensive due to the large size of the geometry of the PMCS. To overcome this obstacle, a pseudo-transient simulation was carried out: first a transient 1D simulation using RELAP5/MOD-3.2 was carried out, for the reactor in an SBO condition for a period of 7 days. From this transient simulation, at any given instant we have the power, temperature and flow conditions inside the Calandria (moderator).

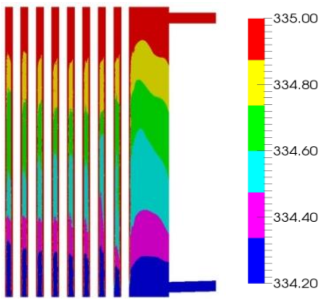

(A)

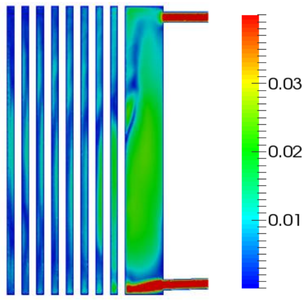

(B)

Figure 6: (A) Temperature (in K) and (B) velocity (in m/s) contours on a plane passing through the Calandria at time t= 12 hours since beginning of SBO.

It was observed that for all time, there is a visible stratification inside the Calandria, which indicates that the flow is buoyancy dominated for all the time of SBO (Fig. 6). Furthermore, the temperatures are higher in the center of the fuel matrix close to the top, whereas the region near the wall is at much lower temperature. This is because the flow is not able to penetrate the fuel channels efficiently in order to carry away heat from them. Hence the CFD simulations could establish that the PMCS is able to remove the heat from the Calandria during a SBO condition.

Important conclusions from the current work are as follows:

- A scaled facility was built in order to understand the thermal hydraulic behavior of the PMCS and to validate various numerical codes. It was observed that, when the power is switched on, the flow initially tends to recirculate within the Calandria vessel. With time as the temperature rises within the Calandria, the buoyancy force becomes sufficiently high, thereafter only the flow starts in the entire loop.

- CFD predictions show that the temperatures inside the Calandria are stratified. Whereas, the hot leg and the cold leg have a uniform temperature. The CFD model predicts that even at the steady state the gross flow in the loop is unable to disrupt the stratification inside the Calandria.
- The steady state CFD simulations are in good agreement with the experimental data (within ±6%).
- The 3D CFD model is used in a unique pseudo-transient approach to simulate the reactor scale moderator during an SBO. The results show that the temperatures in the Calandria are below boiling conditions at all times. The 3D CFD simulations could capture the multidimensional flow inside the Calandria, which reveals that the flow tends to recirculate by going up near the hot tubes and then coming down along the walls of the Calandria.

Thus an extensive analysis was performed on the capability of the PMCS to remove the heat from the Calandria by means of experiments in the scaled facility as well as numerical investigations using 1D system codes (RELAP5-MOD3.2) and 3D CFD codes (OpenFoam 2.2.0).

References

[1] Sinha, R.K., Kakokar, A., (2006) *Design and development of the AHWR—the Indian thorium fuelled innovative nuclear reactor*, Nucl. Engg. and Des. 236, 683-700.

[2] Baek, W.P., Spinks, N.J., (1994) *CANDU Passive Heat Rejection using the Moderator*, International Conference on New Trends in Nuclear System Thermohydraulics, Pisa, May 1994.

[3] Ganguli, A.A., Sathe, M.J., Pandit, A.B., Joshi, J.B., Vijayan, P.K. 2010. *Hydrodynamics and heat transfer characteristics of passive decay heat removal systems: CFD simulations and experimental measurements*. Chem. Engg. Sci. 65(11), 3457-3473.

LIST OF FIGURES

LIST OF TABLES

NOMENCLATURE

$A_{pressure\ tube}$	Total surface area of the pressure tubes (m^2)
C_P	specific heat (J/(kgK))
d	thickness of tube in heat exchanger (mm)
D_h	Hydraulic diameter (m)
DNR	Did Not Report this parameter (-)
dt	diameter of tube (m)
EL	elevation from ground level (mm) [Fig. 2]
F	Friction number (-) [Eq. 4.10]
H	height of tank (m)
D_{HX}	diameter of heat exchanger (m)
D_{Tank}	diameter of Calandria tank (m)
ID	inner diameter (m)
ID_{Loop}	inner diameter of natural circulation loop (mm)
k	turbulent kinetic energy (m^2s^2)
L, L_{HX}	length of heat exchanger (m)
L_{Loop}	length of natural circulation loop (m)
L_{Tank}	length of Calandria tank (m)
Nt	number of tubes inside Calandria
Nt_{HX}	number of tubes in heat exchanger
OD	outer diameter (m)
OD_{Tube}	outer diameter of tube in Calandria (mm)
$OD_{Tube,HX}$	outer diameter of tube in heat exchanger (mm)

Pr_T	turbulent Prandtl number [$= \frac{\nu_T}{\sigma_T}$] (-)
$Q_{radiation}$	Radiation heat transferred to moderator [Eq. 3.1] (W)
Q	Heat source number [$= \frac{\dot{q}_i''' l_o}{\rho C_P u_o \Delta T_o}$, Eq. 4.11] (-)
Ra	Rayleigh number [$= \frac{g\beta\ (T_{surface} - T_{quiescent})x^3}{\nu\alpha}$] (-)
Re	Reynolds number [$= \frac{\rho\ vD}{\mu}$] (-)
Ri	Richarsdon Number [$= \frac{\beta g \rho\ \Delta T_o l_o}{u_0^2}$, Eq. 4.9] (-)
t	time (s)
T_{out}	outlet temperature (K)
$T_{Pressure\ tube}$	temperature of the pressure tube (K)
$T_{Calandria\ tube}$	temperature of the Calandria tube (K)
u	velocity component (m/s)
u_r	steady state velocity in the reference section (heated core) (m/s)
u_r	velocity in the reference section (heated core) (m/s)
w	axial velocity (m/s)
W	width of the tank (m)
W_{Loop}	width of natural circulation loop (m)
y^+	non-dimensional wall distance (-)
z	axial distance from the bottom along the height of the geometry (m)

Acronyms

1D	one dimensional
2D	two dimensional
3D	three dimensional
AECL	Atomic Energy of Canada Limited

AHWR	Advanced Heavy Water Reactor
BARC	Bhabha Atomic Research Centre
CANDU	CANada Deuterium Uranium
CIESV	Condensate Isolation Emergency Stop Valve
CFD	Computational Fluid Dynamics
CT	Calandria Tube
ECCS	Emergency Core Cooling System
GDWP	Gravity Driven Water Pool
HX	Heat Exchanger
ICS	Isolation Condenser System
LDA	Laser Doppler Anemometry
LOCA	Loss of Coolant Accident
MHTS	Main Heat Transport System
NCL	Natural Circulation Loop
PCCS	Passive Containment Cooling System
PCD	circular diameter pitch
PDHRS	Passive Decay Heat Removal System
PEWS	Passive Emergency Water System
PHWR	Pressurized Heavy Water Reactor
PMCS	Passive Moderator Cooling System
PMCTF	Passive Moderator Cooling Test Facility
PT	Pressure Tube
SBO	Station BlackOut
SST	Shear Stress Transport

Greek Symbols

α	thermal diffusivity (m^2/s)
β	thermal expansivity (1/K)
ϵ	emissivity (-)
ε	turbulent energy dissipation rate (m^2s^3)
σ	Stefan-Boltzmann constant
θ	plane of view angle as shown in Figure 8.1 (B)
ξ	plane of view as shown in Figure 8.6 (D)
ξ'	plane of view as shown in Figure 8.6 (D)
ρ	density (kg/m^3)
v	kinematic viscosity (m^2/s)
ψ	any dimensionless parameter (-)
ω	specific dissipation rate (1/s)

Subscripts

T	turbulent property
o	reference section (usually heated length)
i	section of the natural circulation loop

CHAPTER 1:

INTRODUCTION

1.1 Background

The Fukushima Station BlackOut (SBO) scenario has enforced the reactor designers to have a relook on the safety features of the newly designed and existing nuclear reactors. The accident has raised a question on the reliability of conventional safety systems, which are dependent on active components or systems. Hence, the new nuclear reactor designs that are being developed are extensively incorporating passive systems. These systems use entirely passive components or active components in a limited manner (IAEA-TECDOC-1624, 2009). The driving forces in these systems are natural forces such as gravity. These are highly useful in the conditions of a full SBO, where an external supply of electricity is not available for circulating the coolant, such that occurred in the Fukushima incident. In addition, these systems eliminate costs of installation, operation and regular maintenance of the active systems.

1.2 Motivation

One of the advanced nuclear reactor design is the Indian Advanced Heavy Water Reactor (AHWR) (Sinha and Kakodkar, 2006) which is being developed at Bhabha Atomic Research Centre (BARC). It is a 300 MW(e), vertical, pressure tube type, boiling light water cooled, natural circulation nuclear reactor with heavy water moderator (more details in Chapter 3).

The fission heat from the core is removed by means of natural circulation during the normal operation of the reactor as well as during accidental scenarios. The fission heat from the fuel is transferred to the primary coolant in the Main Heat Transport System (MHTS), which results in boiling of the coolant (Fig. 1.1A). The steam-water mixture rises due to buoyancy and enters into a steam drum, where the steam and water separates. The steam is sent to the turbine for electricity generation and after condensation the feed water is returned back to the steam drum. The water from the steam drum returns to the inlet of the fuel channels at the bottom of the Calandria vessel, forming a complete natural circulation loop.

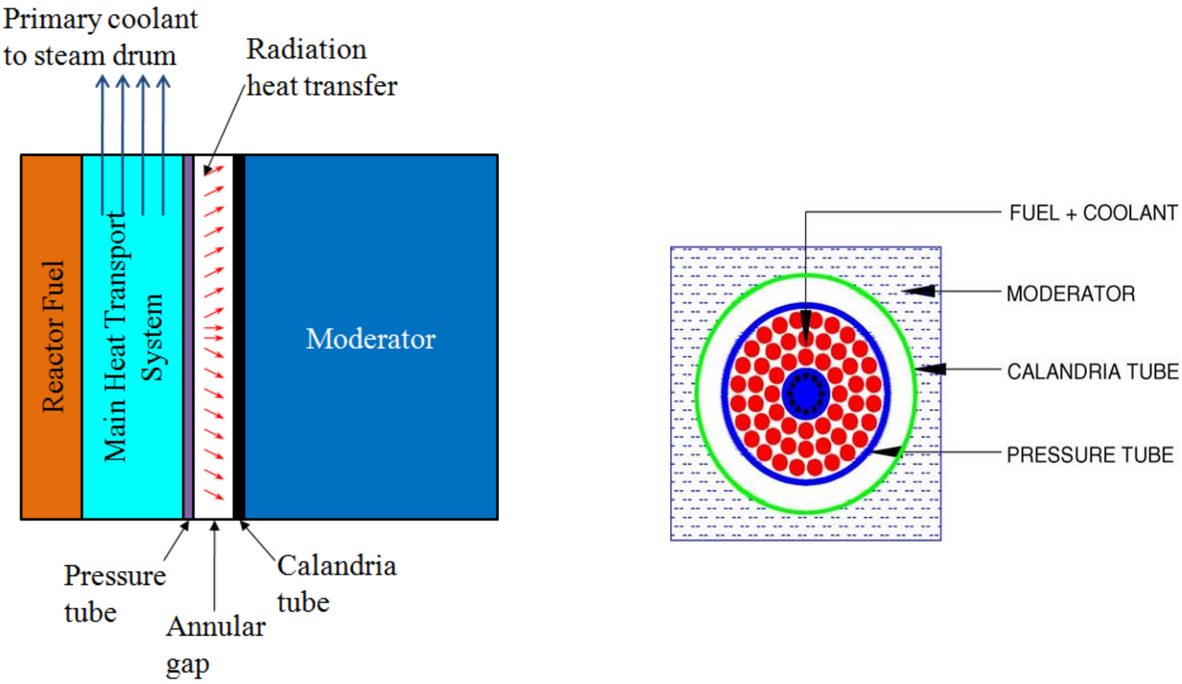

(A) **(B)**

Figure 1.1: (A) Schematic of heat transfer from fuel to moderator in the Calandria (half symmetry from center of fuel channel shown) (B) Structure of fuel channel.

The primary coolant flows through a pressure tube, housing inside the fuel channels of the AHWR, which are located inside the Calandria vessel. A fuel bundle, which consists of 54 fuel rods (Fig. 1.1B), is located inside the pressure tube (which carries the coolant), surrounded by the Calandria tube and separated from the pressure tube by an annulus filled with gas (Fig.

1.1A). The heavy water moderator is filled inside the Calandria vessel surrounding these Calandria tubes. During normal operation of the reactor, heat is continuously generated in the moderator due to neutron moderation and capture, attenuation of gamma radiation as well as due to thermal radiation from the MHTS (i.e. from the heated outer pressure tube wall, which in turn is heated by the coolant). In this process, a total of approximately 52 MW of heat is generated in the heavy water moderator during the normal operation of the reactor. This heat is removed through a pumped moderator cooling circuit, in order to maintain the moderator temperature below the boiling temperature.

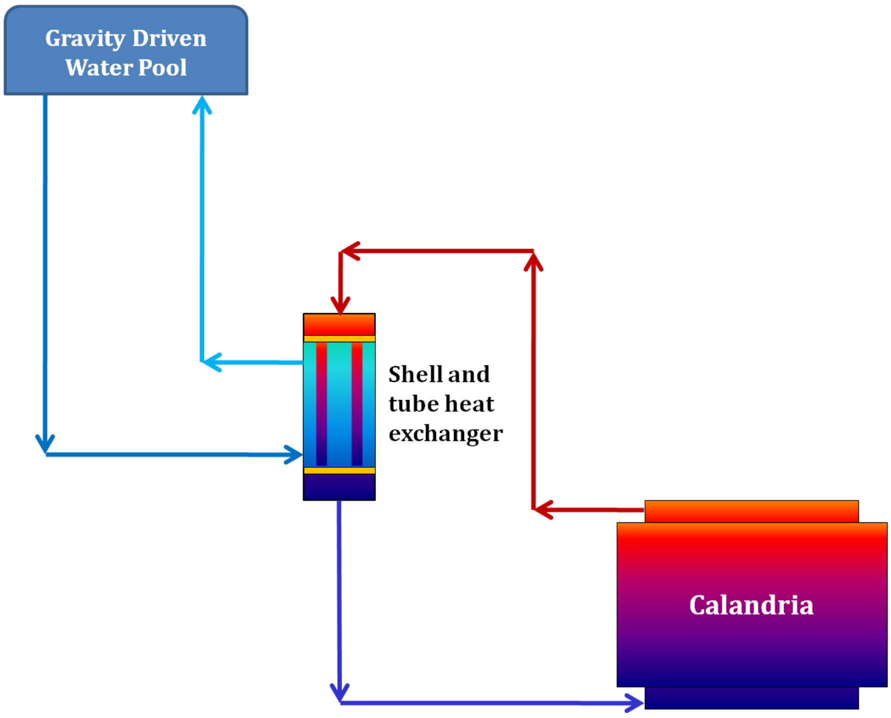

Figure 1.2: Schematic of Passive Moderator Cooling System of Advanced Heavy Water Reactor.

In the event of a prolonged SBO, the reactor trips and the nuclear fission in the fuel stops. As a result, the heat generation due to moderation of neutrons produced from fission reaction also stops. However, the natural radioactive decay of the fission products inside the fuel shall continue generating heat, which in turn is cooled by the MHTS. Now, only the heat transfer from MHTS across the Pressure tube and Calandria tube gap causes the heating of moderator. This thermal radiation heat transfer is estimated to be around 2 MW (Kumar et al., 2015), at the beginning of the reactor trip and slowly reduces as the decay heat generation (hence MHTS temperature) reduces. In such a scenario, the moderator can no longer be cooled by active means due to absence of electricity. Hence, the Passive Moderator Cooling System (PMCS) (Fig.1.2) is designed to remove this heat from the moderator, in order to prevent the pressure inside the Calandria vessel to rise beyond permissible safe limits and also to prevent boiling of the moderator.

Table 1.1: Detailed breakdown of heat deposition in Main heat transport system and moderator.

System	Heat generation mode	Heat deposition (MW)	
		Normal Operation	SBO condition (t=0)
Main heat transport system (coolant)	Fission reaction of Uranium	867	0
	Radioactive decay of fission product	55	55
Calandria vessel (moderator)	Moderation of neutrons, gamma and beta from fission	50	0
	Radiation heat transfer from MHTS across CT and PT gap	2	2

1.3 Objectives

The main objective of this thesis is to simulate the working of the Passive Moderator Cooling System for the advanced reactor under consideration, in an attempt to understand the thermal hydraulic behaviour of this system. In previous literature, a passive moderator cooling system is reported to be developed for the Canadian heavy water reactor CANDU-6 (Baek and Spinks, 1994). This system is a two phase, flashing driven natural circulation system, which is susceptible to flow instabilities. However, in AHWR, the PMCS is a single phase system, which is designed to operate under normal operation (operates along with active pumped cooling system) as well as accidental scenario (only PMCS operates). The PMCS is designed to remove 2 MW heat from the moderator by means of a shell and tube type heat exchanger. The heat generated in Calandria will increase the temperature of the moderator. This hot and less dense moderator fluid rises due to buoyancy and enters the tube side of the shell and tube type heat exchanger. After heat transfer to the shell side the cooled moderator returns to Calandria forming a natural circulation loop. The moderator in tube side is cooled by the water in the shell side, which comes from the Gravity Driven Water Pool (GDWP), forming another natural circulation loop between the shell side and the GDWP. Thus, two interdependent natural circulation loops (coupled natural circulation loops) are formed, one between the Calandria and the tube side of the heat exchanger, and the second one between the shell side of the heat exchanger and the GDWP.

An efficient heat removal from the moderator depends on the flow field inside the PMCS and the flow velocities in the loops. Furthermore, the flow field is inside the Calandria is highly multidimensional because of its large size, which can result in local hotspots and dead zones. Thus it is important to study the thermal hydraulics of the PMCS using the CFD tool under consideration, in order to obtain the detailed temperature and velocity distribution inside the system. Thus the objectives of the current research work are:

1. Establishment of the CFD code to simulate the flow field inside large geometry of Calandria.
2. Establishment of heat removal capability for Calandria tubes for PMCS.

To meet these objectives, the following strategy is undertaken:

1. Building of a scaled experimental facility to simulate the natural convection in the PMCS and conduction of various experiments.
2. Validating the CFD model using experimental data and its application to simulate PMCS.
3. Study of the thermal hydraulics of PMCS under long term transient behavior of SBO.

1.4 Outline of Thesis

This thesis is organised into eight chapters. In chapter 2, a review of the current status of the subject area comprising of the PMCS in various nuclear reactors, natural circulation loops, Calandria and heat exchangers as found in the literature is presented. Chapter 3 describes the important details of the Indian AHWR, the Calandria and the concept of the PMCS in this reactor. Also, a few RELAP5/MOD3.2 simulations results of this system for the AHWR are presented. Chapter 4 gives the description of the Passive Moderator Cooling Test Facility (PMCTF) installed at BARC. Furthermore, the scaling methodology and various experiments performed in the PMCTF are discussed. In chapter 5, RELAP5/MOD3.2 simulations of the PMCTF are discussed. In chapter 6, the CFD model required to simulate the PMCTF and PMCS, is first validated for different cases similar to the actual geometry and thermal hydraulic conditions. Chapter 7 discusses the steady and time dependent CFD simulations of the PMCTF. Chapter 8 discusses the CFD simulations of the Calandria in PMCS of AHWR under prolonged SBO condition. Finally, Chapter 9 provides the summary and conclusions of the current work. In addition, future scope of study is also listed in this chapter.

CHAPTER 2:

LITERATURE REVIEW

2.1 Introduction

The PMCS consists of complex three dimensional components such as the Calandria and the heat exchanger. The flows inside these components are complex due to the intricate geometry of tube banks and also the ongoing natural convection phenomena. Furthermore, the overall system is a set of coupled natural circulation loops. Hence the literature related to the PMCS, natural circulation loop, Calandria and heat exchanger are discussed extensively. The knowledge from the previous literature of these various systems will give an insight into the thermal hydraulics behaviour of the PMCS and also reveal the important scientifically gray areas in this field. Thus, enables to develop a path forward for further research work.

2.2 Passive Moderator Cooling System (PMCS)

A few authors have investigated the concept of a PMCS, mostly for CANDU type reactors. Baek and Spinks (1994) have developed a passive moderator heat removal system for CANDU reactors. In this system, the moderator acts as a heat sink in the event of simultaneous Loss of Coolant Accident (LOCA) and loss of emergency coolant injection system.

Umar et al. (1999) developed a new model of passive moderator system and tested its capability during LOCA scenarios. It was established using the CATHENA code (Hanna, 1998) that the moderator heat exchanger is able to remove heat over a period of 72 hours with no saturated boiling and flow instabilities, inside the Calandria vessel. The proposed system has a 0.7 m riser diameter and 8100 heat exchanger tubes. They further carried out CATHENA simulations to determine the heat transfer coefficient of the heat exchanger. Umar and Vecchiarelli (2000) performed a set of calculations to determine the minimum size of a moderator heat exchanger for the CANDU-6 reactor with a low hydraulic resistance. Furthermore, they used the CATHENA code to study the capability of the designed heat exchanger to remove heat in the long term. In this concept during normal operation, the moderator loop is driven by forced flow. However, during a LOCA event, heat transferred to the moderator is removed by the moderator heat exchanger that is cooled by naturally circulating water from an overhead Passive Emergency Water System (PEWS).

Khartabil (1995) carried out experiments and analysis for a flashing-driven PMCS for CANDU reactors. In this concept, the moderator exits the reactor at a temperature close to saturation so that vapour is generated in a riser connecting the Calandria to a heat exchanger. The two phase flow increases the driving force, making it possible to remove moderator heat passively. These flashing-driven passive systems are prone to flow instabilities at low pressures. Furthermore, a supercritical coolant driven reactor has a potential for flow instabilities due to large variations in the fluid properties near the critical temperature and pressure. Dimmick et al. (2002) worked on the flashing-driven moderator cooling system and looked into the possibility of increasing the primary coolant pressure and temperature to supercritical conditions. For a natural-convection-driven primary flow, the large variations in fluid properties near the critical point provide large density difference, which in turn results in a large buoyancy driving force.

In the reported literature, the concept of a PMCS is discussed for CANDU reactor, which had a horizontal reactor core. The system was designed to be a flashing type system which is capable of removing heat during an accidental condition of LOCA. However, the geometrical condition and heat load in this system resulted in major instabilities in the flow.

2.3 Studies on Natural Circulation Loop (NCL)

The PMCS is essentially a system of two natural circulation loops with integrated complex geometries such as the Calandria and the heat exchanger. Thus, the authors explore the published literature in the field of natural circulation in a loop. There is extensive work on both experimental as well as numerical simulations in a Natural Circulation Loop (NCL). Natural circulation systems have been reviewed by Zvirin (1981) and Grief (1988) which describe various geometries under steady and transient condition under different boundary conditions.

One of the first models as proposed by Welander (1967) consisted of a loop formed by a point heat source and heat sink with imposed temperature and imposed heat transfer coefficient, connected by two adiabatic legs. For this case, since the buoyancy forces and the shear stresses were not in phase, a small perturbation in the temperature field, corresponding to changes in certain thermal boundary conditions, could amplify, causing velocity oscillations and eventually flow reversal. While Nayak et al. (1995) presented 1d conservation equation based mathematical model of a rectangular natural circulation loop (NCL) including both linear and non-linear stability analysis. Vijayan (2002) carried out experiments in a rectangular NCL and gave correlations for steady state flow in laminar and turbulent regimes. Misale et al. (2007) through experiments investigated the effect of power transferred to the fluid and loop inclination for a natural circulation mini-loop. Devia and Misale (2012) carried out an experiment in a rectangular NCL to understand the effect of varying heat sink temperature.

Numerical simulation of stability and transient analysis for the single-phase natural circulation loops have been carried out by many researchers using system codes (Vijayan et al., 1995; Sharma et al., 2002; Ambrosini et al., 2004; Pilkhwal et al., 2007) and other simple tools (Bau and Torrance, 1981; Zvirin, 1981; Chen, 1985; Gordon et al., 1987; Vijayan and

Austregesilo, 1994, Vijayan et al., 2001, 2007; Ambrosini and Ferreri, 1998, 2000, 2003, 2006). With development of computational power and techniques, researchers are progressively inclining towards the use of 3D Computational Fluid Dynamics (CFD) codes for an extensive numerical simulation.

Angelo et al. (2012) presented 3D numerical analysis of a NCL with U-bend heaters and a spiral cooler section. They were able to capture 3D effects such as vortex structures and swirl effects. Wang et al. (2013) have presented a 3D CFD model using a compressible fluid to investigate natural circulation phenomena in a loop and showed good agreement with experimental results. Pilkhwal et al. (2007) discussed the results obtained using one-dimensional and three-dimensional CFD codes for the prediction of the dynamic behaviour observed in experiments carried out in a single-phase natural circulation apparatus. The CFD code was effective in showing the origin of pulsating instabilities observed with the horizontal heater and cooler, which was not captured by the one-dimensional models. The authors concluded that a compromise needs to be achieved between the improved capabilities of CFD codes in providing an accurate modelling of natural circulation flow and the consequent increase in computational cost of the simulations.

From the literature study on natural circulation loops it was understood that the initiation of natural circulation is a highly dynamic phenomena. The flow generally oscillates several times before coming to a stable condition. For some power transients in a horizontal heater and horizontal cooler case, the oscillations may increase or get dampened also. Also, a 3D CFD simulation is able to capture some instability phenomena which are not captured in 1D model. Although a 1D simulation gives a quick and good approximation of the gross thermal hydraulic behaviour of the system.

2.4 Simulation of the flow field inside the Calandria Vessel

The flow inside the Calandria is multidimensional with a large number of Calandria tubes, thus, it is numerically challenging to simulate such a large and complex geometry. To simplify the situation, a porous medium approach (where the tubes are replaced by appropriate distributed hydraulic resistances) was used by the Canadian nuclear industry and developed the MODTURC (MODerator TURbulent Circulation; Huget et al., 1990) and MODTURC-CLAS (MODerator TURbulent Circulation Co-Located Advanced Solution; Huget et al., 1989) codes. The commercial CFD code CFX (CFX-4.2: Solver Manual, 1997) was employed with a porous media approach using segregated (Yoon et al., 2004 and 2006) and coupled solvers (Yoon and Park, 2008). Lee et al. (2013) used a two phase component scale thermal hydraulic code called CUPID (Jeong et al, 2010a and 2010b) to simulate the temperature distribution and the flow pattern in the CANDU natural cooling system.

However, this approach does not provide the flow and temperature details at every location inside the Calandria. In order to ensure the temperature of Calandria tubes are always within permissible safe limits, 3D CFD simulations with all the geometrical details are desirable. Due to recent development in high performance computing capabilities, CFD application of such complex geometries is feasible. Ravi et al. (2008) carried out CFD investigations to study the flow and temperature distribution in the Calandria using 3D Reynolds Average Navier-Stokes (RANS) equations based code. The results were used to define a tolerance band for safe working limits by predicting the hotspots in the Calandria. The hot spots – the region where the temperature is highest in the Calandria are found to be near the upper and lower zones of the Calandria vessel. These occur due to the lack of refreshing mass flux into these zones leading to relatively lower heat removal rate. Kim et al. (2006) assessed the thermal hydraulic characteristics of CANDU-6 reactors for normal operation and transient conditions using FLUENT 6.0 (Fluent, 2001). They developed an optimized calculation scheme by comparing simulation results with experimental data and recommended the scheme for the simulation of reactor operation as well as a transient scenario. Sarchami et al. (2013) performed 3D simulation of CADNU moderator, reporting the asymmetric and fluctuating conditions of temperature and flow in the moderator, during the normal operation of reactor. Seo et al. (2014) have used Particle Image Velocimetry (PIV) to visualize the flow field and measure the velocities inside a scaled CANDU-6 Calandria. They simulated the geometry with CFD code CFX and obtained good agreement with the experimental data.

The multidimensional flow inside the complex geometry of Calandria has been investigated by several authors both experimentally as well as numerically. For experiments various authors considered either a scaled down or an approximately 2D slice of the Calandria vessel. The 3D CFD simulations initially assumed porous media, but later on with progress in computational capability of codes, full geometry of the tube banks were simulated. For the CANDU Calandria vessel the flows were observed to be highly multidimensional and also dynamic in time. During the normal operation of the reactor, the flow inside the Calandria was a mix of momentum and buoyancy dominated.

2.5 3D Simulation of a Heat Exchanger

In the early years, Short (1943) and Donhue (1949) experimentally investigated the heat transfer phenomenon in unbaffled heat exchangers. Short carried out a series of experiments on different heat exchanger sizes and tube layout. Donhue explained that in an unbaffled shell, fluid flows parallel to tube, which is similar to the situation of flow inside a tube. Thus from the experimental data of Short he gave a correlation for heat transfer in the shell side of an unbaffled heat exchanger by modifying the Sieder and Tate [Sieder et al. (1936)] correlation for heat transfer in pipe. However, the limitation of the correlation lies in the fact that the experimental range of Reynolds number considered was extremely limited.

The work was further extended by Kim and Aicher (1997) who experimented on shell side heat transfer of 32 different types of heat exchangers. They examined Ds = 34 mm to 150 mm, L = 920 to 2000 mm, NT = 1 to 91 and Re = 500 to 50000. They gave a correlation in terms of porosity instead of ratio of shell to tube diameter. They also signified the heat transfer in the nozzle region is higher than in parallel region by 40 %. This work was extended further by Aicher and Kim (1998) by using the double pipe heat exchangers. They found out that the influence of cross flow is higher in the case of shorter heat exchangers, and smaller ratio of free cross sectional area of nozzle to that of shell side. They developed a correlation to describe the Nusselt number for highly turbulent flow Re > 10000.

Uzzan et al (2004) develop a analytical solution for temperature profiles within a double pipe heat exchanger with counter current flow. The results were compared with experimental data. Dirker and Meyer (2004, 2005) found out that the existing correlations for heat transfer coefficients in concentric annuli were not in good agreement with each other. Experiments were carried out to develop a new correlation which included the ratio of the annular diameters. Gnielinski (2009) analyzed a large number of experimental data from the literature to find the suitability of various heat transfer and friction factor correlations and brought out their limitations. Therefore, he provided improved correlations for the inner as well as for the outer wall of the annulus. Van Zyl et al (2013) carried out extensive experiments on concentric annuli, emphasizing that the heat transfer coefficient and the friction factor depend on the annular diameter ratio as well as the direction of heat flux across the tube wall.

With improvement in computational techniques and machines, scientists progressively started using CFD as a quick and efficient tool to assess the flow distribution and heat transfer in various types of heat exchangers. Prithiviraj and Andrews (1998a, 1998b, 1999) developed a 3D numerical code based on distributed resistance method along with volumetric porosities and surface permeability to model the tubes in a baffled shell and tube heat exchanger. In this method, a single computational cell may have multiple tubes. Further, this method also simulated pressure drop and temperature fields, where the CFD predictions agreed with the experimental values within 7.4% and 15%, respectively. Wang et al. (2009) investigated the overall heat transfer rate and pressure drop through shell side with helical baffles by using commercial CFD code FLUENT and the authors obtained good agreement between the CFD predictions and the experimental measurements. Ozden and Tari (2010) presented the CFD application for simulating the shell side of a small heat exchanger using FLUENT. The simulations were performed using standard k-ε, realizable k-ε model and Spallart-Allmaras turbulence models. The studies are focused on the effects of various types of baffle and their cut, spacing etc. on the pressure drop and heat transfer.

Bhutta et al. (2012) reported an extensive review of literature on CFD simulations performed in the field of heat exchangers. Various studies on flow maldistribution, fouling, pressure drop and heat transfer in heat exchangers were compiled systematically in this review paper. Zeng et al (2012) investigated into the effect of length by diameter ratio of a shell and tube heat exchanger on the fluid flow maldistribution and heat transfer performance; and to mitigate the same issue, a multi parallel channel inlet and outlet structure was proposed. The simulations were carried out assuming porous media approach in commercial CFD software FLUENT. Afrianto et al (2014) investigated the effect of mass flow rate and heat transfer characteristics of LNG flow in a 1-2 pass shell and tube heat exchanger with segmental baffles using ANSYS Fluent 12.

The field of heat exchanger is investigated extensively since early as 1943. Several authors have carried out multiple experiments on various heat exchanger geometries and provided a correlation for the heat transfer. These geometries that have been investigated have high length to diameter ratio, in order to improve heat transfer. However, the heat exchanger in the PMCS and also the Calandria vessel (which is similar to the geometry of shell side of a shell and tube heat exchanger) has very low length to diameter ratio. Hence the conventional heat transfer correlations are not applicable. Thus, there is a need to simulate these geometries using 3D CFD simulations.

In addition to these complex geometries, for the past 25 years, (CFD) computational fluid dynamics is being increasingly used because of the developments in the computational power as well as numerical techniques [Ranade and Joshi (1989, 1990a, 1990b) Ranade et al. (1992), Thakre and Joshi (1999), Joshi (2002), Bhole et al. (2007), Tabib and Joshi (2008), Murthy and Joshi (2008)]. In the published literature, the knowledge of flow pattern has been employed for the estimation of equipment performance such as mixing [Joshi and Sharma (1978), Joshi (1980),1982, Ranade et al. (1991), Patwardhan and Joshi (1999), Sahu et al. (1999), Nere et al. (2003), Kumaresan and Joshi (2006)], heat transfer [Joshi et al. (1980), Dhotre and Joshi (2004)], sparger design [Kulkarni et al. (2009)], gas induction (Joshi and Sharma (1977), Murthy et al. (2007b), solid suspension [Raghava Rao and Joshi (1988), Rewatkar and Joshi (1991), Murthy et al. (2007a)]. Joshi and Ranade (2003) have discussed the perspective of computational fluid dynamics (CFD) in designing process equipment with their views on expectations, current status and path forward.

2.6 Closure

An extensive literature survey related to the PMCS has brought forth the following scientifically unresolved issues:

1. Complex multidimensional flow inside a 3D structures- heat exchanger and Calandria.

2. Flow initiation from rest phenomena in natural circulation system.

3. Thermal hydraulic behaviour of a coupled natural circulation loops.

In the reported literature, the PMCS has been studied under two phase (flashing type) conditions or forced flow conditions. Moreover, the Calandria geometry (for CANDU reactors) is horizontal and simulated under a forced flow boundary condition. However, the PMCS considered in the current study consists of a vertical Calandria vessel in which the flow is single phase within a natural circulation loop. The feasibility and efficiency of such a system needs to be assessed before it is implemented in the reactor design. Therefore, it was thought desirable to set up a scaled experimental facility for the PMCS. For flow simulation, the open source code OpenFoam 2.2.0 was used. The results obtained using this code was compared with the experimental data. In future, this code will be useful to simulate various operational and accidental scenario of the reactor for the reactor scale PMCS.

CHAPTER 3:

PASSIVE MODERATOR COOLING SYSTEM CONCEPT

3.1 Introduction

Many new reactor designs are including passive systems, which has the advantage of being operational without any power supply. The Indian Advanced Heavy Water Reactor (AHWR) is one of such designs, that has several in-built passive systems. In this chapter the salient features of the AHWR are described. In light of the Fukushima accident, a Passive Moderator Cooling System (PMCS) was conceptualised, which safeguards the reactor Calandria from overheating and pressurisation by cooling the moderator by passive means. The PMCS consists of the Calandria and GDWP, connected via an intermediate shell and tube heat exchanger, forming a coupled natural circulation loop system. The geometrical details and working of the Passive Moderator Cooling System (PMCS) of AHWR are explained. However before implementing any design in the reactor it must be first rigorously tested. For an initial assessment the system was simulated using a 1D system code, RELAP5/MOD3.2 and the thermal hydraulic behaviour is discussed in brief.

3.2 System Description

3.2.1 Advanced Heavy Water Reactor

To enhance fuel utilization, India has developed a nuclear power program using a closed nuclear fuel cycle. Plutonium from the spent fuel of Pressurized Heavy Water Reactors will be recycled and used as fuel in the Fast Breeder Reactors, in order to breed more fissile fuel.

Ultimately, in order to achieve energy security in the country, India will install reactors based on thorium-^{233}U fuel cycle, which will keep breeding new fuel from the fertile thorium (whose reserves are abundantly present in India). In order to timely develop the thorium based technologies an Advanced Heavy Water Reactor (AHWR) is designed (Fig. 3.1. It is 300 MW(e), vertical, pressure tube type, boiling light water cooled, natural circulation nuclear reactor with heavy water moderator. The fuel contains $(Th\text{-}Pu)O_2$ and $(Th\text{-}^{233}U)O_2$ pins.

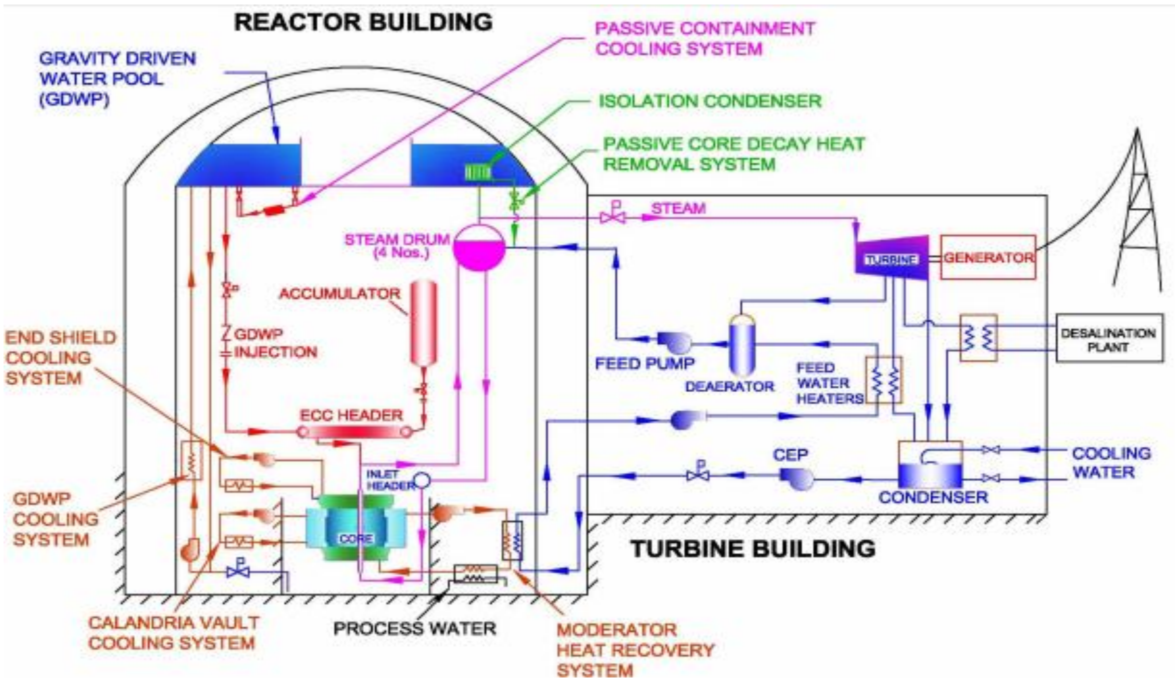

Figure 3.1: Schematic of Advanced Heavy Water Reactor.

The reactor core is housed in a low-pressure cylindrical reactor vessel called the Calandria, which contains the heavy water (acts as moderator and reflector). The Calandria houses vertical coolant channels consisting of pressure tubes, inside which the fuel cluster is inserted. The Calandria tube envelops each pressure tube and an air annulus separates the two tubes proving a thermal insulation between the hot coolant channel and the cold moderator. The light coolant is circulated by natural convection through the tail pipes to the steam drum, where the steam is separated and supplied to the turbine. Four steam drums receive water at

403 K and returns sub-cooled coolant at the reactor inlet. An 8000 m^3 capacity gravity driven water pool (GDWP), is located at the top off the containment which serves as a heat sink to various passive safety systems. Further details of the design of this reactor is given in published literature (Sinha and Kakodkar, 2003, 2006; Sinha et al., 2000).

Due to the generation of radioactive isotope Tritium and high cost of production of heavy water, heavy water as a coolant requires implementation of a costly heavy water management and recovery system. On the other hand, light water as a coolant can be used to achieve boiling inside the core, generating steam at higher pressure than a pressurized non-boiling system. The core of AHWR is designed as vertical in order to remove the core heat by natural circulation. Finally, heavy water is chosen as moderator due to its excellent fuel utilization properties. Hence, the AHWR adopts the well-proven pressure tube type technology (derived from PHWR) and employs natural circulation to remove core heat during normal operation of the reactor, by means of boiling in the core (as in a conventional Boiling Water Reactor). In addition to this, several passive safety systems have been incorporated in the reactor design, e.g. the passive decay heat removal system, the passive containment cooling system, the PMCS, etc.

3.2.2 Calandria

The Calandria vessel in consideration is a vertical cylindrical tank with inner diameter of shell being 6.9 m and height 5.3 m. There are 513 Calandria tubes (fuel channels) in this tank whose outer diameter is 0.168 m and are arranged in a square pitch layout (pitch = 0.225 m). Inside the Calandria tubes, the primary coolant flows inside another concentric tube (namely the pressure tube) separated from the Calandria tube by an air gap. There are 16 inlets and 16 outlets located near the bottom and top of the Calandria, respectively.

3.2.3 Passive Moderator Cooling System

In the event of a prolonged SBO, the reactor trips and the nuclear fission in the fuel stops. As a result, the heat generation due to moderation of neutrons produced from fission reaction also stops. However, the natural radioactive decay of the fission products inside the fuel shall continue generating heat, which in turn is cooled by the MHTS. Now, only the heat transfer from MHTS across the pressure tube and Calandria tube gap causes the heating of moderator. This thermal radiation heat transfer is estimated to be around 2 MW (Kumar et al., 2015), at the beginning of the reactor trip and slowly reduces as the decay heat generation (hence MHT temperature) reduces. In such a scenario, the moderator can no longer be cooled by active means due to absence of electricity. Thus, the objective of the PMCS is to remove this 2 MW heat from the moderator generated by radiation heat transfer across pressure tube and Calandria tube gap in case of a prolonged SBO and maintaining its temperature below the permissible safe limit (100 ºC) for at least 7 days.

3.2.3.1 Geometrical details

The Calandria vessel is a cylindrical vessel housing the 513 Calandria tubes, which are surrounded by the heavy water moderator. There are 16 outlets located uniformly along the top of the tank. These outlets join to a common ring header, from which a single pipe leaves towards the tube side of a single pass shell and tube heat exchanger located at an elevation of 2.1 m from the Calandria vessel. The outlet of the tube side is connected to a ring header from which 16 pipes connect to the bottom of the Calandria acting as the inlets to the Calandria. The shell side of heat exchanger is water coming from an overhead tank with a huge inventory of water (8000 m^3), called the GDWP tank, and located at a height of 40 m.

The heat exchanger is a shell and tube heat exchanger with shell diameter of 1.345 m and height of 3.5 m. There are 3461 tubes with outer diameter 12.7 mm. Hot heavy water moderator flows through the tube side, whereas cooler GDWP light water flows through the shell side of the heat exchanger. Both the tube side and the shell side fluid work at atmospheric pressure.

3.2.3.2 System working

The PMCS removes 2 MW heat from the moderator by means of a shell and tube heat exchanger (HX in Fig. 3.2) placed at an elevated position with respect to the Calandria (Fig. 3.2). The heat generated in the Calandria increases the temperature of the moderator. This hot and less dense moderator fluid rises upwards due to buoyant force and through the hot leg and enters the tube side of the shell and tube type heat exchanger. This in turn is cooled by the water coming from the GDWP (a large overhead tank) into the shell side of the heat exchanger, again by means of natural circulation. Thus, two interdependent natural circulation loops are formed: one between the Calandria and the tube side of the heat exchanger, and the other between the shell side of the heat exchanger and the GDWP.

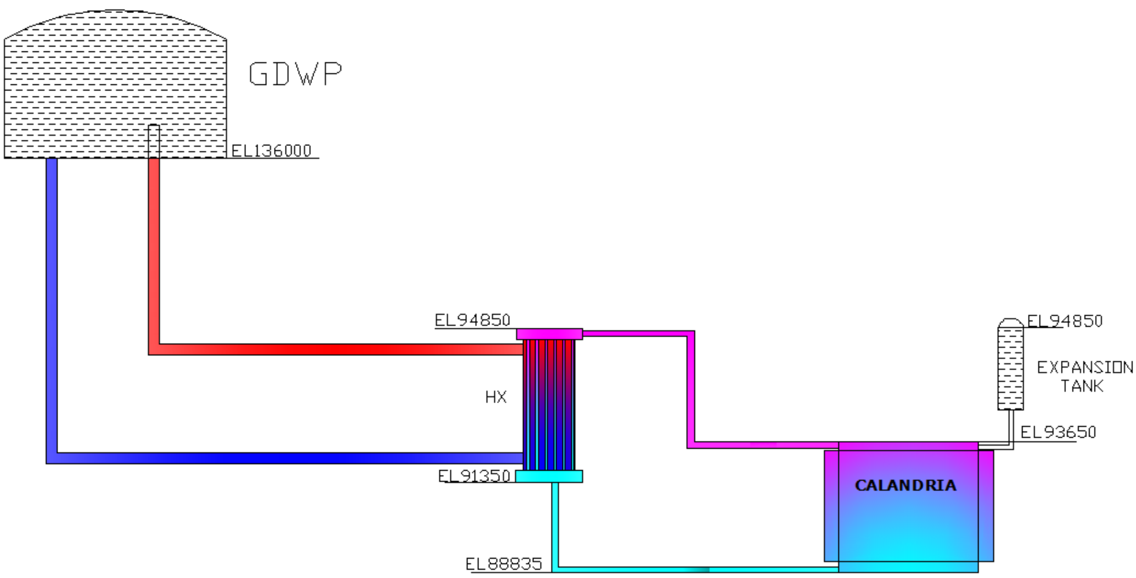

Figure 3.2: Schematic of Passive Moderator Cooling System.

The estimation of 2 MW heat generation in the moderator is given as follows: The MHT coolant is at an average temperature of 272.5 ºC. The pressure tube is also assumed to be at this temperature. The moderator is initially present at an average temperature of 67.5 ºC.

For radiation heat transfer: $Q_{radiation} = \epsilon \cdot \sigma \cdot A_{pressure\ tube} \cdot (T^4_{pressure\ tube} - T^4_{Calandria\ tube})$

$$= 0.5 \times 5.67 \times 10^{-8} \times 903 \times (545.5^4 - 340.5^4)$$

$$= 1.923 \text{ MW}$$

Where, ϵ is the emissivity of stainless steel 304, σ is the Stefan-Boltzmann constant, $A_{pressure\ tube}$ is the heat emitting surface area (total surface area of the pressure tubes) and T is the absolute temperature (K).

3.3 RELAP modelling of PMCS

In an earlier study, a reactor-scale 1D transient simulation (using RELAP5/MOD3.2) was performed for the reactor including the MHTS and the PMCS, in the event of a station blackout scenario (Kumar et al, 2013). The results indicate that the systems remain within the defined safety limits for more than 9 days.

In this previous study (Kumar et al., 2013), various systems of the reactor viz Main Heat Transport System (MHTS), Isolation Condenser System (ICS), Emergency Core Cooling System (ECCS), Passive Containment Cooling System (PCCS), and Primary Containment volumes, i.e. V1 and V2 along with the Passive Moderator Cooling Systems were integrally simulated with the system code RELAP5/MOD3.2.

A prolonged SBO condition has been considered for analyzing the decay heat removal capability of the reactor. When the simulation starts, the system is assumed at a condition of rest. The power is first increased slowly to the normal operating power (920 MW) and kept constant for 7500 s. After this, the SBO is initiated (which is considered as time t = 0 s). With initiation of the SBO, the reactor is shut down (trips). The PMCS system is plugged in from the time SBO is initiated. The heat from the MHTS is modeled to be transferred to the moderator by radiation mode of heat transfer. The moderator temperature is initially at 67.5 ºC. It was observed that after 2.5 days, the moderator and the shell side of the heat exchanger mass flow rates stabilize at 10 kg/s and 21 kg/s, respectively (Fig. 3.3A). Also, the temperature difference between the inlet and outlet of Calandria (moderator) is maintained at an almost constant value of 3 ºC (Fig. 3.3B). The analysis led to the conclusion that the concept works. Furthermore, the system is able to maintain the moderator temperature below boiling conditions for a time period of 7 days without any operator intervention.

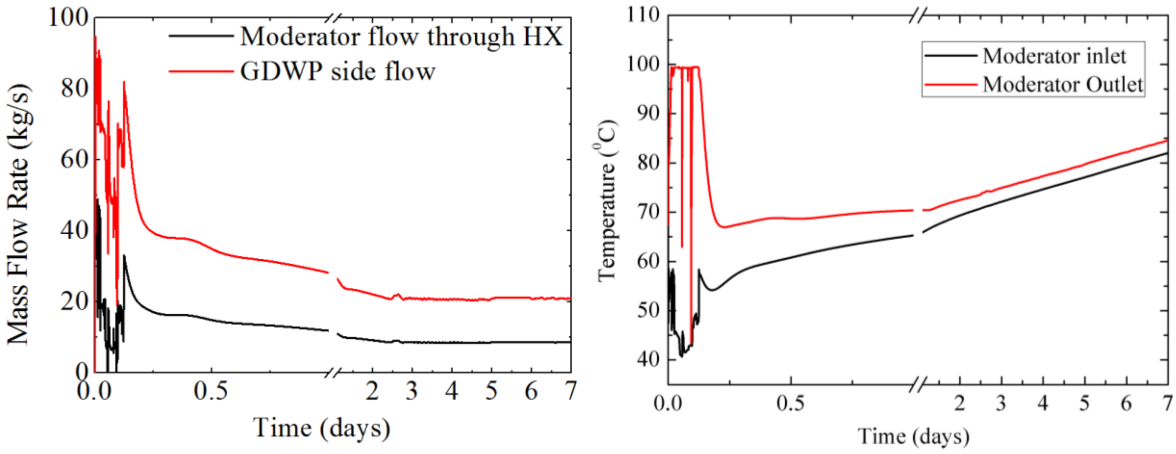

(A) **(B)**

Figure 3.3: Variation of (A) moderator and GDWP side mass flow rates (B) Moderator inlet and outlet temperature for 7 days.

3.4 Closure

Although the working of this concept was proven by performing numerical analysis using 1D numerical code, the PMCS consists of complex three dimensional components such as the Calandria and the heat exchanger. The thermal-hydraulic behavior of such a complex natural circulation system needs to be assessed even more comprehensively, before it is implemented in the reactor design. One of the best methods to do so is by performing experiments in a scaled experimental facility. The experimental facility will give much required insights into the working of a coupled natural circulation loop.

CHAPTER 4:

SCALING AND EXPERIMENTS IN PASSIVE MODERATOR COOLING TEST FACILITY

4.1 Introduction

As explained in the previous chapter a PMCS design in the AHWR was analyzed using a 1D code. It was concluded that the system is capable of limiting the temperature of the moderator below boiling conditions in a SBO condition for a period of 7 days. However the system has complex three dimensional components such as the Calandria and the heat exchanger. Thus a scaled experimental facility of the AHWR PMCS was built. The experimental facility description, the scaling methodology and the various experiments performed in this system are described in this chapter. The experiments performed in this facility will give insights into the working of the PMCS and also the thermal hydraulic behavior of the coupled natural circulation loop. Finally, the results from the experiments will be used to validate various numerical codes, which can be used later for reactor scale simulations.

4.2 Scaling Methodology

In order to predict the flow and heat transfer in the PMCS, a scaled facility was built. It is necessary to maintain the geometrical and dynamic similitude in the facility for accurate predictions. To achieve this, a systematic scaling procedure must be followed. Several authors have reported on the scaling methodologies and scaled facility experiments [Carbiener and

Cudnik (1969), Nahavandi et al. (1979), Ishii and Kataoka (1983), Kiang (1985), Ishii et al. (1998), Kim et al. (2005, 2007), Park et al. (2007)].

For the single phase flow in the present case, one dimensional area averaged mass, momentum and energy balance equations were used. Using boundary conditions for these equations, similarity groups were identified and finally the important dimensionless numbers characterizing the geometric, kinematic, dynamic and energetic similarity parameters were derived. The present analysis considers the following assumptions:

1. The viscous heating is negligible.
2. The heat losses to ambient are negligible.
3. Boussinesq approximation is valid, i.e. fluid properties can be considered to be constant in the governing equations except for the density in the buoyancy force term which is assumed to vary linearly with temperature as

$$\rho = \rho_o\{1 - \beta(T - T_o)\} \qquad ...(4.1)$$

4. Since the analysis is for single phase liquid conditions, the fluid is assumed to be incompressible.

The governing equations for a one-dimensional flow around a loop compose of several sections can be given as follows (Kiang, 1985):

Continuity equation:

$$u_i = \frac{a_o}{a_i} u_r \qquad ...(4.2)$$

Integral momentum equation:

$$\rho \frac{du_r}{dt} \sum_i \frac{a_o}{a_i} l_i = \beta g \rho \Delta T l_h - \frac{\rho u_r^2}{2} \sum_i \left(\frac{fl}{d} + K\right) \left(\frac{a_o}{a_i}\right)^2 \qquad ...(4.3)$$

Energy equation:

$$\rho C_P \left(\frac{\partial T_i}{\partial t} + u_i \frac{\partial T_i}{\partial x}\right) = \dot{q}_i''' \qquad ...(4.4)$$

where u_i is the velocity in the i^{th} section, u_r is the velocity in the core, a_o is the core flow area and l_h is the vertical separation between the hot and the cold thermal center in the loop. u_r is a function of time, but during a steady-state natural circulation it is denoted by u_o and it is the reference velocity used in non-dimensionalization.

The non-dimensionless parameters are defined as follows:

$$u_i^* = \frac{u_i}{u_o}, u_r^* = \frac{u_r}{u_o}, a_i^* = \frac{a_i}{a_o}, l_i^* = \frac{l_i}{l_o}, l_h^* = \frac{l_h}{l_o}, x_i^* = \frac{x_i}{l_o}, t^* = \frac{tu_o}{l_o}, T^* = \frac{T}{\Delta T_o}, \text{ and } \Delta T^* = \frac{\Delta T}{\Delta T_o}. \quad ...(4.5)$$

where ΔT_o is the maximum temperature difference in the loop during steady state natural circulation. With these dimensionless parameters, the conservation equations can be non-dimensionalized, so that

$$u_i^* = \frac{u_r^*}{a_i^*} \quad ...(4.6)$$

$$\frac{du_r^*}{dt^*}\sum_i \frac{l_i^*}{a_i^*} = \frac{\beta g \rho\ \Delta T_o l_o}{u_0^2}\Delta T^* l_h^* - \frac{u_r^{*2}}{2}\sum_i \frac{\left(\frac{fl}{d}+K\right)_i}{a_i^{*2}} \quad ...(4.7)$$

$$\frac{\partial T_i^*}{\partial t^*} + u_i^* \frac{\partial T_i^*}{\partial x^*} = \frac{\dot{q}_i''' l_o}{\rho C_P u_o \Delta T_o} \quad ...(4.8)$$

The three dimensionless numbers in Eqs. 4.6, 4.7 and 4.8 are named as follows:

1. Richardson number, Ri = $\frac{\beta g \rho\ \Delta T_o l_o}{u_0^2}$, ...(4.9)
2. Friction/Orifice number, F= $\left(\frac{fl}{d} + K\right)$, ...(4.10)
3. Heat source number, Q = $\frac{\dot{q}_i''' l_o}{\rho C_P u_o \Delta T_o}$. ...(4.11)

The model is operated with the same fluid at the same pressure and temperature as the prototype (Table 4.1). This means the fluid properties are same, i.e. $\rho_R = (C_P)_R = \beta_R = 1$.

Table 4.1: Initial conditions of the PMCS and PMCTF

Parameters	PMCS	PMCTF	Ratio (model/prototype)
Primary loop pressure	1 atm	1 atm	1
Secondary loop pressure	1 atm	1 atm	1
Calandria inlet temperature	333 K	333 K	1
Calandria outlet temperature	353 K	353 K	1
GDWP temperature	313 K (Ambient temperature)	308 K (Ambient temperature)	~1

To achieve geometrical and dynamic similitude, the ratio of various dimensionless parameters in the prototype and the model must be equal. For any dimensionless parameter ψ:

$$\psi_R = \frac{\psi_{model}}{\psi_{prototype}} = 1 \quad ...(4.12)$$

This gives:

$a_{iR}^{*} = 1,$ ➔ similarity in flow area ...(4.13)

$l_{iR}^{*} = l_{hR}^{*} = x_{iR}^{*} = 1,$ ➔ similarity in length and height ...(4.14)

$t_{R}^{*} = 1,$ ➔ $t_R = \left(\frac{l_o}{u_o}\right)_R$ ...(4.15)

$T_{R}^{*} = 1,$ ➔ $T_R = (\Delta T_o)_R$ ...(4.16)

$Ri_R = 1,$ ➔ $(\Delta T_o)_R = \frac{u_{0R}^2}{l_{oR}}$ ...(4.17)

F_R=1, ➔ preservation of flow resistance ...(4.18)

Q_R= 1, ➔ $\dot{q}_R^{'''} = u_{oR}^3 / l_{oR}^2$ ...(4.19)

The requirement of fluid property matching demands T_R=1. Thus, $(\Delta T_o)_R = T_R = 1$. Thus the Richardson number matching requires:

$$u_{oR} = \sqrt{l_{oR}} \quad ...(4.20)$$

With the relationship between u_o and l_o being fixed, the time and heat source scaling become:

$$t_R = \sqrt{l_{oR}} \text{ and } \dot{q}_R^{'''} = 1/\sqrt{l_{oR}} \qquad ...(4.21)$$

In order to satisfy the similarity between the prototype and the model, all the above ratio between the prototype and model should be satisfied. The length and the flow area ratio of the PMCTF were 1/10 and 1/100 respectively. This is because of the restrictions in available experimental space and power supply. The PMCTF uses water as the working fluid same as in the prototype. Furthermore, the thermal hydraulic conditions in the model are similar to the prototypic pressure and temperature conditions. This selection achieves a fluid property similarity between the AHWR PMCS and PMCTF. Stainless steel is the main construction material for most of the components to minimize the corrosion problems. The various ratios of the scaled facility ratios are listed in Table 4.2. Major scaled design data is summarized in Table 4.3.

Table 4.2: Similarity parameters for Passive Moderator Cooling Test Facility.

Parameter	Scaling Law	Design
Length	l_R	1/10
Area	a_R	1/100
Temperature	1	1
Velocity	$\sqrt{l_R}$	1/3.16
Time	$\sqrt{l_R}$	1/3.16
Power	$a_R\sqrt{l_R}$	1/316

Due to the available size of materials for the construction of the Calandria tank vessel and the pipe size, some distortion in the scaled ratio has occurred. The total loop elevation was scaled according to the available total height in the experimental area. However the scaled value of the height of the primary loop was too small, hence the height was left as the full height of the prototype.

Table 4.3: Design values of PMCS and PMCTF.

Parameter	PMCS (Prototype)	Ideal model value	PMCTF (actual model)
Calandria			
Height (m)	5.3	0.53	0.6
Flow area (m^2)	26.02	0.26	0.16
Power (W)	2×10^6	6.33×10^3	6.5×10^3
Heat Exchanger			
Height (m)	3.5	0.35	0.6
Flow area (m^2)	0.0036	3.65×10^{-5}	0.00069
Pipe flow area (m^2)	0.071	0.0007	0.0022
Loop elevation			
Total	47	4.7	4.7
Primary (m)	2.1	0.21	2.1
Secondary (m)	39.4	3.94	2.6

4.3 Experimental Setup

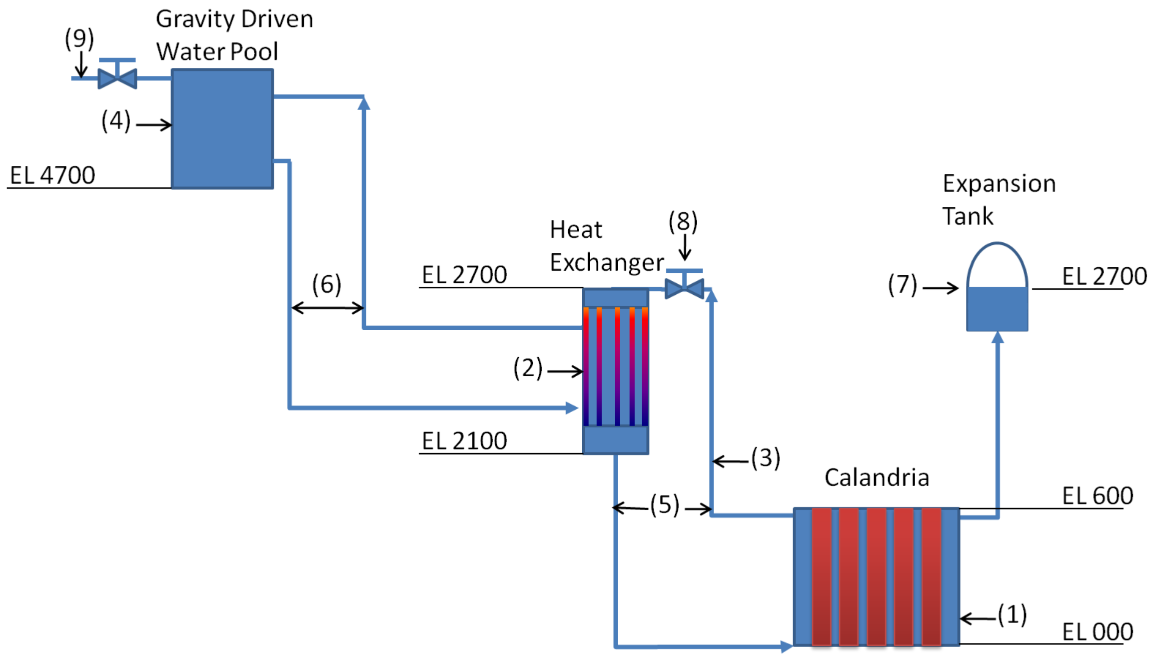

Figure 4.1: Components of the passive moderator cooling test facility (1) Calandria vessel (2) heat exchanger (3) hot leg (4) gravity driven water pool (GDWP) (5) primary natural circulation loop and (6) secondary natural circulation loop (7) expansion tank (8) vent and (9) overflow line.

The schematic of the PMCTF is shown in Fig. 4.1. The Calandria vessel is a 0.6 m ID carbon steel cylindrical tank with 19 electrical heater tubes (in two rings with PCD of 0.24 m and 0.48 m) that simulates the fuel channels of the reactor. These were arranged in two circular rings as shown in Fig. 4.2. The heat exchanger is a shell and tube type heat exchanger designed to remove 6.5 kW. The shell inner diameter is 0.0525 m with 40 tubes of 0.006 m OD. The pipes connecting Calandria and heat exchanger are of 0.0525 m ID. The shell side of the heat exchanger is connected to the GDWP tank. The GDWP tank was a large 0.8 m x 1.2 m x 1 m steel tank, which was open from the top. An expansion tank (height 0.7 m and 0.3 m diameter) was connected to the top of the Calandria vessel and was located at the highest elevation of the primary loop. Fig. 4.2 B and C show the Calandria vessel and the heat exchanger of the experimental facility. To take care of heat loss to the atmosphere, the loop was insulated with ceramic wool in order to minimize heat losses to the ambience. The geometrical details are summarized in Table 4.4.

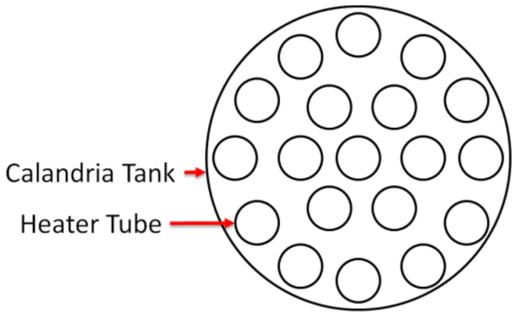

(A)

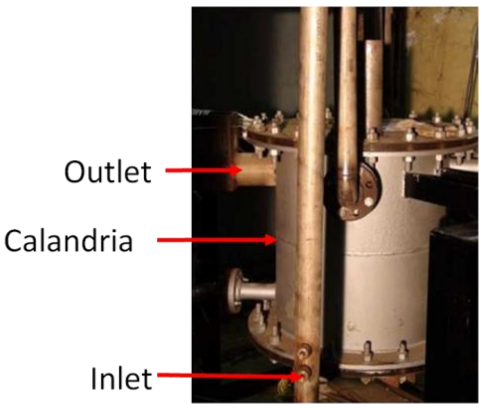

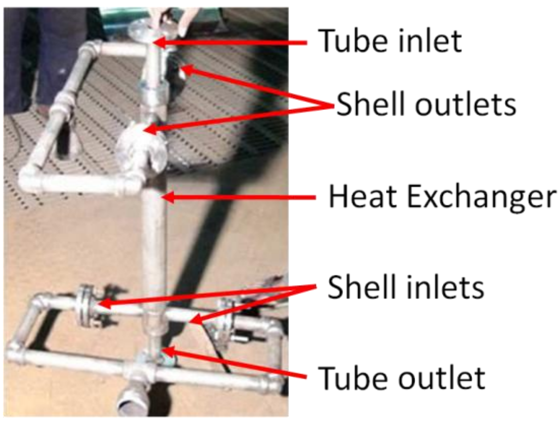

(B) **(C)**

Figure 4.2: (A) Top view sketch of Calandria showing the tubes; Components in the experimental setup (B) Calandria vessel (C) heat exchanger

4.4 Instrumentation

Fifty seven thermocouples were located at a distance of 2 mm on nineteen Calandria tubes, distributed uniformly among all the tubes. This gave a 3D temperature profile inside the Calandria at all times. Furthermore, thermocouples were also placed at the inlet and outlet of the Calandria, tube side of the heat exchanger and shell side of the heat exchanger. These are mineral insulated 0.5 mm diameter chromel-alumel thermocouples (K-type). Thermocouples were calibrated in the range of 0-150 ºC with a measuring accuracy of 0.4 % (± 0.6 ºC). Heater power could be controlled using dimmerstat and measured with the help of Wattmeter having an accuracy of 0.5 %. All temperature data were recorded at a frequency of 10 seconds and fed to a data logger from Yokogawa.

Table 4.4: Geometrical details of the prototype PMCS and the scaled model (PMCTF)

Component	Dimensions	AHWR PMCS	PMCTF
Calandria	Diameter of shell, D_{Tank} (m)	6.9	0.6
	Outer diameter of fuel channel, OD_{Tube} (m)	0.168	0.09
	Length, L_{Tank} (m)	5.3	0.6
	Total no. of tubes, Nt	513	19
Heat Exchanger	Diameter of shell, D_{HX} (m)	1.35	0.0525
	Outer diameter of tube, $OD_{Tube,HX}$ (mm)	12.7	6
	Length, L_{HX} (m)	3.5	0.6
	Total no. of tubes, Nt_{HX}	3431	40
	Thickness of tube, d (mm)	2.5	0.7

4.5 Experimental Methodology

The experimental procedure is as follows: the primary loop was filled with demineralized light water through the top expansion tank (#7 in Fig. 4.1). In this process, any air trapped in the loop was vented through a nozzle (#8 in Fig. 4.1) present at the top horizontal section of the primary loop. The water level in the expansion tank was filled upto 0.55 m. The secondary loop was then filled through the GDWP tank to the overflow line (#9 in Fig. 4.1), 0.05 m below the top surface of the GDWP. The data recorders were enabled and then the heater power input was activated. The matrix of experiments that were performed are listed in Table 4.5.

Table 4.5: Matrix of experiments performed in Passive Moderator Cooling Test Facility

Experiment	Power Input		
	Input	Time interval	Maximum power
1 h power step up	500 W step	1 h	3 kW
4 h power step up	500 W step	4 h	5 kW
1 kW const power	const. 1 kW	7 days	1 kW

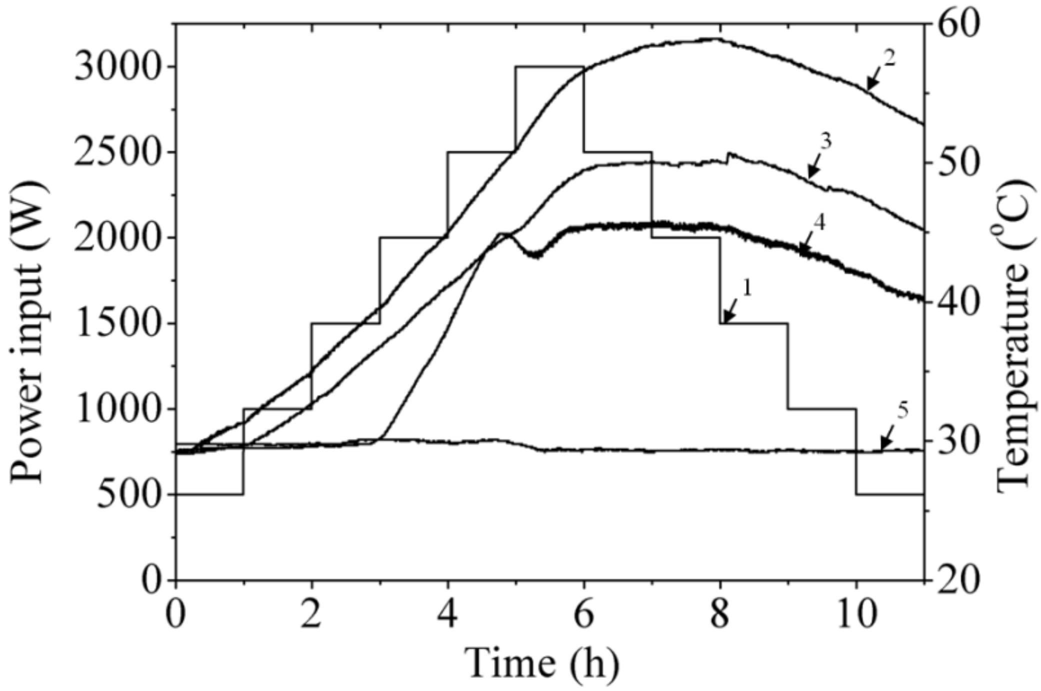

Figure 4.3: Power and temperature plot with time for the one hour power step up experiment (1) power input, (2) Calandria outlet temperature, (3) Calandria inlet temperature (4) heat exchanger shell side outlet temperature and (5) heat exchanger shell side inlet temperature.

4.6 Results and Discussion

4.6.1 Power transient experiment for natural circulation studies

A set of power step up and power step down experiments was conducted in the test facility. Because SBO is a time decaying power transient scenario, this set of experiments would demonstrate the behaviour of the PMCS in such a power varying case.

4.6.1.1 One hour power step up experiment

The power input to the Calandria was increased in steps of 500 W for a constant time interval of 1 h to a maximum power level of 3000 W and then decreased in steps of 500 W back to 0 (Fig. 4.3).

4.6.1.1.1 Flow initiation from rest in Calandria

Fig. 4.4 shows the time variation of Calandria and heat exchanger tube side inlet and outlet temperatures. The time varying development of temperature can be explained in following 4 stages:

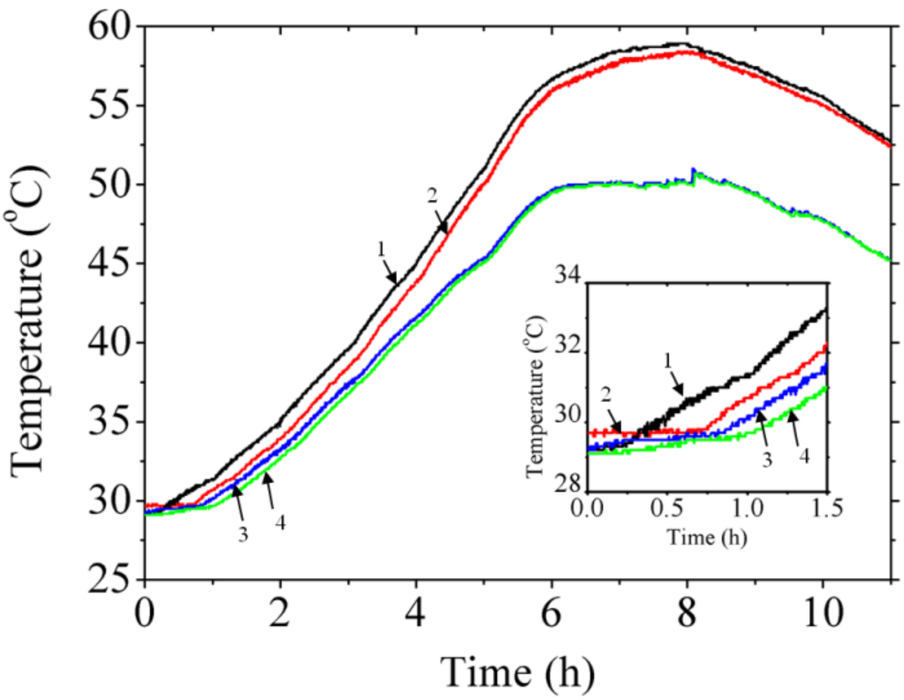

Figure 4.4: Temperature plot with time for the one hour power step up experiment (1) Calandria outlet temperature, (2) heat exchanger tube side inlet temperature, (3) heat exchanger tube side outlet temperature, and (4) Calandria inlet temperature.

<u>Stage1: Stationary primary and secondary loops</u>

When the power is switched on, the fluid near the hot tubes get heated, rises due to buoyancy and gets piled up at the top of Calandria. Simultaneously, relatively colder fluid moves from within the Calandria to replace this hot fluid, thus forming recirculation’s within the Calandria. The rising hot fluid keeps piling up at the top of Calandria, i.e. temperature inside the Calandria gets stratified. Some heat is also lost in heating the structural material of the system and also minor losses to the ambience through any uninsulated surface such as the nozzle and expansion tank. At time 0.25 h, the Calandria outlet temperature starts to increase (inset of Fig. 4.4). However, the temperature at the inlet of the tube side of the heat exchanger does not increase, i.e. the primary side major flow does not reach the tube inlet. This hot fluid leaks out of the outlets of the Calandria gets mixed with the cold fluid within the pipes and the cold fluid enters back through the outlets only.

Stage2: Circulation in primary and stationary secondary loop

At 0.75 h, the hot fluid exiting the Calandria reaches the tube inlet, and then progressively with time, it reaches the tube side outlet and finally the Calandria inlet. This is because by this time, the buoyancy head developed in the primary loop becomes sufficient to overcome the hydraulic resistance of the entire primary loop and starts a flow in this loop.

Stage3: Circulation in both primary and secondary loops

At 3 h, the power input has risen sufficiently high, in order to produce a large enough temperature difference in the secondary loop that starts a natural circulation in this loop also. This can be observed by the rise in shell outlet temperature. The circulating fluid in the secondary loop promotes heat transfer from the primary side. Thus, the temperature difference between the inlet and the outlet of the Calandria and also across the heat exchanger tube side increases. Further, the temperature at the shell side outlet increases sharply and then becomes constant after a small oscillation.

Stage 4: Decrease in power

At 6 h, the power has begun to decrease, as shown in Fig. 4.3. However, the Calandria outlet temperature continues to rise. Only after about 8 h, temperatures at all the locations begin to decrease. The inlet temperature is maintained at a constant value as the secondary side mass flow is sufficiently high enough to cool the primary fluid.

Fig. 4.5 shows the time variation of temperature at five locations along the axial height of the central tube. It is clear that the temperatures are stratified and the degree of stratification increases with time. Even after 6 h, when the power input has started to reduce, the temperatures remain stratified.

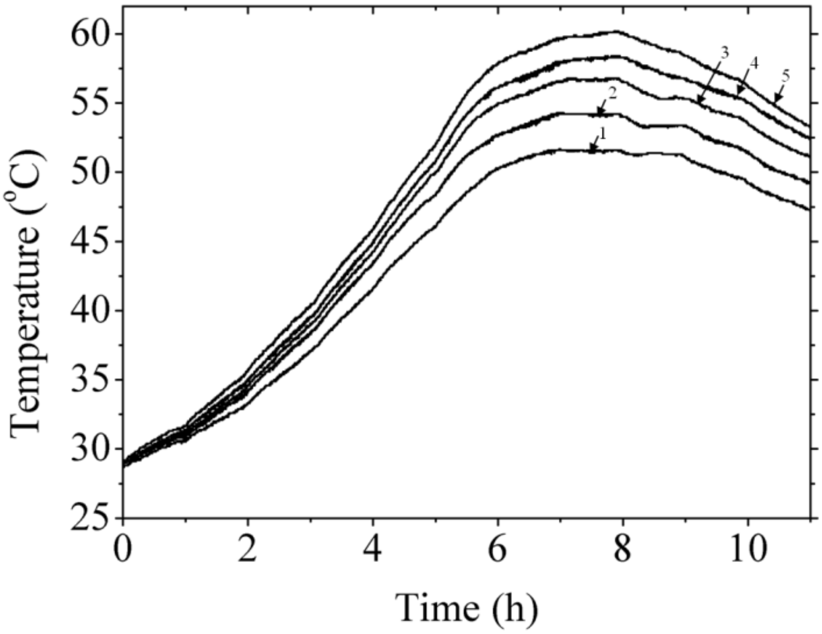

Figure 4.5: Temperature plot with time for the one hour power step up experiment at various axial locations near the central tube (1) z=50mm, (2) z=175mm, (3) z=300mm (4) z=425mm and (5) z=550mm.

4.6.1.1.2 Temperature contours inside the Calandria

The 2D temperature contours on a plane (Fig. 4.6 (A), (B)) passing though the centre of the Calandria is shown in Fig. 4.6 C. These contours have been plotted using the experimental data of the thermocouples located on this plane. The data was post processed using software Origin8©**.** The central tube being unheated, the central part of the contour has lower temperature zone. The top of the Calandria has been seen to be at higher temperatures than the lower part, indicating that the hot fluid rises upward and continues to accumulate (i.e., stratification). It is observed that the temperature contours remain almost the same until 3000 s. Only the magnitude of temperature continues to increase.

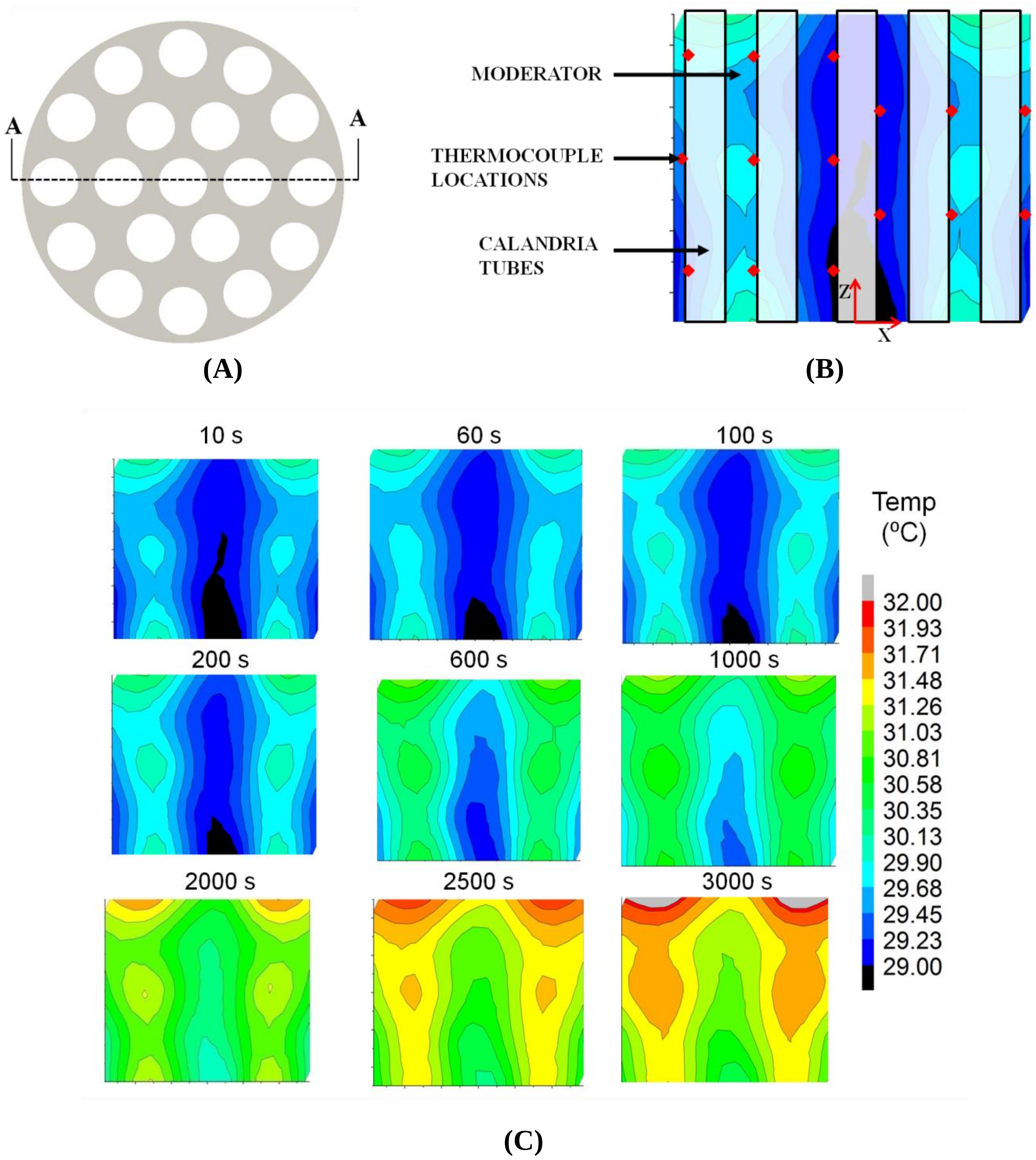

Figure 4.6: (A) Plan view of Calandria with the location of section AA, (B) elevation view of section AA with the locations of tubes and thermocouples (red diamonds) and (C) experimental temperature contours till 3000 s on this plane.

Fig. 4.7 shows the time varying temperature contours for the entire duration of the experiment, taken at an interval of 2 h with a total time of 10 h. It is observed, that, initially the temperature contours are according to the local heat source present (i.e., locations where hot tubes are present have higher temperature) overlapped with a higher temperature zone near the top (i.e., stratification). After 2 h, both the temperature and the stratification continuously increase inside the Calandria. After 6 h, when the heat input has started to reduce, the stratification increases even more. Thus, the major flow throughout the entire loop is unable to affect the stratification inside the Calandria.

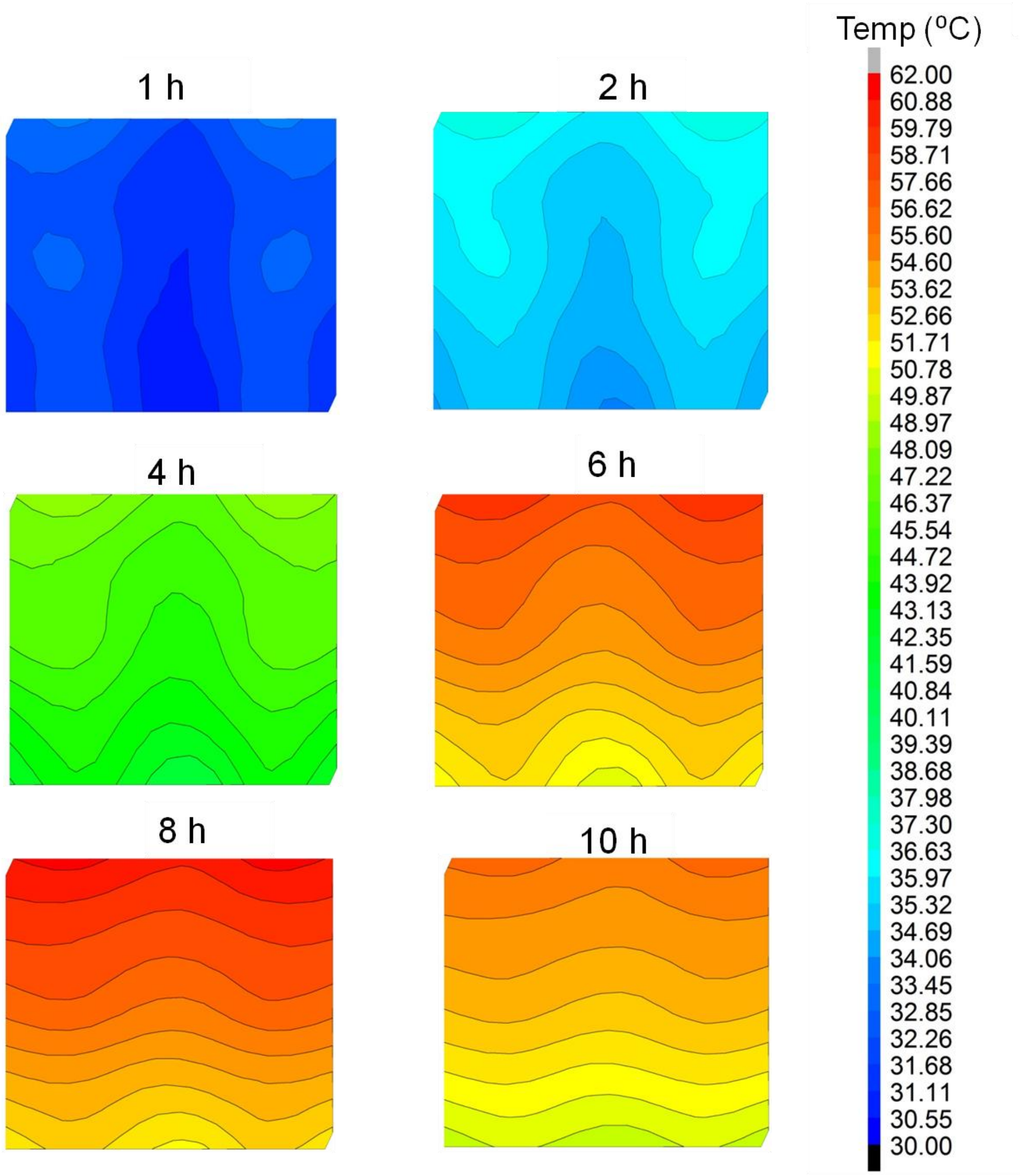

Figure 4.7: One hour power step up experimental temperature contours (in °C) on a plane passing through the centre of Calandria for entire duration of the one hour power step up experiment.

Fig. 4.8 (A) and (B) show the plane of view and the locations of the thermocouples in the Calandria. Fig. 4.8 (C) and (D) show the time variation of temperature contour on an axial plane at the inlet and outlet of the Calandria vessel, respectively. It was observed at the inlet plane (Fig. 4.8 (C)) that the temperature contours demonstrates consistent trends, only the magnitude of temperature continue to increase with time variation. Until 1 h, the temperature variation on this plane is about 1 ºC, whereas after 1 h the temperature variation is about ≈2 ºC. The cold region (i.e., in blue) is located surrounding the centrally unheated pipe, whereas the cold flow in the outer edge is the incoming flow through the inlet of the Calandria.

In the outlet plane contours (i.e., Fig. 4.8 (D)), the temperature contour plots are more dynamic. With time, the hot and cold regions are observed to move around relatively more than at the inlet plane. This is because of the mixing of the spreading external loop flow inside the Calandria, and the buoyant flow in this plane. The temperature difference within this plane is ≈1 ºC up until 1 h. This temperature difference starts to increase with time (i.e., increase in power) and then reduces after 8 h. From these temperature contours it is clear that the flow and temperature distribution inside this system is highly multi-dimensional.

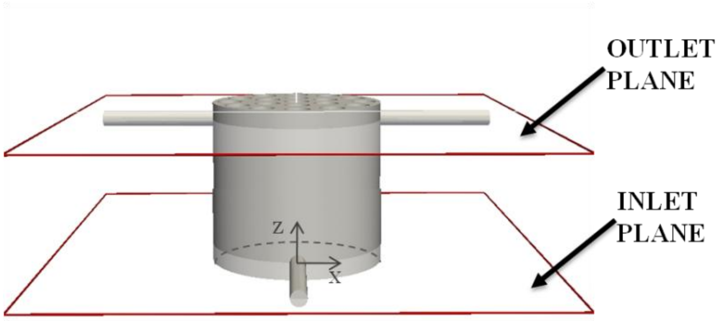

Fig 4.8 (A)

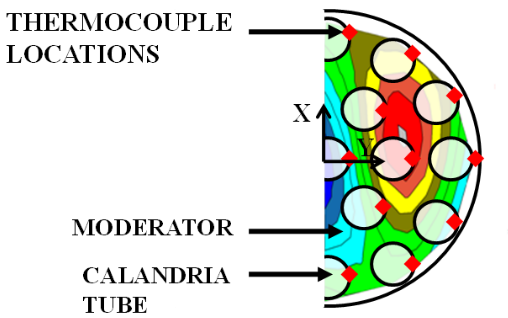

Fig 4.8 (B)

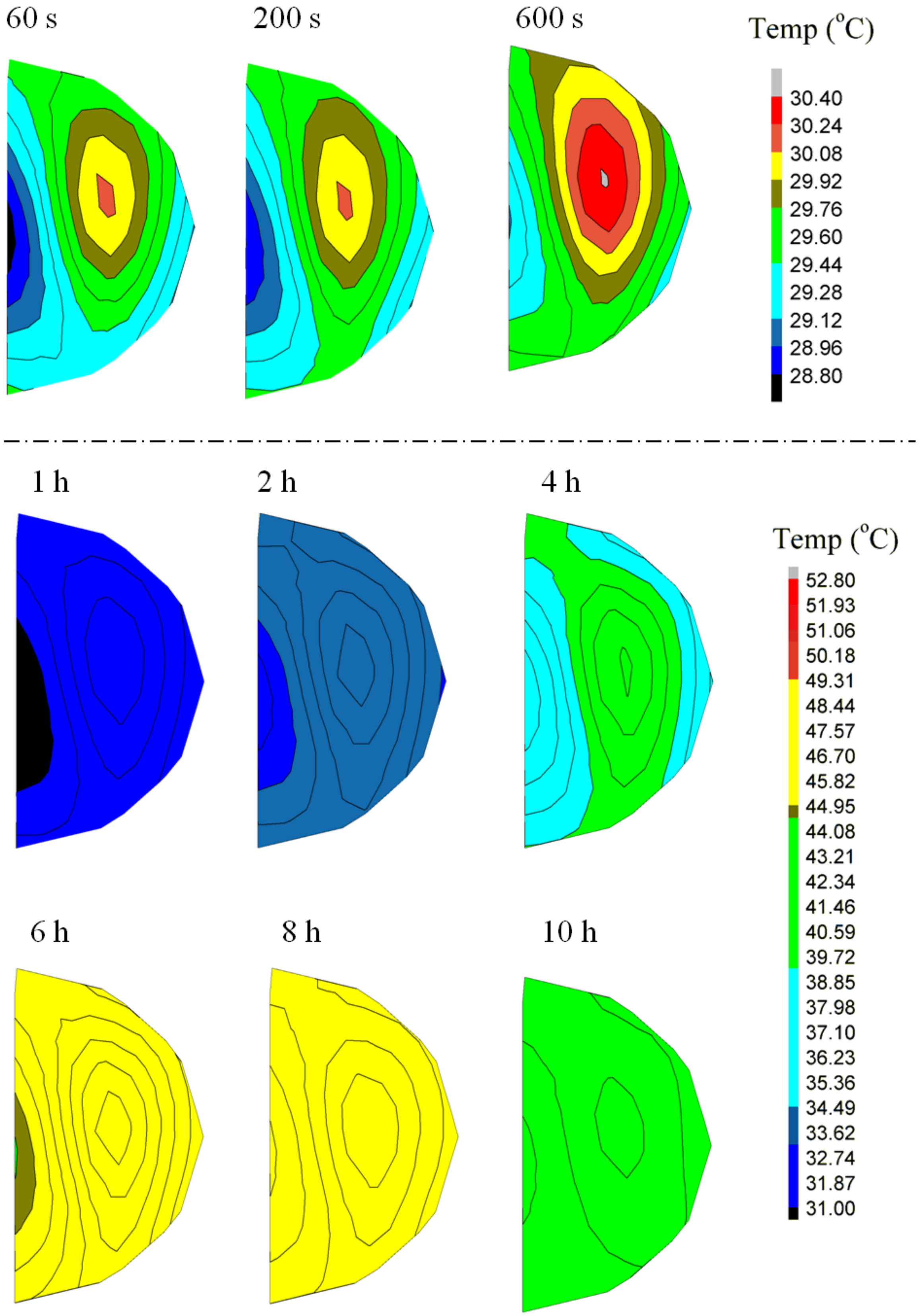

60 s
200 s
600 s
Temp (°C)
30.40
30.24
30.08
29.92
29.76
29.60
29.44
29.28
29.12
28.96
28.80
1 h
2 h
4 h
Temp (°C)
52.80
51.93
51.06
50.18
49.31
48.44
47.57
46.70
45.82
44.95
44.08
43.21
42.34
41.46
40.59
39.72
38.85
37.98
37.10
36.23
35.36
34.49
33.62
32.74
31.87
31.00
6 h
8 h
10 h

Fig. 4.8 (C)

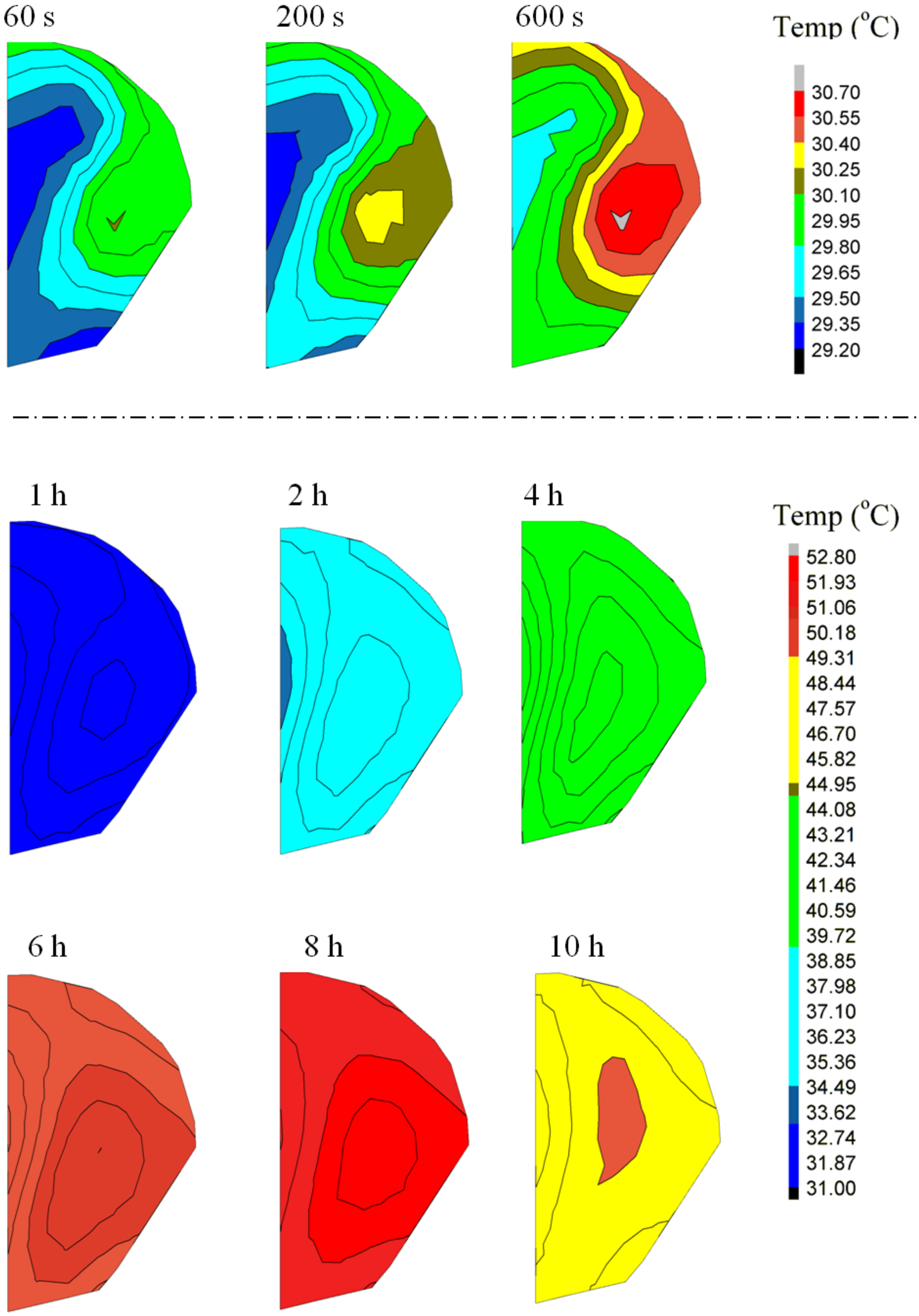

(D)

Figure 4.8: (A) Planes of viewing in Calandria (B) locations of tubes and thermocouples (red diamonds); One hour power step up experimental temperature contours (in °C) from t = 60 s to 10 h, on an axial plane of Calandria (C) z = 50 mm (Inlet Plane) and (D) z= 550 mm (Outlet plane).

4.6.1.2 Power step up experiment

In order to observe a steady behavior at any given power input, the constant time duration for a given power was increased to 4 h (Fig. 4.9).

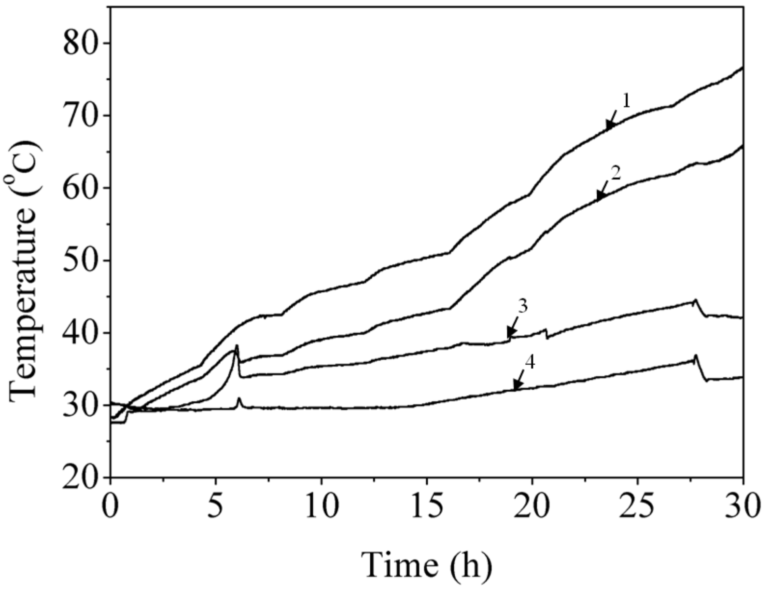

Figure 4.9: Temperature plot with time for "four hours 500 W power step up" experiment (1) Calandria outlet temperature, (2) Calandria inlet temperature (3) Heat exchanger shell side outlet temperature and (4) Heat exchanger shell side inlet temperature.

In this case also, similar to previous experiment, till time 6 h, the temperature difference between the inlet and outlet of Calandria is comparatively lower (~2 ºC). Until this time, there is no circulation in the secondary loop and the temperature at the shell side outlet keeps on increasing. At 6 h, we observe the characteristic spike and drop in temperature of secondary side water. At this time, the circulation in the second loop starts, which leads to the mixing of the hot fluid at the shell side outlet with the GDWP water and hence there is a sharp drop in the temperature of the secondary side. This could also be noted by a corresponding increase in the temperature difference across the inlet and outlet of the Calandria.

Due to the longer transient nature of the experiment, a rise in the temperature of the shell side inlet temperature is also observed (~14 h). The experiment had to be stopped before reaching the target maximum power of 5 kW, as the temperature at one of the thermocouples located inside the Calandria had reached above 80 ºC, which was set as power circuit trip value according to the safety regulations in the laboratory.

4.6.2 Constant power experiment

For this experiment, the loop was given a constant low power of 1 kW for a period of 7 days. The temperature versus time graph is shown in Fig. 4.10. The loop is under transient behavior for the first 8 h. After which the loop enters into a slow transient, with overall rise in temperature while essentially maintaining the same temperature difference. After 2 days, the temperature difference across Calandria is almost at a constant value of 5 ºC. It is interesting to note that the shell side inlet temperature rises by merely 2 ºC since the commencement of the experiment.

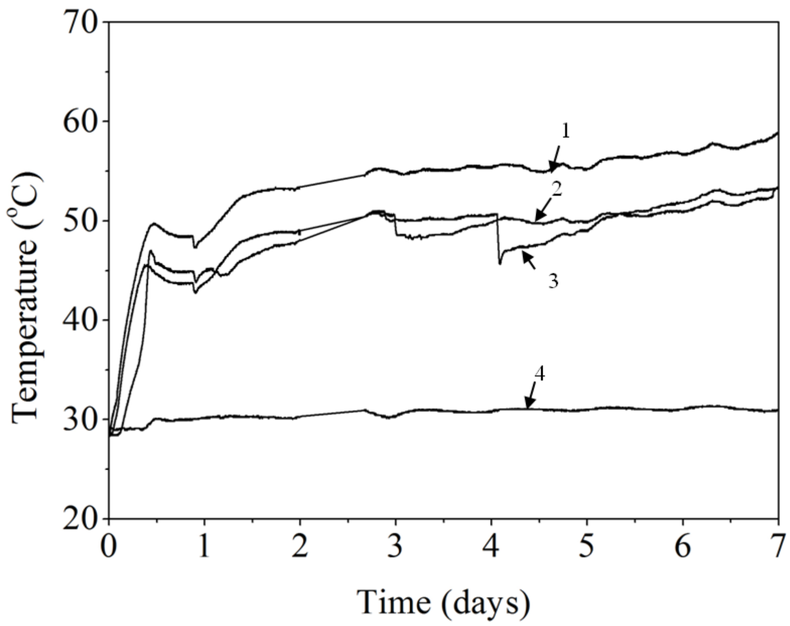

Figure 4.10: Temperature plot with time for "1kW constant power" experiment(1) Calandria outlet temperature, (2) Calandria inlet temperature (3) Heat exchanger shell side outlet temperature and (4) Heat exchanger shell side inlet temperature.

Fig. 4.11 shows the time varying temperature contours on a plane passing through the centre of the Calandria for the entire duration of the experiment. As before, it is observed that the temperatures initially (1 h) in the Calandria the temperatures are higher near the hot tubes. Thereafter, the contours show stratification for the entire duration of the experiment.

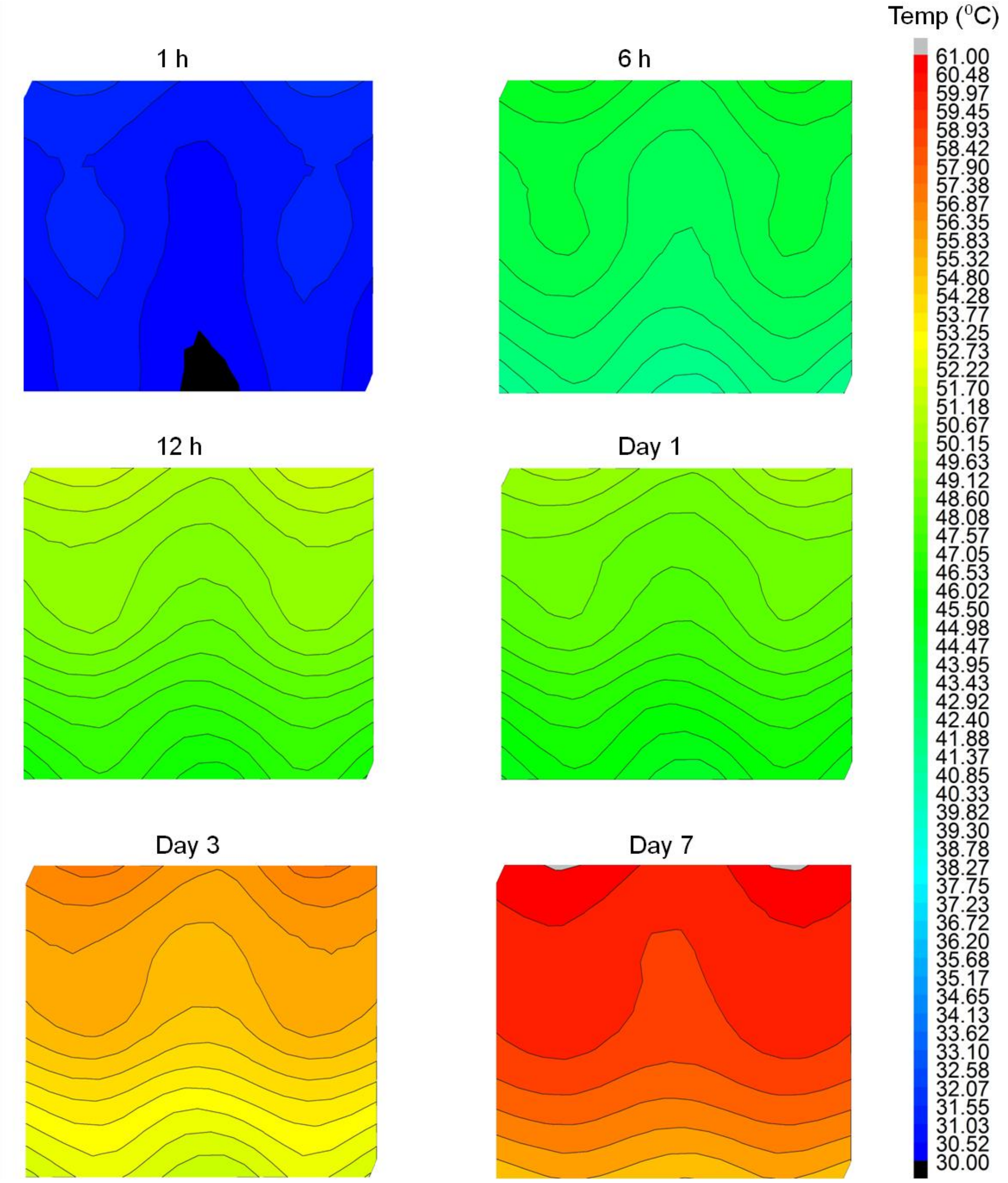

Figure 4.11: Experimental temperature contours (in °C) on a plane passing through the centre of Calandria for entire duration of the 1kW constant power experiment.

4.7 Closure

The scaling methodology and various natural circulation experiments performed in the scaled PMCTF were discussed. Stepwise power increase and decrease transients were studied.

Also data was generated for 1 kW constant power run for 7 days. Starting from a state of rest, the system shows multidimensional flow inside Calandria for the initial time period. Only after the Calandria temperatures have risen sufficiently high enough that the buoyancy head is more than the resistive force in the entire loop, a gross flow begins in the loop. Furthermore, this gross flow is unable to break the stratified contour inside the Calandria. Thus, the thermal hydraulic behaviour of a coupled natural circulation loop was investigated and understood.

The results from these experiments can now be used to validate the numerical codes. Firstly, a 1D system code, namely RELAP5/MOD3.2 shall be used to simulate these experiments. This validated code shall be used in future for reactor scale transience studies for the PMCS.

CHAPTER 5:

RELAP SIMULATIONS OF PASSIVE MODERATOR COOLING TEST FACILITY

5.1. Introduction

A 1D code was used (RELAP5/MOD3.2) to simulate the transient flow of the various experiments performed in the PMCTF. The results of the code are compared to the experimental data. Once the code is validated for this coupled natural circulation system, it will be useful to simulate various operational and accidental scenario of the reactor for the reactor scale PMCS.

5.2. Nodalisation details

Both the primary and secondary loops of the PMCTF were simulated, including heat transfer across the heat exchanger tubes. The geometrical details are as explained in section 4.2 (Table 4.1). All the tubes of the heat exchanger were grouped as a single equivalent channel having the flow area and heat transfer area. Similarly, the Calandria vessel also was simulated as an equivalent channel. All the Calandria tubes were lumped together into one having the same heat transfer area and heater power input as the actual tubes. Both the Calandria and the heat exchanger length were divided into uniform 20 nodes. The GDWP was simulated as a pipe volume with 20 nodes of water and top 2 nodes with air connected to an atmospheric volume. The connecting pipes were nodalised with 0.1m nodes. The heat input to the Calandria tube was given as a constant heat flux. The working fluid was light water in both the loops. Fig. 5.1 shows the nodalisation of RELAP geometry, in which some extra pipe lengths were

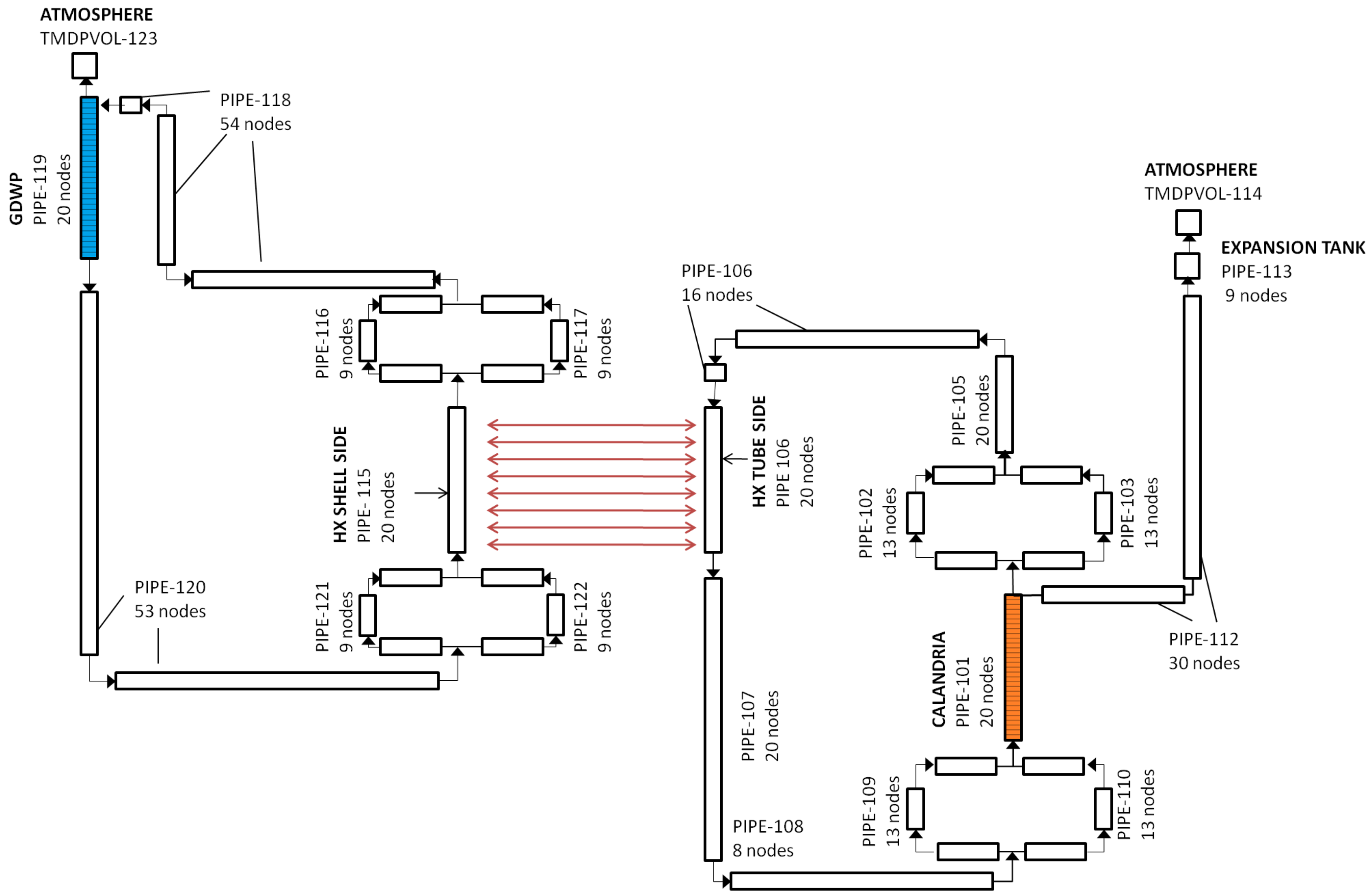

Figure 5.1: RELAP5 nodalisation of PMCTF.

added to the loops, to account for 3D to 1D transformation of the loop.

5.3. Solution methodology

The RELAP5 (Reactor Excursion and Leak Analysis Program) (RELAP Manual, 1995) code is an advanced, reactor thermal-hydraulic simulation code, developed at Idaho National Engineering and Environmental Laboratory (INEEL). It is a one dimensional, transient, two-fluid model for flow of a two-phase steam-water mixture that can contain non-condensable components in the steam phase and/or a soluble component in the water phase. The appropriate empirical correlations are considered within the code to estimate the hydraulic resistance and the heat transfer.

The scenarios simulated were: (1) 4 h power step up experiment and (2) 1 kW constant power run for 7 days. The boundary conditions are listed in Table 5.1.

Table 5.1: Initial and boundary conditions for RELAP5 simulations.

Input Parameter	Boundary Condition	RELAP5 simulation	
		4 h step up	7 d 1 kW power
Calandria heater tube wall	No slip, Constant surface heat flux	500 W step	1000 W
Calandria Shell Wall	No slip, Adiabatic wall	0	0
Heat Exchanger tube wall	No slip, Constant temperature	-	-
Pipe walls	No slip, Adiabatic walls	0	0
Initial temperature of fluid	constant temperature	303 K	303 K
Initial mass flow rate	none	0	0

5.4. Results- Comparison with experimental data

5.4.1. Four hour power step up experiment

The comparison of RELAP5/MOD3.2 predictions and the experimental results is shown in Figure 5.2. The standard deviation of temperature for Fig. 5.2 A and B are 6% and 8% , respectively. The gross temperature increment pattern is quite close to that of the experimental observation.

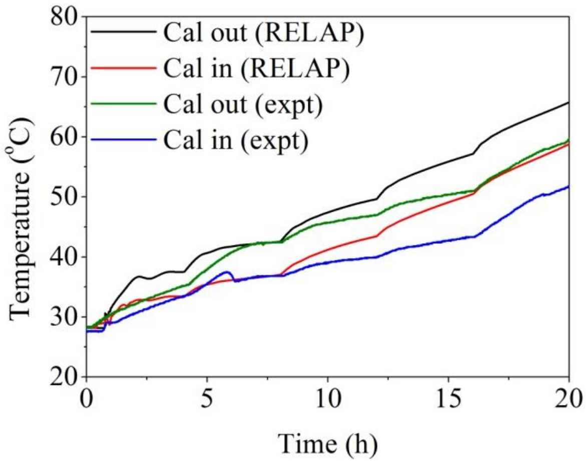

(A)

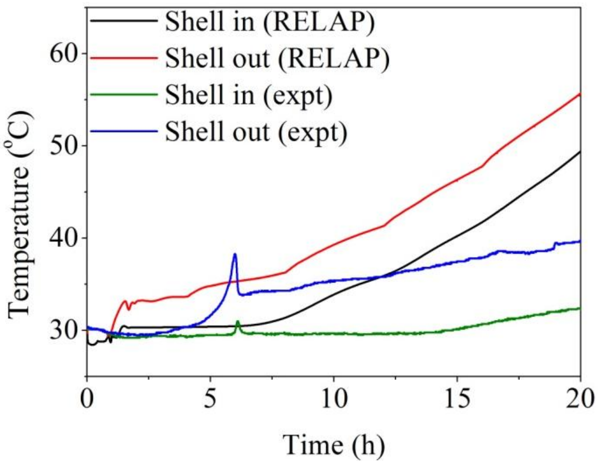

(B)

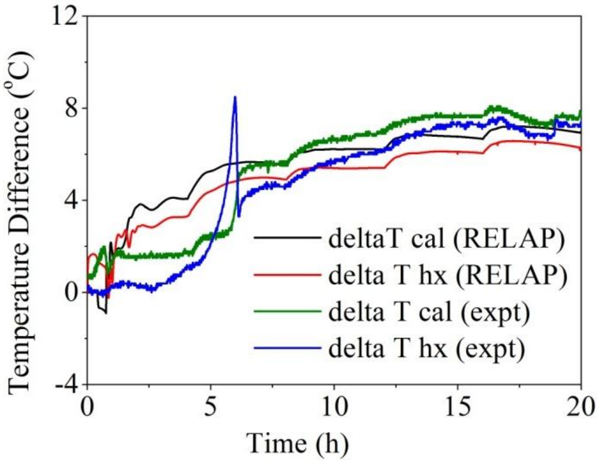

(C)

Figure 5.2: Comparison of temperature with time for "four hour power step up" experiment using RELAP analysis (A) Calandria inlet and outlet (B) Heat exchanger shell side inlet and outlet (C) delta T across the inlet and outlet of Calandria and heat exchanger.

RELAP being a 1D code is not able to capture the initial period (time < 6 h) in which there are internal recirculatory flows within the Calandria. This is because, in 1D case, as soon as the heat input to Calandria begins, the hot fluid rises due to buoyancy and exits the Calandria, rising further upward through the pipes. In turn, to maintain continuity, the cold fluid gets sucked in through the inlets of the Calandria, completing the flow in the entire loop. Thus, unlike in the real experiment where a temperature difference across the inlet and outlet of Calandria is observed from the beginning. Also on the shell side a similar phenomena is seen. The temperature at the shell side inlet, keeps on increasing in the RELAP simulations. However, in the experiment this temperature remains almost constant till 14 h. This is an indication to a possible heat loss to the environment from the top open surface of the GDWP tank and un-insulted sides, which was not considered in the RELAP simulation. After 6 h, the temperature difference across Calandria is in close agreement with the experimental data.

5.4.2. Constant power experiment

The temperature profile from RELAP simulation for the 7 day experiment at constant power of 1 kW is shown in Fig. 5.3. The predicted temperature profiles at the outlet and inlet of Calandria tend to agree reasonably with the experimental data (with the standard deviation of 7%), specially in the long duration (>1 day). However, in the initial transient phase (<0.5 day) the temperatures calculated by the RELAP model at the inlets and outlets of Calandria and heat exchanger increases much earlier than in the actual experiment.

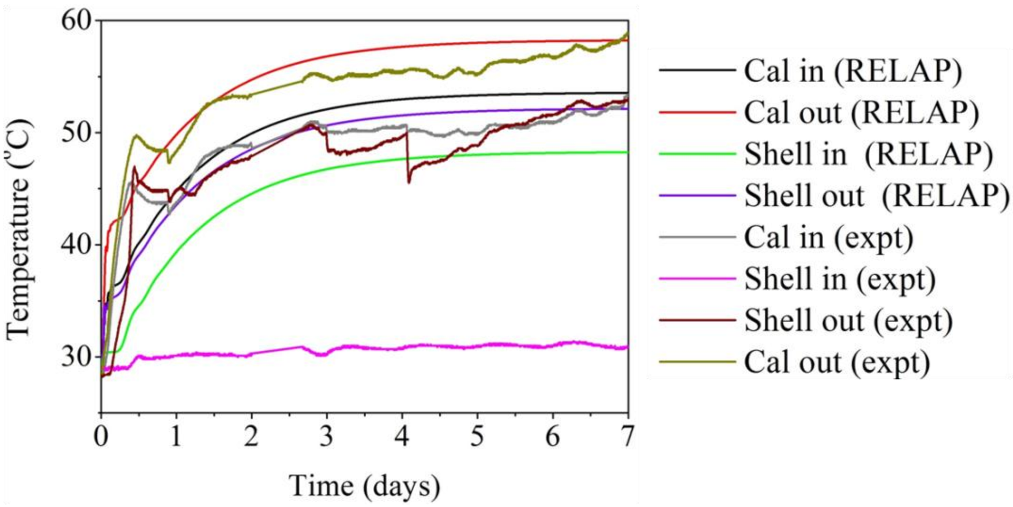

Figure 5.3: Comparison of temperature with time for "1kW steady constant power" experiment using RELAP analysis.

5.5. Closure

The 1D RELAP code is able to capture the gross temperature development in the system. Also, a long transience could be easily and quickly simulated using this code. However, the code is unable to capture all the phenomena in the PMCS test facility experiments, especially the initial transient, when the temperatures in the Calandria rises without a gross flow in the loop. This initial transient phase is even more crucial for an SBO as the highest heat flux occurs in this phase. Thus, the system must be assessed for cooling accurately during this time. Therefore, it was thought desirable to undertake 3D CFD simulations.

CHAPTER 6:

CFD MODEL VALIDATION

6.1. Introduction

In this chapter, the 3D CFD model will be validated against published literature data and experiments. It is important to assess the capability of the CFD code (OpenFOAM 2.2.0) to simulate the various multidimensional and natural convection phenomena such that occurring inside the PMCTF, before it is used to simulate the actual PMCTF experiments. This will give a firsthand knowledge of the sensitivity of the various parameters in the code and also prepare the 3D model for further analysis. The PMCS mainly comprises of a complex 3D geometry of the Calandria which is similar to a shell and tube heat exchanger and also the natural convection phenomena. Thus we simulate various types of systems in order to capture these various geometries and phenomena.

6.2. Numerical modelling

6.2.1. Governing equations

The flow is assumed to be steady, incompressible, 3-dimensional and turbulent. Fluid properties are assumed to be constant, i.e. fluid properties are not varying within the considered temperature range. The governing equations for the Newtonian, incompressible turbulent flow are given by:

Continuity equation:

$$\frac{\partial \bar{u}_j}{\partial x_j} = 0 \qquad \text{...(6.1)}$$

Momentum transport equation:

$$\frac{\partial \bar{u}_i}{\partial t} + \frac{\partial}{\partial x_j}\left(\bar{u}_j \bar{u}_i\right) - \frac{\partial}{\partial x_j}\left\{\nu_{eff}\left[\left(\frac{\partial \bar{u}_i}{\partial x_j} + \frac{\partial \bar{u}_j}{\partial x_i}\right) - \frac{2}{3}\left(\frac{\partial \bar{u}_k}{\partial x_k}\right)\delta_{ij}\right]\right\} = -\frac{1}{\rho}\frac{\partial \bar{p}}{\partial x_i} + S_M \qquad ...(6.2)$$

where $\nu_{eff} = \nu_0 + \nu_T$

The buoyancy effect is modeled by the inclusion of a source term in the momentum equation as follows:

$$S_M = \left(\rho - \rho_{ref}\right) g_i \qquad ...(6.3)$$

where ρ is the fluid density and ρ_{ref} is the fluid reference density.

Since the pressure gradient is relatively small in the natural circulation loop and density variations are due to only temperature variations, the Boussinesq approximation was used as follows:

$$S_M = -\rho_{ref}\,\beta g_i\left(T - T_{ref}\right) \qquad ...(6.4)$$

where β is the thermal expansivity $\beta = -(1/\rho).\,\partial\rho/\partial T|_P$

The reference temperature is taken equal to the temperature on the heat exchanger tube surface for each simulated case. All the thermal properties are defined at this reference temperature.

Energy conservation equation:

$$\frac{\partial \bar{T}}{\partial t} + \frac{\partial}{\partial x_j}\left(\bar{T}\bar{u}_j\right) = \frac{\partial}{\partial x_j}\left[\left(\frac{\nu_t}{Pr_T} + \frac{\nu_0}{Pr}\right)\frac{\partial \bar{T}}{\partial x_k}\right] \qquad ...(6.5)$$

where Pr_T is the turbulent Prandtl number.

6.2.2. Turbulence model

To model the turbulence the standard k-ε model and the SST k-ω models have been employed. The equations of the models are described below:

6.2.2.1. The standard k-ε model (Launder and Sharma, 1974)

The eddy viscosity is modeled as follows:

$$\mu_t = C_\mu \frac{k^2}{\varepsilon} \qquad ...(6)$$

Turbulent kinetic energy (k) transport equation:

$$\frac{\partial(\rho k)}{\partial t} + \nabla.\left(\overline{u_j}\rho k\right) = \nabla.\left[\left(\mu + \frac{\mu_t}{\sigma_k}\right)\nabla.k\right] + G_k + G_b - \rho\varepsilon \qquad ...(6.7)$$

Turbulent dissipation rate (ε) transport equation:

$$\frac{\partial(\rho\varepsilon)}{\partial t} + \nabla.(\rho\varepsilon\overline{u_j}) = \nabla.\left[\left(\mu + \frac{\mu_t}{\sigma_\varepsilon}\right)\nabla.\varepsilon\right] + C_{1\varepsilon}(G_k + C_{3\varepsilon}G_b) - C_{2\varepsilon}\rho\frac{\varepsilon^2}{k} \qquad ...(6.8)$$

where $G_k = -\rho\overline{u_i' u_j'}\frac{\partial\overline{u_j}}{\partial x_i}$, $G_b = -\beta g\frac{\nu_t}{\sigma_t}\frac{\partial\overline{T}}{\partial z}$ and $\beta = -\frac{1}{\rho}\left(\frac{\partial p}{\partial T}\right)_P$

The model constants are given as follows:

$C_{1\varepsilon}$=1.44, $C_{2\varepsilon} = 1.92, C_{3\mu\varepsilon} = 0.09, \sigma_k = 1.0,$ and $\sigma_\varepsilon = 1.3$

6.2.2.2. The SST k-ω model (Menter, 1994)

The eddy viscosity is modeled as follows:

$$\nu_t = \frac{a_1 k}{max\,(a_{1,}\omega, SF_2)} \qquad ...(6.9)$$

Turbulent kinetic energy (k) transport equation:

$$\frac{\partial k}{\partial t} + \overline{u_j}\frac{\partial k}{\partial x_j} = P_k - \beta^* k\omega + \frac{\partial}{\partial x_j}\left[(\nu + \sigma_k\nu_t)\frac{\partial k}{\partial x_j}\right] \qquad ...(6.10)$$

where, $$P_k = min\left(\tau_{ij}\frac{\partial U_i}{\partial x_j}, 10\beta^* k\omega\right)$$

Turbulent dissipation rate (ε) transport equation:

$$\frac{\partial\omega}{\partial t} + \overline{u_j}\frac{\partial\omega}{\partial x_j} = \alpha S^2 - \beta\omega^2 + \frac{\partial}{\partial x_j}\left[(\nu + \sigma_\omega\nu_T)\frac{\partial\omega}{\partial x_j}\right] + 2(1 - F_1)\sigma_{\omega 2}\frac{1}{\omega}\frac{\partial k}{\partial x_i}\frac{\partial\omega}{\partial x_i} \qquad ...(6.11)$$

Each of the constants is a blend of an inner (1) and outer (2) constant, blended via:

$$\phi = \phi_1 F_1 + \phi_2 (1 - F_1) \qquad ...(6.12)$$

where ϕ_1 represents constant 1 and ϕ_2 represents constant 2. Additional functions blended via:

$$F_1 = \tanh\left\{\left\{min\left[max\left(\frac{\sqrt{k}}{\beta^* y\omega}, \frac{500\nu}{y^2\omega}\right), \frac{4\sigma_{\omega 2} k}{CD_{k\omega} y^2}\right]\right\}^4\right\}$$

$$F_2 = \tanh\left[\left[max\left(\frac{2\sqrt{k}}{\beta^* y\omega}, \frac{500\nu}{y^2\omega}\right)\right]^2\right]$$

where $CD_{k\omega} = max\left(2\rho\sigma_{\omega 2}\frac{1}{\omega}\frac{\partial k}{\partial x_i}\frac{\partial \omega}{\partial x_i}, 10^{-10}\right)$, y is the distance from the field point to the nearest wall and S is an invariant measure of the strain rate. The model constants are given as follows:

$\alpha_1 = \frac{5}{9}, \alpha_2 = 0.44, \beta_1 = \frac{3}{40}, \beta_2 = 0.0828, \beta^* = \frac{9}{100}, \sigma_{k1} = 0.85, \sigma_{k2} = 1, \sigma_{\omega 1} = 0.5, \sigma_{\omega 2} = 0.856.$

6.2.3. Boundary Conditions Modelling

6.2.3.1. Inlet

At inlet, the Dirichlet boundary conditions are specified for all the mean velocity components and temperature while homogeneous Neumann boundary conditions are specified for the pressure. For turbulent kinetic energy k, constant value can be prescribed based on the background disturbances usually measured in terms of turbulent intensity (I), defined as:

$$I = \frac{\sqrt{\frac{2k}{3}}}{U_\infty} \qquad ...(6.13)$$

In current analysis inlet intensity of 5 % has been used. This gives the value of k at inlet.The inlet value of ε is calculated using the following equation as has been explained in Biswas and Eswaran (2002):

$$\varepsilon = \frac{k^{3/2} C_\mu^{3/4}}{0.07\ L_{char}} \qquad \text{...(6.14)}$$

where L_{char} is taken as the hydraulic diameter.

6.2.3.2. Outlet

At the outlet boundary, homogeneous Neumann boundary condition can be prescribed for all the scalars except the pressure.

$$\frac{\partial f}{\partial x} = 0; \qquad f = u, T, k, \varepsilon \qquad \text{...(6.15)}$$

For pressure a constant value equal to zero or ambient pressure is assigned at the outlet.

6.2.3.3. Wall

At solid no-slip wall (both stationary as well as moving) boundaries, the standard wall function treatment is applied for all the velocity components and turbulence quantities (k, ε). For the pressure homogeneous Neumann boundary condition ($\partial p/\partial x = 0$) is applied.

Near the wall turbulent fluctuations tend to zero and flow very close to the wall is laminar in the so-called laminar sub-layer. In this sub-layer the velocity gradient is very high compared to the region outside it. Thus to give proper boundary conditions at the wall for the RANS mean velocity equations, the grid-points near the wall have to be very close to be able to properly resolve this high gradient. But an alternative is to assume a fully developed turbulent boundary layer and then apply velocity and scalars boundary values using analytical expressions such as log-law. This approach is termed as wall function approach. The velocity scale near the wall which is also called friction velocity, u_τ, is defined as,

$$u_\tau = \sqrt{\frac{\tau_w}{\rho}} \qquad \text{...(6.16)}$$

where τ_w is the shear stress near the wall. It has been shown in Pope (2000) in the wall region,

$$u^+ = y^+; \qquad for\ y^+ \leq 10.9; \qquad viscous\ sub-layer$$

$$u^+ = \frac{1}{\kappa} ln(Ey^+); \qquad for\ \ 300 > y^+ \geq 10.9; \qquad log-layer$$

...(6.17)

where κ is the von-Karman constant (=0.42) and E = 9.0.

In the logarithmic region, the viscous stresses are low, and the turbulent shear stress is approximately equal to the wall shear stress. Hence

$$\mu_t \frac{\partial u}{\partial y} \approx \tau_{wall} = \rho u_\tau^2 \qquad \text{...(6.18)}$$

At the wall, u, v, w→0 and k→constant, so the modelled equation for k (Eq. 7) gives

$$0 = \mu_t \left(\frac{\partial u}{\partial y}\right)^2 - \rho\varepsilon \qquad \text{...(6.19)}$$

where log-law gives (Eq. 17)

$$\frac{\partial u}{\partial y} = \frac{u_\tau}{\kappa y} \qquad \text{...(6.20)}$$

Substituting this along with the definition of μ_t (Eq. 6) we get:

$$k = C_\mu^{-1/2} u_\tau^2 \text{ and } \varepsilon = \frac{u_\tau^3}{\kappa y} \qquad \text{...(6.21)}$$

As k becomes a constant value in the log layer, we can prescribe the homogenous Neumann boundary contition for k at the wall, (∂k/∂y = 0). However, for SST k-ω model near the wall k approaches zero.

The ε at wall is computed from Eq. (21) as:

$$\varepsilon = \frac{u_\tau^3}{\kappa y} = \frac{C_\mu^{3/4} k_P^{3/2}}{\kappa\, y_P} \qquad \text{...(6.22)}$$

The ω value in the wall cell is computed from the Menter's model as follows:

$$\omega = 10\, \frac{6\upsilon}{\beta\,(y_P)^2} \qquad \text{...(6.23)}$$

6.2.4. Solution Methodology

The computational work was carried out on the open source solver OpenFoam 2.2.0 using the buoyantBoussinesqSimpleFoam solver. It is a fully three-dimensional CFD tool, based on the finite volume method. The steady state, Reynolds averaged Navier-Stokes equations of motion and the equation of energy were solved for an incompressible Newtonian fluid. The upwind scheme was used for discretisation of convection terms (detailed discussion in section 6.3.2. The diffusion terms were discritised using central differencing scheme which is second order accurate. SIMPLE (Semi-Implicit Method for Pressure Linked Equations) algorithm was selected for pressure-velocity coupling with relaxation factors of 0.3 for pressure and 0.7 for momentum (detailed discussion in section 6.3.4). The SIMPLE algorithm is a guess-and-correct procedure for the calculation of pressure on the staggered grid arrangement. In a staggered grid, the scalar variables of the conservation equations are solved on the nodes of the grid, whereas the vector quantities are solved on the cell faces. All the solutions were considered fully converged when sum of scaled residuals was below 10^{-7} (detailed discussion in section 6.3.3). Before stopping the calculations, relative variations of key physical variables, such as flow velocities and temperature were imposed to be lower than 10^{-4} m/s and 10^{-3} K, respectively.

6.3. Parametric sensitivity analysis

The flow inside a double pipe heat exchanger is similar to that of a flow in an unbaffled heat exchanger. We have selected (a) the studies of Kim and Aicher (1997) and Aicher and Kim (1998) for experimental Nusselt number comparison; and (b) Uzzan et al. (2004) for the comparison of experimental temperature profiles in a unbaffled heat exchanger as an exercise to validate the code. Furthermore, the sensitivity of various numerical parameters is also studied. The above mentioned geometries are described in Table 6.1.

Table 6.1: Geometrical parameters for unbaffled heat exchangers from reported literature used for code validation: Uzzan et al. (2004)- U010210011, Aicher and Kim (1998)- A010340013 and Kim and Aicher (1997)- C070501612.

System	U010210011	A010340013	C070501612
Shell Diameter, Ds (m)	0.0209	0.034	0.05
Tube outer diameter, d (m)	0.0109	0.013	0.012
Tube bundle geometry and pitch (m)	-	-	Triangular, 0.016
Number of tubes, N_T	1	1	7
Heat Exchanger Length, L (m)	3.78	2	0.92
Hydraulic diameter, D_h (m)	0.0109	0.021	0.01113

6.3.1. Turbulence model

6.3.1.1. Pipe in pipe heat exchanger

The annular flow in a double pipe heat exchanger experiment of Uzzan et al. (2004) was simulated and the geometry is summarised in Table 6.1. The fluid flowing on the shell is water, and for CFD simulations, constant properties were taken at the inlet temperature. A constant temperature profile from experiment was imposed as boundary condition on the tube surface along with a no slip boundary condition. The outer wall of the heat exchanger was considered to be adiabatic and no slip. The inlet mass flow rate is 3.8 lpm at 336 K for case A and at 290 K for case B. The outlet is kept at constant atmospheric pressure and zero gradient velocity. The steady state incompressible flow equations were solved according to the solution methodology (Section 6.2.4). The comparison of CFD simulations using different turbulent models and experimental data is shown in Fig. 6.1 A and B.

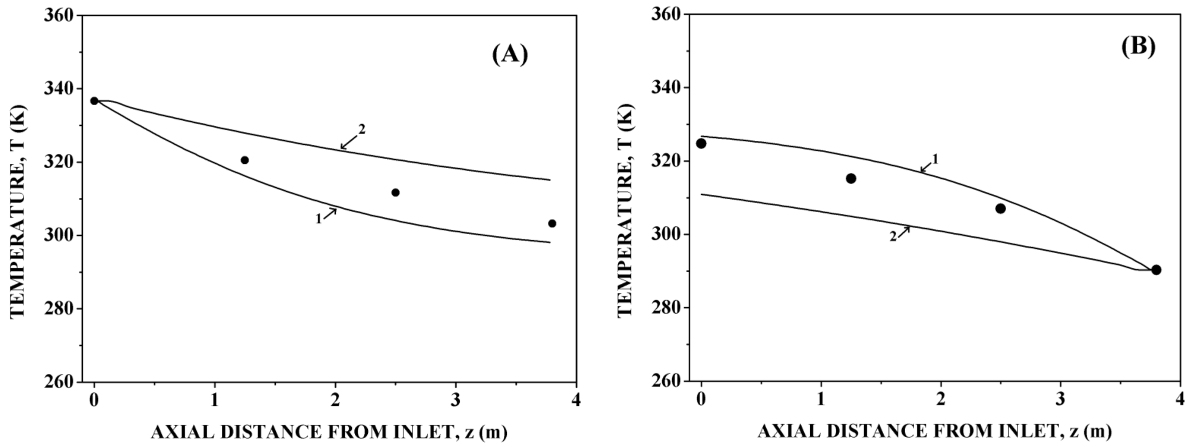

Figure 6.1: Comparison of temperature along axial length of the heat exchanger shell side Uzzan et al. (2004) for a shell side inlet mass flow of 3.8 lpm and inlet temperature of (A) 336K and (B) 290K from CFD simulation using different turbulence models: (1) the standard k-ε model, (2) the k-ω model, and (•) the experimental data.

It was observed that the standard k-ε and SST k-ω models are able to get good predictions results within ±2% and ±4% respectively. At high Re, standard k-ε model performs relatively better and also requires relatively coarse mesh. For this simulation, the grid has 0.5 million cells and the y^+ value is 44 on the first node from the heat transfer surface. Whereas, the mesh requirement for the SST k-ω model is 1.44 million and the y^+ value is 0.36 on the first node from the heat transfer surface. Despite this fine mesh, which becomes computationally expensive, the SST k-ω turbulence model is not able to capture the temperature profile as good as the standard k-ε model. Thus it is clear that for high Re cases, standard k-ε model works better. It is also observed that the standard k-ε model tends to overestimate the heat transfer slightly, whereas the SST k-ω model under predicts the heat transfer.

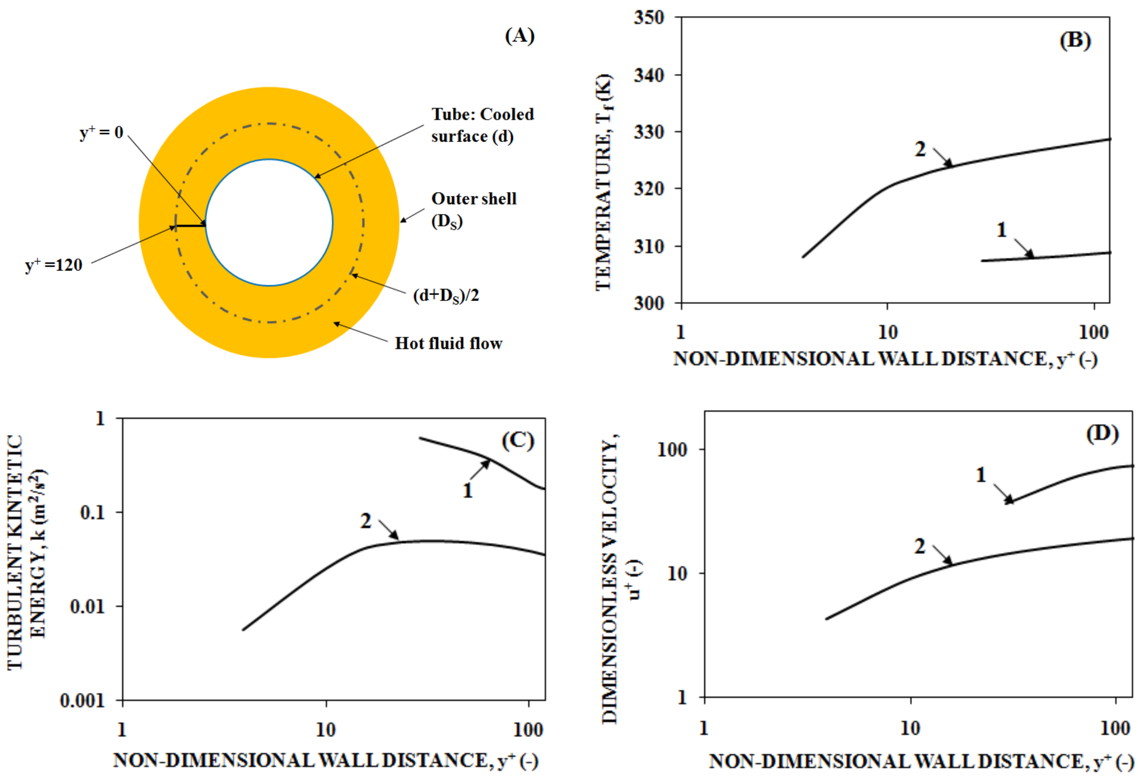

Figure 6.2: (A) Cross section of the annulus showing the location of y^+ plots from the inner tube wall to the center of the annular region for the Case A of Uzzan et al. (2004). Variation of (B) shell side fluid temperature, (C) turbulent kinetic energy and (D) dimensionless velocity with non-dimensional wall distance (y^+) using: (1) the standard k-ε model (2) the SST k-ω model.

Figs. 6.2 B - D shows the variation of shell side fluid temperature, turbulent kinetic energy and dimensionless velocity with non-dimensional wall distance (y^+) for the Case A of Uzzan et al. (2004) from the inner tube wall to the centre of the annular region (Fig. 6.2 A). It was observed for the case of standard k − ε model, that the temperature is lower and for the SST k − ω model it is much higher. This has been explained by the k vs y^+ plot (Fig. 6.2 C). It can be seen that the turbulence predicted by the standard k − ε model is higher than the SST k − ω model, and hence the higher turbulence will result in higher heat transfer coefficient. Fig. 6.2 D shows the u^+ vs y^+ plot. For y^+ <10, the SST k–ω model predicts $u^+ = y^+$. Thus it is able to capture the viscous sub layer in the range of y^+ <10. Thus the large velocity gradients near the wall are captured. However, it is unable to predict the transition to the turbulent layer (y^+ >30), since the turbulent kinetic energy predicted in the core flow region is lower (Fig. 6.2 C). This is maybe due to the incorrect blending functions for the high Reynolds number under consideration. The standard $k - \varepsilon$ model has the first grid in y^+ <10 and the wall behavior is modelled using the standard wall functions as described in Section 6.2.3.3.

6.3.1.2. Double pipe heat exchanger

The shell side (annular) flow of the double pipe heat exchanger from the experiment of Aicher and Kim (1998) was simulated (Table 6.1). The fluid flowing in the shell is water and was considered with constant properties at the inlet temperature. A constant temperature of 450 K was imposed on the tube surface along with no slip boundary condition. The outer wall of the heat exchanger was considered adiabatic and no slip. Water flows in with Reynolds number in the range of 1000 to 7000 and with an inlet temperature of 303 K. The number of grids for the standard k-ε model ranges between 1.8-1.9 million and boundary layer meshing was done around the tubes as shown in Fig. 6.4 B and distance was maintained from the wall such that calculated average y^+ is approximately 20 on the first node from the heat transfer surface; whereas for SST k-ω model for grid size of 4.2-4.8 million it is less than 1 on the first node from the heat transfer surface. The comparison of CFD simulations with experimental data using the two turbulent models is shown in Fig. 6.3 A. The Nusselt number predicted by the standard k-ε model and SST k-ω model are in close agreement within ± 18 % and ± 20 %, respectively. It was also observed that for Re<2000, the SST $k-\omega$ model predicts the Nusselt number slightly better than the standard $k-\varepsilon$ model. This is because the former is able to resolve the viscous sublayer flow near the wall which is the heat transfer region. Hence, a more accurate result is obtained. However, for Re>4000, i.e. in the turbulent regime, the standard k − ε model predictions are better as this model is developed for high Reynolds number flows.

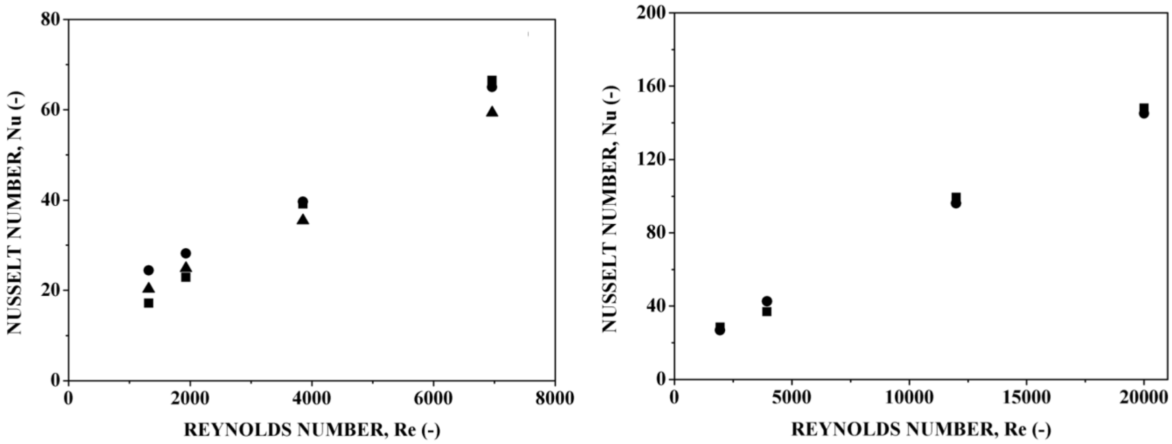

(A) (B)

Figure 6.3: Comparison of Nusselt number versus Reynolds number for the experiment of (A) A010340013 from Aicher and Kim (1998) and (B) C070501612 from Kim and Aicher (1997): (•) experimental data, CFD simulation using (■) the standard k-ε model, and (▲) the SST k-ω model

6.3.1.3. Unbaffled heat exchanger

Next, the shell side of an unbaffled shell and tube heat exchanger with 7 tubes (Kim and Aicher (1997)) was simulated (Table 6.1). Grid size of approximately 2.1 million cells was used for the said geometry. The initial and boundary conditions are same as for the double pipe heat exchanger as described in Section 6.3.1. The fluid flowing in the shell is water with constant properties taken at inlet temperature. A constant temperature of 450 K was applied on the tube surface along with no slip boundary condition. The outer wall of the heat exchanger was considered adiabatic together no slip boundary conditions. Inlet temperature of 303 K is specified for all Reynolds number ranging from 2000 to 20,000. It was pointed out in Section 6.3.1.1 and 6.3.1.2 that the standard k − ε model gives relatively accurate predictions. Therefore, for the current simulations only standard k − ε was used. First grid point distance from the tube wall was maintained to give y^+ nearly 20. In Fig. 6.3 B, it is observed that the CFD predictions are in good agreement with the experimental data.

6.3.2. Discretisation Scheme

A sensitivity study was carried out by considering three discretisation schemes for convection term: (a) first order upwind scheme, (b) second order upwind scheme and (c) QUICK scheme (a third order scheme). The results are summarised in Table 6.2.

Table 6.2: Variation of outlet temperature with various numerical settings for Uzzan et al. (2004) Case A, A010340013 from Aicher and Kim (1998) and C070501612 from Kim and Aicher (1997).

Numerical setting	Outlet Temperature, T_{out} (K)		
	Uzzan et al. Case A (2004)	A010340013 from Aicher & Kim (1998)	C070501612 from Kim & Aicher (1997)
Convection Scheme			
Upwind	297.50	324.39	346.17
Second order upwind	297.76	324.47	346.55
Convergence criteria (Residuals limit)			
0.1	333.75	-	-
0.3	302.59	-	-
0.7	298.27	-	-
1.2	298.22	-	-
Relaxation parameter for pressure			
0.1	297.23	324.39	346.17
0.3	297.50	324.39	346.17
0.7	297.62	324.57	Diverged
1.2	297.28	diverged	Diverged
Prandtl turbulent number, P_{rt} (-)			
0.3	296.60	-	346.08
0.7	297.50	-	346.17
0.9	297.95	-	346.16

For the case of Uzzan et al. (2004) Case A, it was observed that the first and the second order upwind schemes give practically the same value of outlet temperature (3). However, for QUICK scheme the solution was found to diverge. A similar observation was made for the case of A010340013 (Re=4000) from Aicher and Kim (1998); and C070501612 from Kim and Aicher (1997) (Re=4000). Further, for the present complex geometry of a heat exchanger with multiple tubes or baffles, the residuals were found to diverge for both the higher order schemes. Therefore, for all the simulations in the present work, the first order upwind scheme has been employed.

6.3.3. Convergence criteria

A convergence criteria study was carried out, in which the sum of scaled residuals was fixed between 10^{-3} and 10^{-9} for the case of Uzzan et al. (2004) Case A. The value of exit temperature (T_{out}) was then compared with the experimental value as shown in Table 6.2. It was observed that the T_{out} value remains constant (variation is less than 0.01 %) when the residual converges to a value below 10^{-7}. Thus for the present work 10^{-7} was taken as convergence criteria.

6.3.4. Relaxation parameter

A sensitivity study was carried out by varying the relaxation parameter with the values of 0.1, 0.3, 0.7 and 1.2. This study was performed for the geometry of Uzzan et al. (2004) Case A, A010340013 (Re= 4000) from Aicher and Kim (1998) and C070501612 (Re= 4000) from Kim and Aicher (1997). Firstly, in all the cases of relaxation parameter, the value of Tout was found to remain almost constant (within 0.5 K) and these Tout values are listed in the Table 6.2. It was observed that for the simpler geometry of pipe in pipe heat exchanger of Uzzan et al. (2004) the solution converged for all the values of relaxation factor. However, for A010340013 the solution diverged for over-relaxation parameter value of 1.2 and for C070501612 the solution diverged for the relaxation parameter value of 0.7 as well as 1.2. It is thus recommended not to use an over-relaxation parameter. In the present work, a value of 0.3 has been used for all the simulations.

6.3.5. Turbulent Prandtl number

The turbulent Prandtl number was varied in the range of 0.1, 0.7 and 1, for the cases of Uzzan et al. (2004) Case A and C070501612 (Re= 4000) from Kim and Aicher (1997). In all the cases, it was observed that (see table 6.2) the solution converges to an almost constant value of T_{out} (within 1 K). The Prandtl number is taken as 0.7 in further simulations.

6.4. Heat Exchanger

The geometry of the Calandria is similar to the geometry of the shell side of a shell and tube heat exchanger. Thus a set of simulations were carried out to assess the capability of the CFD code to simulate such complex flows.

6.4.1. Geometry and meshing

The dimensions of the considered heat exchanger geometries simulated in the present work are enlisted in Table 6.3. The geometry consists of the shell side of the heat exchanger with inlet and outlet. The inlet and outlet nozzle diameter was 79.8 mm. The schematic of the geometry is shown in Fig. 6.4 A.

Table 6.3: Geometrical parameters for heat exchanger.

System	hx150	hx300	hx600
Diameter of shell, D_s (m)	0.15	0.3	0.6
Diameter of tube, d (m)	0.02	0.02	0.09
Length, L (m)	0.6	0.6	0.6
Total no. of tubes, N_T	19	61	19
Hydraulic diameter, D_h (m)	0.025	0.043	0.089

Initially, for the geometry of hx150, a coarse mesh was generated containing 350,000 cells. Near the tube and shell wall, the meshing consists of a boundary layer made up of structured cells. In between these wall regions, the mesh consists of unstructured tetrahedral cells. The meshing near a tube wall has been shown in Fig. 6.4 B. Successively; the mesh was refined to a medium size containing 750,000 cells. And finally a fine mesh was created with 1,100,000 cells. The mesh independence results are listed in Table 6.4. It was observed that the variation in outlet temperature for the medium and fine mesh is very small. Thus in order to save computational time and power, the medium mesh size (750,000 cells) was selected for further studies. Similar mesh independence studies were performed for the other two systems, namely hx300 and hx600. For hx300 and hx600 2,500,000 and 3,500,000 cells were employed.

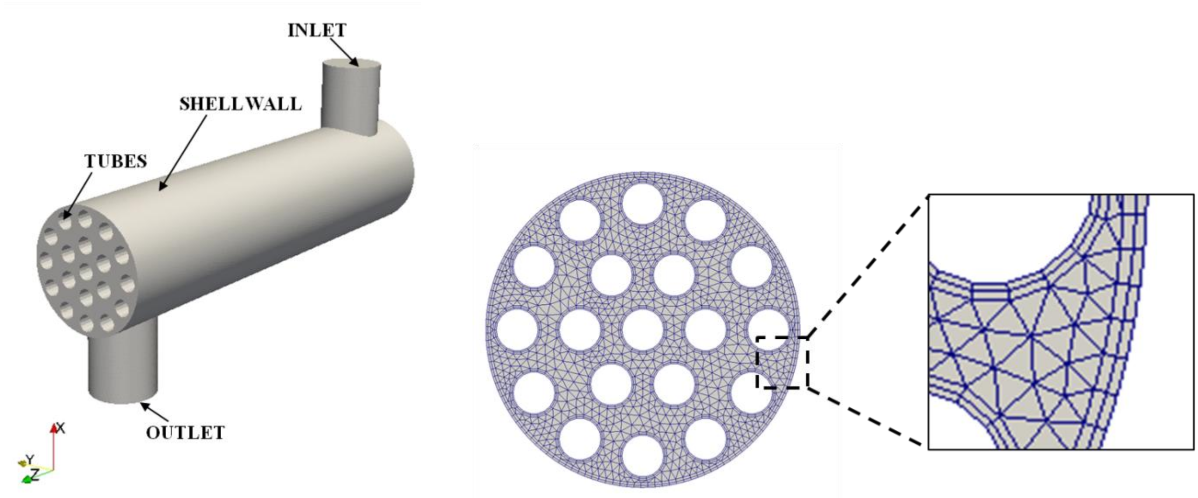

(A) **(B)**

Figure 6.4: (A) Geometry of heat exchanger (B) Cross section of hx150 showing the CFD mesh.

Table 6.4: Variation of outlet temperature with flow rate and grid points for heat exchanger.

HX	Flow (kg/s)=	0.5		5	
	Mesh Size	T_{out} (K)	Difference %	T_{out} (K)	Difference %
hx150	350,000	330.21	1.4	308.34	2.0
	750,000	335.54	0.2	312.00	0.8
	1,100,000	334.99	0.0	314.65	0.0
hx300	1,400,000	354.66	2.2	312.62	2.9
	2,500,000	360.58	0.6	320.92	0.4
	4,200,000	362.62	0.0	322.08	0.0
hx600	1,500,000	349.19	1.9	315.87	3.3
	3,500,000	354.69	0.4	325.62	0.3
	6,700,000	355.97	0.0	326.73	0.0

6.4.2. Numerical modelling

6.4.2.1. Governing equations

The governing equations are described in section 6.2.1. The standard k-ε model was selected to perform further simulations, according to the discussion in section 6.3.1. The physical properties of the fluid for simulation are listed in Table 6.5.

Table 6.5: Physical properties of fluid used for CFD simulations.

Fluid density (ρ) (kg/m^3)	995
Kinematic viscosity (ν) (m^2/s)	0.9×10^{-6}
Thermal diffusivity (α) (m^2/s)	1.58×10^{-7}

6.4.2.2. Solution Methodology

The solution methodology is described in section 6.2.4.

6.4.2.3. Boundary conditions

The boundary conditions for the CFD simulation of the heat exchanger are listed in Table 6.6.

Table 6.6: Boundary conditions for CFD simulation of heat exchanger.

Input Parameter	Boundary Condition	Value
Inlet	Velocity-inlet	0.1 m/s, 0.5 m/s,1 m/s
Outlet	Pressure- outlet	Atmospheric pressure
Tube wall	No slip, Constant wall temperature	450 K
Shell Wall	No slip, No heat flux	-
Turbulence	Turbulence Intensity	5 %
Temperature of fluid	Inlet temperature	300 K

6.4.3. Results and Discussion

The temperature contours of hx150 for a mass flow of 0.5 kg/s is shown in Fig. 6.5. The plane shown is the central plane along the length of the heat exchanger and cross-sectional planes at inlet (z/L= 0.1) and outlet (z/L= 0.9). For the same locations, the velocity vector plots are shown in Fig. 6.6. In Fig. 6.6 A, there is a region of recirculation formed in the outlet nozzle due to the flow separation. This results in a dead zone. In the inlet plane (Fig. 6.6 B), we can observe the impingement of fluid on the tubes. This causes a major pressure drop across the heat exchanger at this point. The fluid is unable to penetrate uniformly through the tubes and thus we observe a relatively higher fluid temperature at the far end of the shell (Fig. 6.5 C).

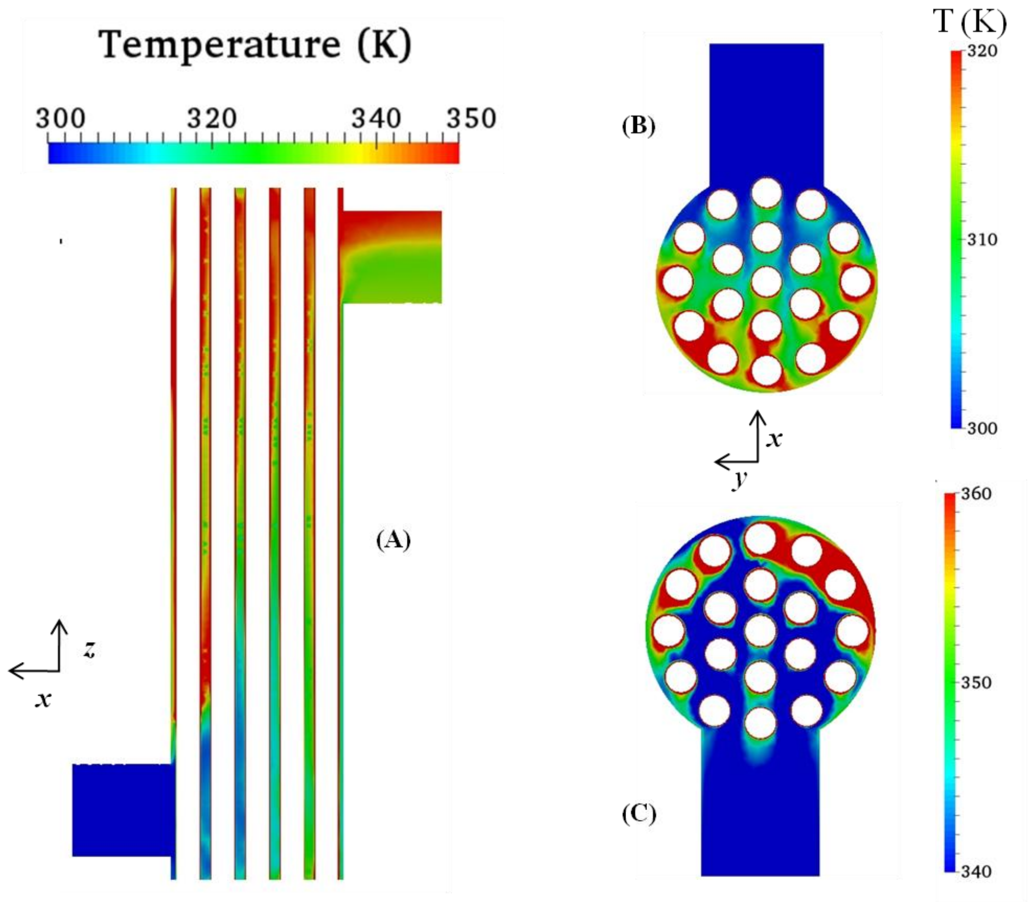

Figure 6.5: Temperature contours of hx150 at three different planes at steady state for mass flow of 0.5 kg/s. (A) Central axial plane; (B) inlet plane; (C) outlet plane.

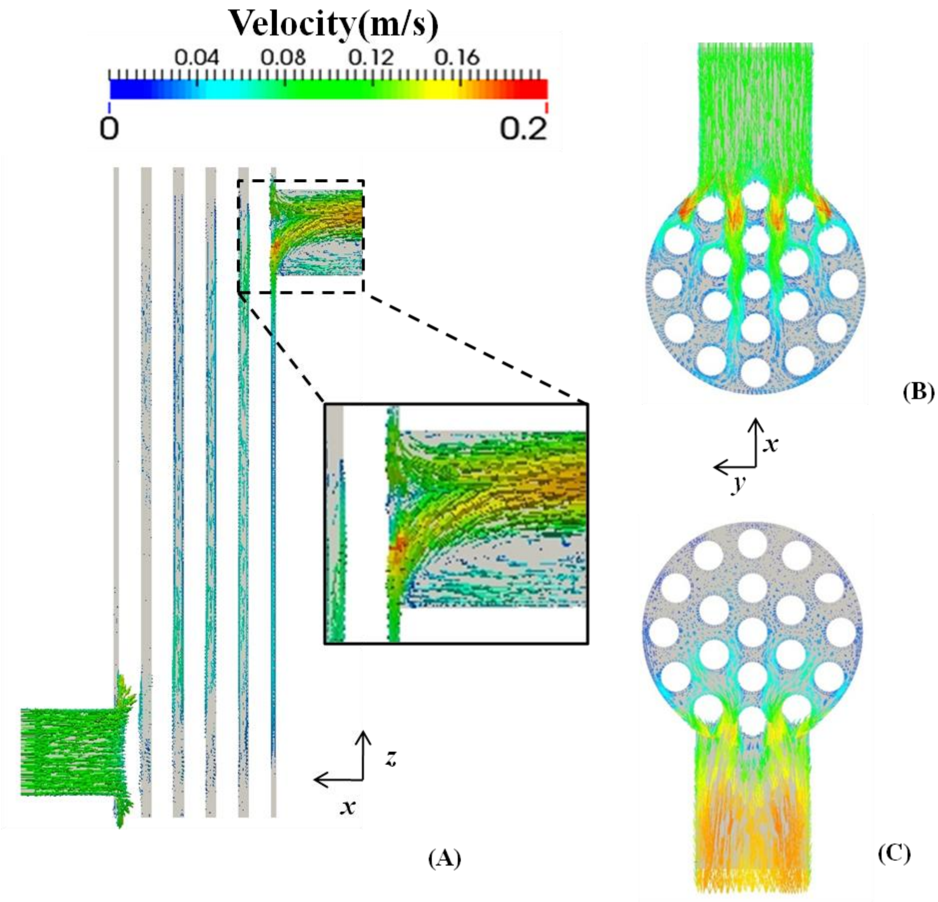

Figure 6.6: Flow distribution of hx150 at three different planes at steady state for mass flow of 0.5 kg/s. (A) Central axial plane; (B) inlet plane; (C) outlet plane.

Fig 6.7 A shows the variation of axial velocity with from the wall to the opposite side along the diameter (x-direction) at various axial locations on the xz plane (z/L = 0.1, 0.3, 0.9) for mass flow rate = 0.5 kg/s. The axial velocity peaks in between the tubes, and is zero at the surface of tubes. At z/L = 0.1, which is the inlet plane, the axial velocity is low since the flow enters radially through the inlet. At z/L = 0.3, the flow is converted in axial direction, thus all the peaks of axial flow are maximum. Thereafter, successively we observe that the maximum peak begins to shift towards the left, i.e. towards the outlet. Finally, at the outlet plane, at z/L = 0.9, the flow is maximum outside the tube banks, which is observed as a peak at y/DS = 0. The axial flow velocity inside the heat exchanger is maximum near z/L = 0.3, which is equals to 0.067 m/s.

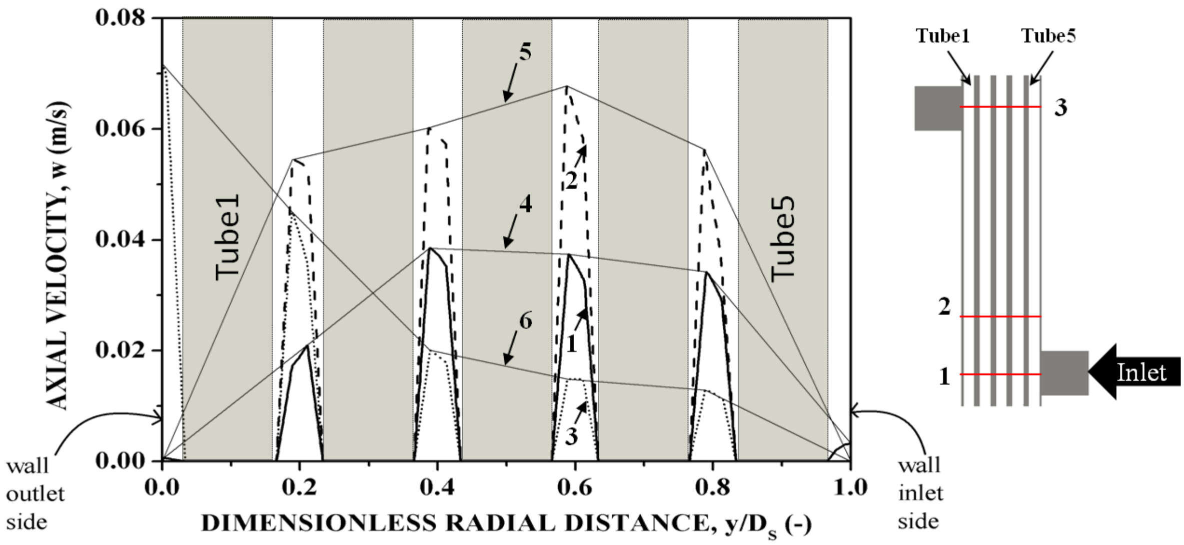

(A)

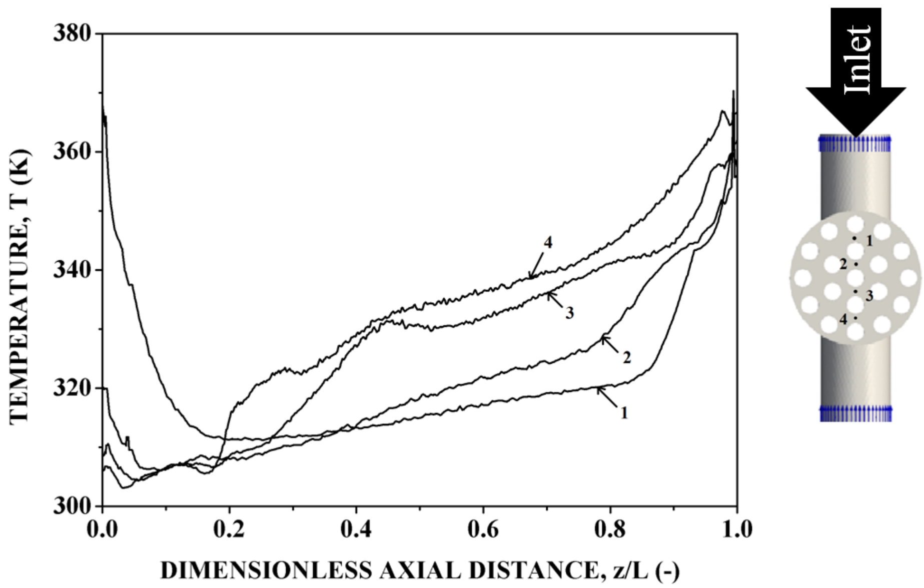

(B)

Figure 6.7: (A) Variation in axial velocity with dimensionless radial distance and mass flow rate of 0.5 kg/s at axial locations (1) z/L= 0.1; (2) z/L= 0.3; (3) z/L= 0.9. Lines passing through the axial velocity peaks in the axial locations: (4) z/L= 0.1; (5) z/L= 0.3; (6) z/L= 0.9. (B) Variation in temperature with dimensionless axial distance and mass flow rate= (A) 0.5 kg/s (B) 5 kg/s at radial locations (1) y/D_S = 0.2; (2) y/D_S = 0.4; (3) y/D_S = 0.6 (4) y/D_S = 0.8.

Fig 6.7 B shows the temperature plot along the axis of the heat exchanger for mass flow rate= 0.5 kg/s at various radial locations(for instance, namely y/D_S = 0.2, 0.4, 0.6, 0.8 are named as points 1, 2, 3 and 4; respectively). The location of 0.2 is closest to the outlet and 0.8 is closest to the inlet. For the axial region $z/L < 0.1$ at point 1, the temperature is much higher than the other radial locations. This is because the flow is low and is diverted upwards by the tube bank before reaching this region. Thus, there is a reduced heat transfer and the fluid temperature rises. As we go along the length of the heat exchanger, near $z/L = 0.1$ the temperature drops, due to mixing of incoming cold fluid. The fluid temperature rises slowly with a smaller gradient in the region $0.2 < z/L < 0.8$. This is because in this region the velocity is high enough to efficiently carry away heat from the tubes. In the region beyond $z/L = 0.8$ (above the outlet), an increase in temperature is observed again due to reduction of velocity.

6.5. Natural circulation in a tank

In this section, the simple natural circulation phenomena that of heating inside a tank is undertaken by simulating the geometry of Ganguli et al. (2010).

6.5.1. Geometry and meshing

The geometry of Ganguli et al. (2010) consists of a cylindrical tank of diameter 0.3 m and height 0.3 m. At the centre of the tank a single hot tube of diameter 0.02 m is present. Steam at a constant temperature of 413 K is passed through this tube. The tank was filled with water. A 5 degree wedge of the geometry was simulated with assumption of symmetry. The geometry was meshed in a non-uniform manner (Fig. 6.8), with fine mesh near the hot tube and the top surface in order to capture the gradients in a better manner. After a grid independence study the mesh size of 120,000 cells was selected.

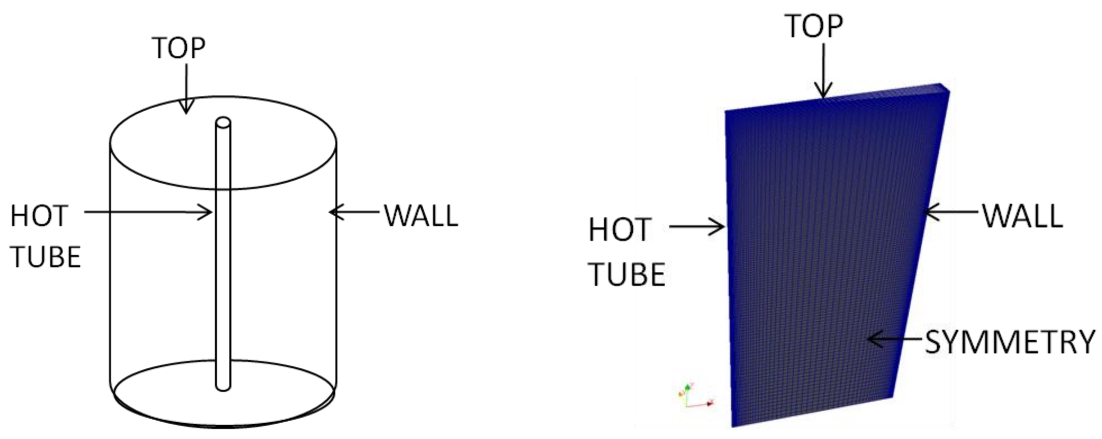

(A) (B)

Figure 6.8: (A) Schematic and (B) the meshed geometry for 1 tube in cylindrical tank.

6.5.2. Numerical modelling

6.5.2.1. Governing equations

In order to solve unsteady single phase fluid flow inside the natural circulation loop, the governing equations (continuity, momentum, and energy) with appropriate turbulence model and boundary conditions must be solved. The governing equations are listed in section 6.2.1. The SST k- ω and the standard k-ε turbulence model were compared with the experimental results to observe their performance (detailed equations in section 6.2.2). CFD simulations are carried out in opensource CFD code OpenFoam 2.2.0.

6.5.2.2. Solution methodology

For the three dimensional model the following assumptions are made:

1. The fluid is Newtonian and incompressible.
2. Boussinesq approximation is valid, i.e. density differences are only important in producing buoyancy.
3. Fluid properties are constant except in the formulation of buoyancy term.

The implicit scheme is used for time discretization in transient solution and QUICK scheme for discretization of convection terms. These discretized equations were solved using SIMPLE algorithm for steady state and PISO algorithm for transient solution. All the solutions were considered fully converged when the residuals was below 10^{-4}. The case was run for single phase transient simulation for 200 s. After a time step independence study, the time step of 10^{-3} s was selected.

6.5.2.3. Boundary conditions

Table 6.7: Boundary conditions for CFD simulation of natural convection in a tank.

Boundary Conditions	Temperature	Velocity
Hot tube	Constant temp. = 413 K	No slip, u=0
Wall	Adiabatic wall	No slip, u =0
Top	zero gradient	zero gradient
Initial Conditions		
Fluid	T = 300 K	u =0

6.5.2.4. Grid independence

The geometry was meshed in a non-uniform manner (Fig. 6.8 B), with fine mesh near the hot tube and the top surface in order to capture the gradients in a better manner. After a grid independence study the mesh size of 120,000 cells was selected.

6.5.3. Results and Discussion

In order to understand the natural convection the temperature contours were plot with time (Fig. 6.9). It is observed that initially that close to the hot tube there is a steep temperature gradient whereas in the bulk the temperature is more or less constant. This is because the fluid close to the hot tube gets heated and rises up due to buoyancy. This can also be seen in the velocity contours (Fig. 6.10), where there is region of high velocity near the hot tube and negligible velocity in the bulk. The fluid rising near the hot tube, takes a turn near the top surface and is converted into radial outward velocity until it reaches the wall. Thus the top surface also is seen as a high velocity region in the velocity contour (Fig. 6.10 B).

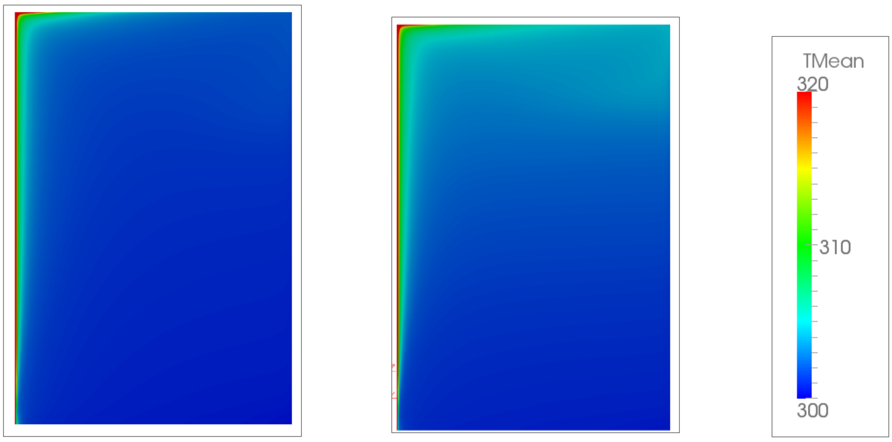

(A) **(B)**

Figure 6.9: Temperature contours on x-z plane in a cylindrical tank at time (A) 100 s (B) 200 s.

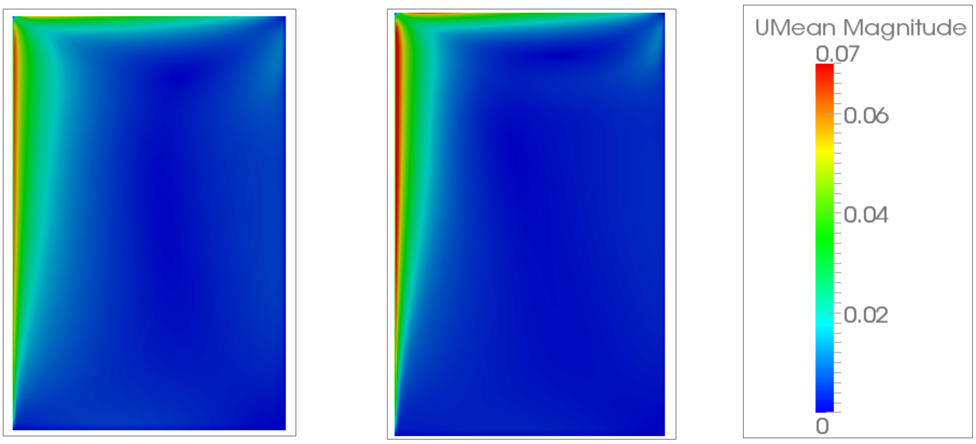

(A) **(B)**

Figure 6.10: Velocity contours on x-z plane at time (A) 100 s (B) 200 s.

The hot fluid reaches the wall and turns downward, setting up a natural circulation inside the tank. This is seen in the radial profile of axial velocity (Fig 6.11 A) as a very high upward velocity near the hot tube, then it reaches zero near the bulk and close to the tank wall it goes negative. The hot liquid rising near the tube get piled up at the top due to buoyancy and we see a steep gradient in the temperature, which is seen as a sharp rise in temperature close to the top surface for x = 3 mm plot in Fig. 6.11 B.

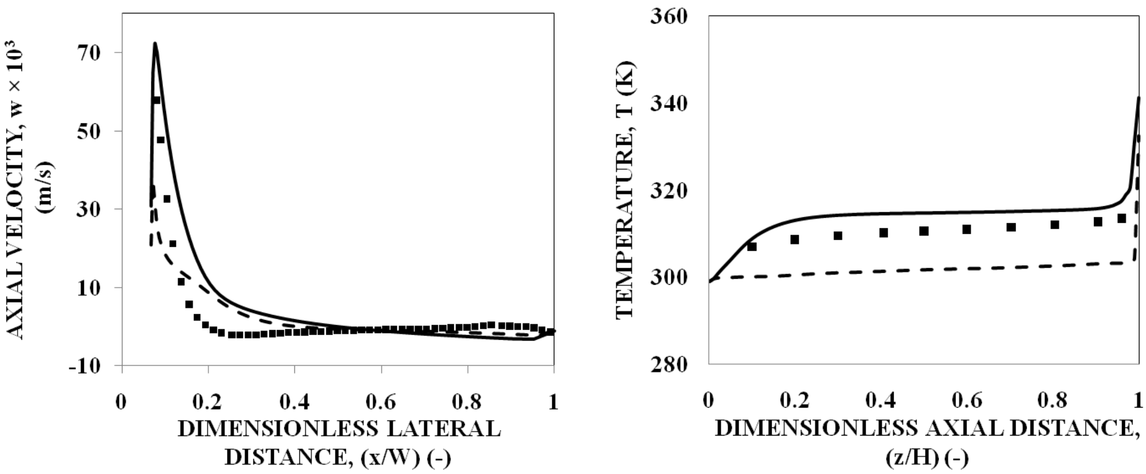

(A) **(B)**

Figure 6.11: Code validation for natural convection from reported literature (Ganguli et al, 2010) (A) Axial velocity plot along the radial distance at mid level of the tank at 200 s, and (B) Temperature plot along axial height at a distance 3 mm from the central heated tube, (—): SST k-ω model, (- - -): standard k-ε model and (◆): experimental data (PIV and HFA).

The simulations were carried out using two different turbulence models: namely the standard k-ε model and the SST k-ω model. The axial velocity and the temperature plot are shown in Fig. 6.11. It was observed that the results of the SST k-ω model are closer to the experimental data as compared to the standard k-ε model. This is because the standard k-ε model performs better in high Reynolds number flows, whereas the velocities in a natural convection system are very low.

6.6 Closure

It can be concluded that the CFD code OpenFOAM-2.2.0 is capable of capturing flow and temperature details for natural convection flows in a simple geometry and forced flows in complex geometries such as shell and tube heat exchangers. In the next chapter, we shall assess the capability of the code to simulate complex geometries under natural circulation flows. Furthermore, through these simulations, the various numerical settings such as the discretisation schemes, relaxation parameter, and turbulence model were selected.

CHAPTER 7:

3D CFD SIMULATIONS OF THERMAL HYDRAULIC CHARACTERISTICS IN THE PASSIVE MODERATOR COOLING TEST FACILITY

7.1. Introduction

In this chapter, the various experimental conditions in the scaled experimental facility are simulated using the validated CFD model. The objective of this exercise is to assess the capability of the code to simulate multi dimensional flow in a natural circulation system. This will lead to an understanding of the physics of a coupled natural circulation system by studying the detailed temperature and flow pattern inside the system. Finally this benchmarked code shall be used to simulate the PMCS of the AHWR.

Table 7.1: Geometrical details of the reactor scale PMCS and the scaled model.

Component	Dimensions	PMCTF
Calandria	Diameter of shell, D_{Tank} (m)	0.6
	Outer diameter of fuel channel, OD_{Tube} (m)	0.09
	Length, L_{Tank} (m)	0.6
	Total no. of tubes, Nt	19
Heat Exchanger	Diameter of shell, D_{HX} (m)	0.0525
	Outer diameter of tube, $OD_{Tube,HX}$ (mm)	6
	Length, L_{HX} (m)	0.6
	Total no. of tubes, Nt_{HX}	40
	Thickness of tube, d (mm)	0.7
Piping	Diameter of pipe (m)	0.0525

7.2. Geometrical Details

For the current work, only one of the two natural circulation loops in the PMCS was simulated, namely the primary loop. This includes the Calandria connected to the tube side of the heat exchanger. The setup of the PMCTF is already discussed in Fig. 4.1 in Chapter 4. The dimensions are described in Table 7.1. The simulated CFD geometry is shown in Fig. 7.1

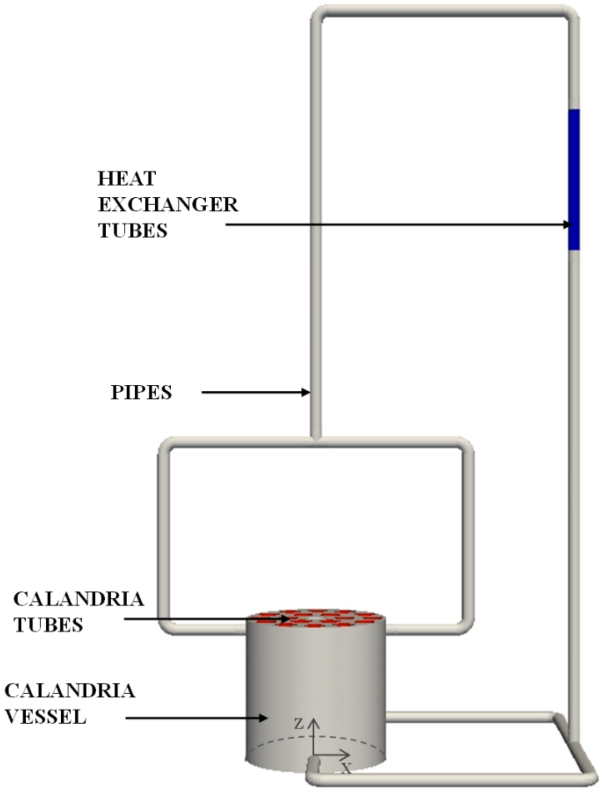

Figure 7.1: Geometry of PMCS loop for CFD simulations.

7.3. Numerical modelling

7.3.1. Governing equations

In order to solve single-phase (liquid) fluid flow behaviour inside the PMCS loop, the governing transport equations (continuity, momentum, and energy) with appropriate turbulence model and boundary conditions need were solved. CFD simulations were performed using opensource CFD code (OpenFoam 2.2.0). The governing equations are described in detail in Chapter 6, Section 6.2.1.

7.3.2. Solution methodology

The following assumptions are made for the three dimensional CFD simulations:

4. The fluid is Newtonian and incompressible.
5. The Boussinesq approximation is valid.

6. Fluid properties are constant except in the formulation of buoyancy term.
7. Heat loss to ambient through walls is neglected (i.e., adiabatic walls).
8. The surface of tubes in the heat exchanger is kept at a constant temperature.
9. For the standard k-ε and SST k-ω turbulence models, the turbulence is assumed to be homogenous and isotropic.
10. In these turbulence models, eddy diffusivity for k, ε and ω have been empirically correlated to eddy diffusivity for momentum.

The turbulence model selected for this study is the SST k-ω model. As discussed in section 6.5, this turbulence model is able to predict the natural convection phenomena fairly well. The details of the equations related to this model is given in section 6.2.2 of Chapter 6. Modelling of the convection term in the governing equations was done using the second order upwind scheme. A Semi-Implicit Method for Pressure Linked Equation method (SIMPLE) was used for steady state simulations, which is a pressure-velocity coupling numerical algorithm. Whereas, the Pressure-Implicit with Splitting of Operators scheme (PISO) was adopted to solve the velocity-pressure coupled equations in the time-dependent simulations. The first order implicit scheme was used to treat time dependent terms in the simulations. An under-relaxation factor of 0.3 was used for pressure and 0.7 for the momentum equations. All the solutions were considered as fully converged when the average of scaled residuals was below 10^{-4}. All the computations were carried out in a parallel manner on a cluster using 32 cores.

7.3.3. Boundary conditions

Steady state CFD simulations were carried out for the “four hour 500 W power step up” experiment (Section 4.6.2). In these simulations, the experimental temperature data and power at the end of every four hour was given as input conditions to steady state simulations. The Calandria tube surfaces were given a constant surface heat flux as boundary condition, which was calculated from the total heater power. The heater power ranged from 500 W to 2000 W, as in the experiment. The heat exchanger tube was given a constant temperature boundary condition, where the temperature was calculated by averaging the temperatures at the inlets and outlets of both shell and tube side of the heat exchanger in the experiment for the four hour 500 W power step up experiment. The Calandria shell and pipe wall surfaces were considered adiabatic walls. Finally, a no-slip and smooth boundary condition was applied to all the walls. The boundary conditions are listed in Table 7.2. For the time dependent study, heater power of 500 W was considered. Also, the temperature on the heat exchanger tube surface and the initial fluid temperature were taken as 303 K. This is because the working fluid is at 303 K at the beginning of the experiment. The flow was considered to be stagnant initially.

Table 7.2: Boundary and initial conditions for pseudo steady CFD simulation of PMCTF for the four hour 500 W power step up experiment.

Input Parameter	**Boundary Condition**	**Value**			
Calandria heater tube wall	No slip, Constant surface heat flux	500 W	1000 W	1500 W	2000 W
Heat exchanger tube wall	No slip, Constant temperature	305.1 K	308.7 K	310.9 K	313.6 K
Initial temperature of fluid	constant temperature	305.1 K	308.7 K	310.9 K	313.6 K

7.3.4. Grid independence

Fig. 7.2 A shows the computed mesh on a cross-section through the Calandria and B shows the boundary layer mesh near the hot tubes. Fig. 7.2 C and D show the mesh near the top of the heat exchanger and the junction of outlets of Calandria. The mesh near the wall regions have two boundary layers made up of hexahedral cells. Most of the pipes were swept with hexahedral cells, whereas the complex region as the junctions were meshed with tetrahedral cells. The boundary layer growth is 1.5 times, i.e. the second layer thickness is 1.5 times that of the first layer. The boundary layer was constructed such that the y+ value of the first node from the wall is maintained <1. A mesh independence study was carried out with three different mesh sizes: (1) 0.46 million, (2) 1.13 million and (3) 3.43 million cells. The mesh size increment was kept at the rate of ~ 2.5 times.

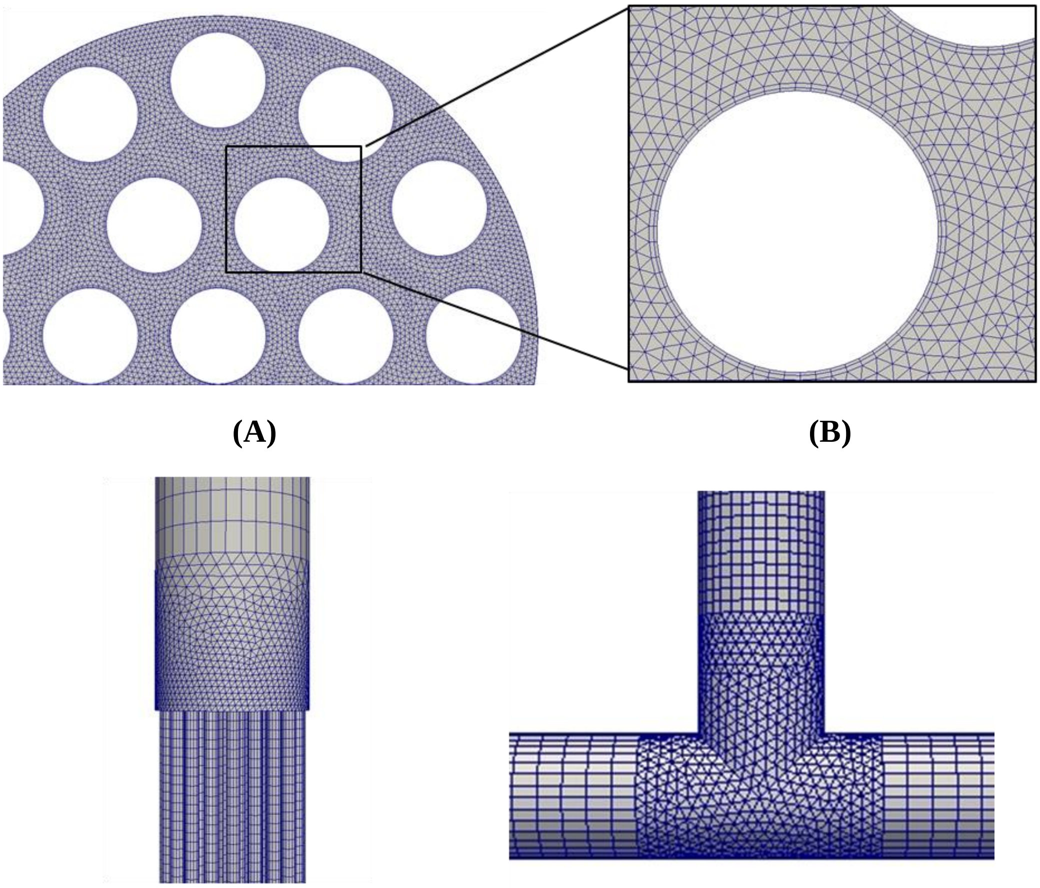

(A) **(B)**

(C) **(D)**

Figure 7.2: Mesh of PMCS loop in CFD- (A) Calandria (B) zoomed section of meshing around a Calandria tube (C) heat exchanger top section and tubes (D) junction of outlets from Calandria.

A steady state simulation was performed for a constant heater power of 500 W (more details of boundary conditions in Section 7.3.3). The results are shown in Fig. 7.3 A where the temperature difference between the outlet and inlet of the Calandria plot for different mesh sizes. Fig. 7.3 B shows the axial variation of temperature along the z-axis at a location of 3 mm from the central tube of Calandria. This variation between point (2) and (3) in temperature difference across Calandria was approximately 8 %, whereas the absolute value of the temperature at the Calandria outlet varied within 0.05 %. The calculations are performed for the mesh with 1.13 million elements.

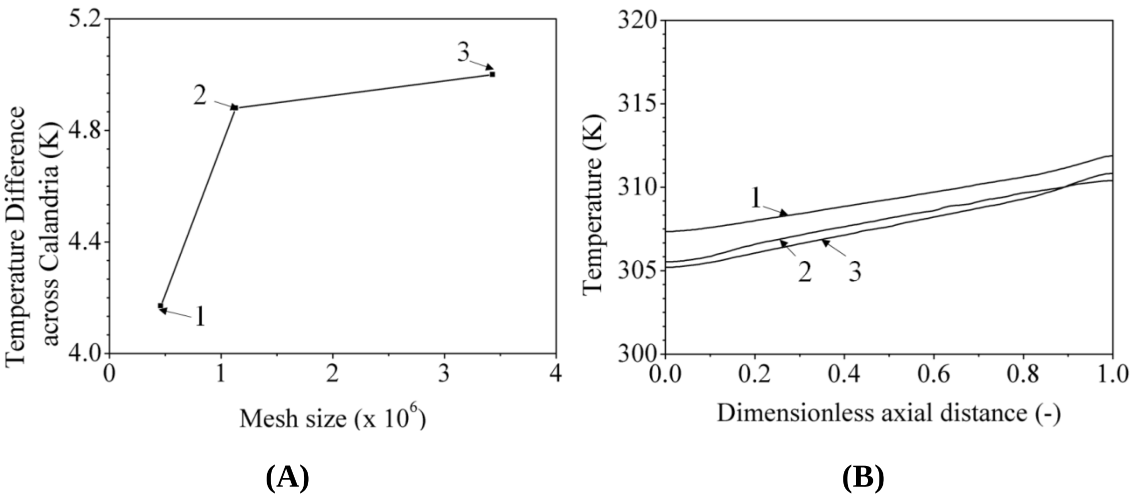

Figure 7.3: (A) Temperature difference between the outlet and inlet of the Calandria for grid sizes: (1) 0.46 million cells, (2) 1.13 million cells and (3) 3.43 million cells and (B) variation of temperature along the axial height of the Calandria at a location 3mm away from the surface of the central tube.

7.3.4. Time step independence

A time step independence study was performed for the constant heater power of 500 W. The different time steps considered for the time dependent studies were 10^{-2} s, 10^{-3} s, 10^{-4} s and 10^{-5} s. The simulations were executed till 30 s and the temperatures inside the Calandria were compared. For a time step of 10^{-4} s and 10^{-5} s, the change in temperature difference was less than ± 0.04 % and hence 10^{-4} s was used for time dependent simulations.

7.4. Results and Discussion

First the results of the steady and time dependent simulations are discussed in order to understand the details of the thermal hydraulic behaviour. Next the results from the CFD simulations are compared with the experimental data from the PMCTF.

7.4.1. Pseudo Steady state simulations

For the total heater power of 500 W, the steady state temperature and the velocity vectors on a plane passing through the center of the Calandria and heat exchanger tubes are shown in Fig. 7.4.

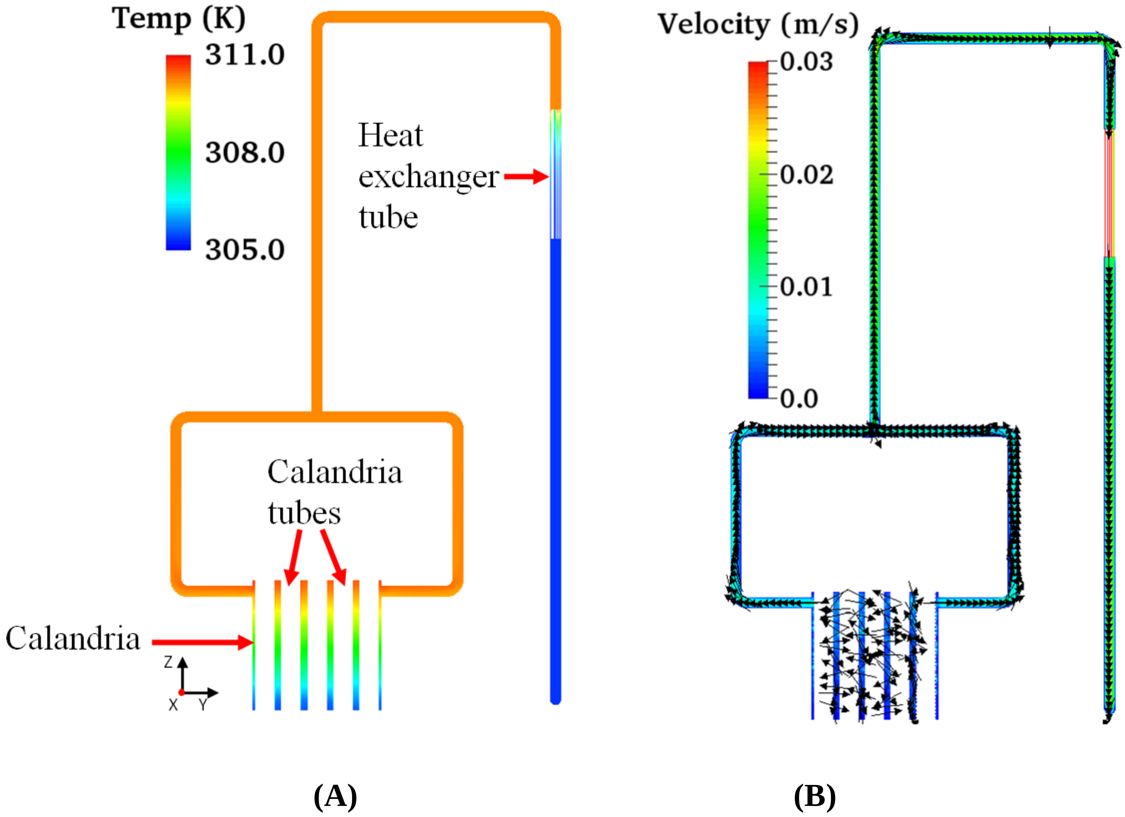

Figure 7.4: Steady state (A) contours of temperature and (B) velocity vectors on a vertical plane passing through the center of Calandria, the outlets of Calandria and the heat exchanger tube section for heat power 500 W.

It can be observed that, at steady state, the temperature inside the Calandria is stratified. Above the Calandria, the temperature is uniform from the outlets through the riser (hot leg) until the heat exchanger entry. Similarly, from the exit of heat exchanger through the downcomer (cold leg) until the inlets of the Calandria where the temperature is fairly uniform again. The 3D structures namely the Calandria and the heat exchanger tubes where the heat transfer occurs only show temperature variations. The temperature difference between the hot leg and the cold leg at steady state was found to be ≈4.9 K. The maximum temperature inside the loop occurs inside the Calandria, which is predicted to be 310.8 K, which was higher than the hot leg temperature 310.2 K. The down comer (cold leg) was present at a constant temperature of 305.3 K. The velocity vectors (Fig. 7.4 B) show that the flow exiting from the Calandria at the two outlets meet together to form a single flow towards the heat exchanger. It is also observed that the velocity vectors inside the Calandria are not defined in a single direction, but exist in all the directions.

In Fig. 7.5, the same contours and velocity vectors are shown for a plane passing through the inlets of the Calandria (XZ plane). The Calandria temperature contour show stratification. In the velocity contour (Fig. 7.5 B) the incoming fluid is observed to flow past the first tube and reach the vicinity of the central tube.

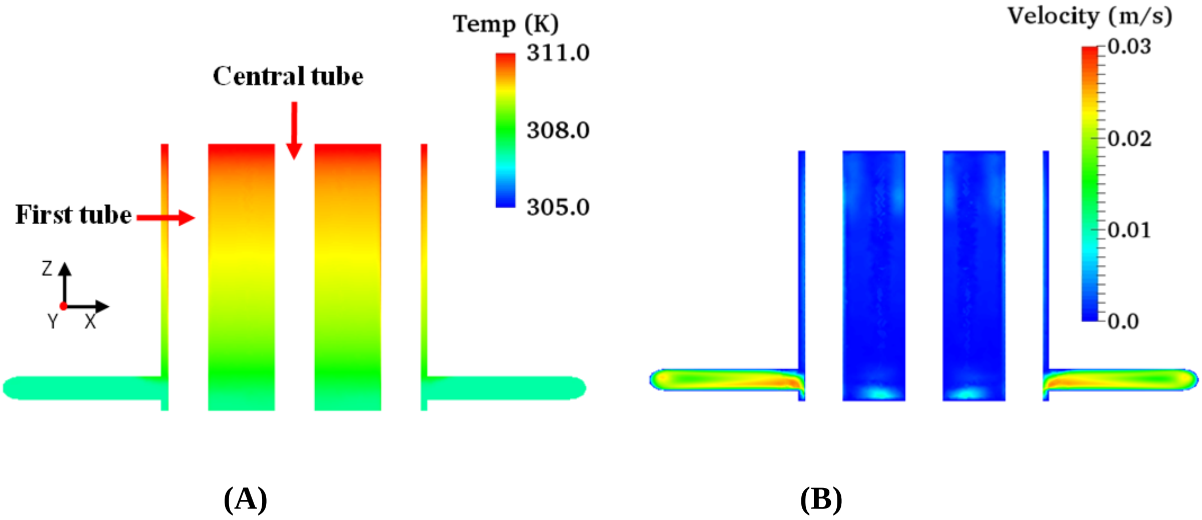

Figure 7.5: Steady state contours of (A) temperature and (B) velocity on a vertical plane passing through the center and the inlets of Calandria for heat power 500 W.

Fig. 7.6 shows the velocity contour on a cross sectional plane passing through the inlet (z/L_{Tank}= 0.08) of the Calandria vessel. It is observed that the inlet nozzle opens directly onto one of the tubes inside Calandria, which causes the majority of the flow to divert inwards into the tube bank. This flow slowly keeps penetrating through the tube bank and also branches after impinging on them. A high velocity region is observed between the second and third rings of tubes. It is observed that due to the larger flow area of the Calandria than the inlets, the incoming flow spreads out and becomes negligible as compared to the inlet velocity.

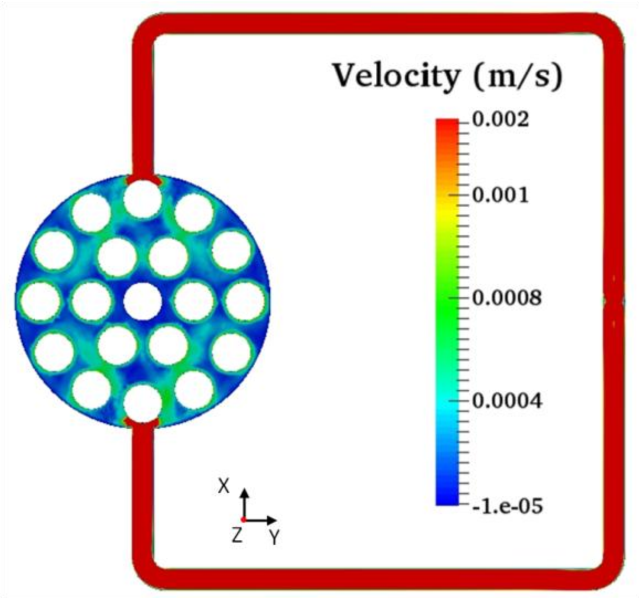

Figure 7.6: Steady state contours of velocity on a plane normal to z axis and passing through the Calandria and the inlets of Calandria.

In Fig. 7.7 A and B, the steady state temperature contours are shown for heater input of 500 W and 2000 W, respectively. The steady state contours for different powers show similar trends, only the magnitude of temperature throughout the Calandria increases. For a power of 500 W and 2000 W, the difference in the hottest and coolest fluid inside the Calandria increases from ~5.5 K to ~15.4 K.

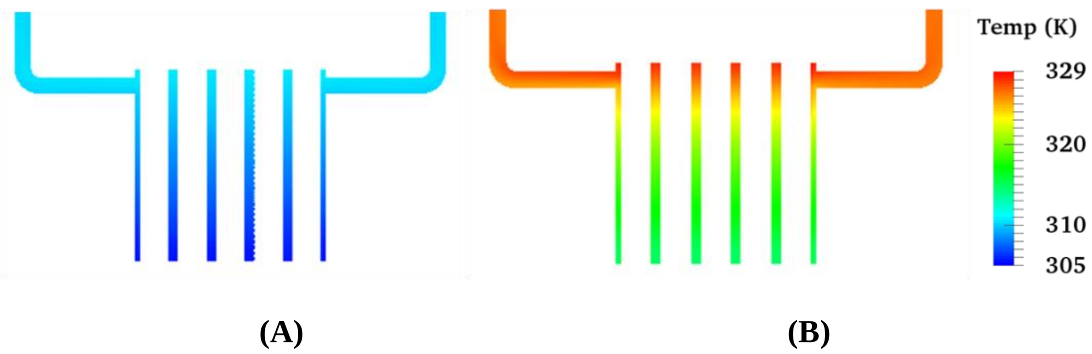

Figure 7.7: Steady state temperature contours for heater power input (A) 500 W and (B) 2000 W.

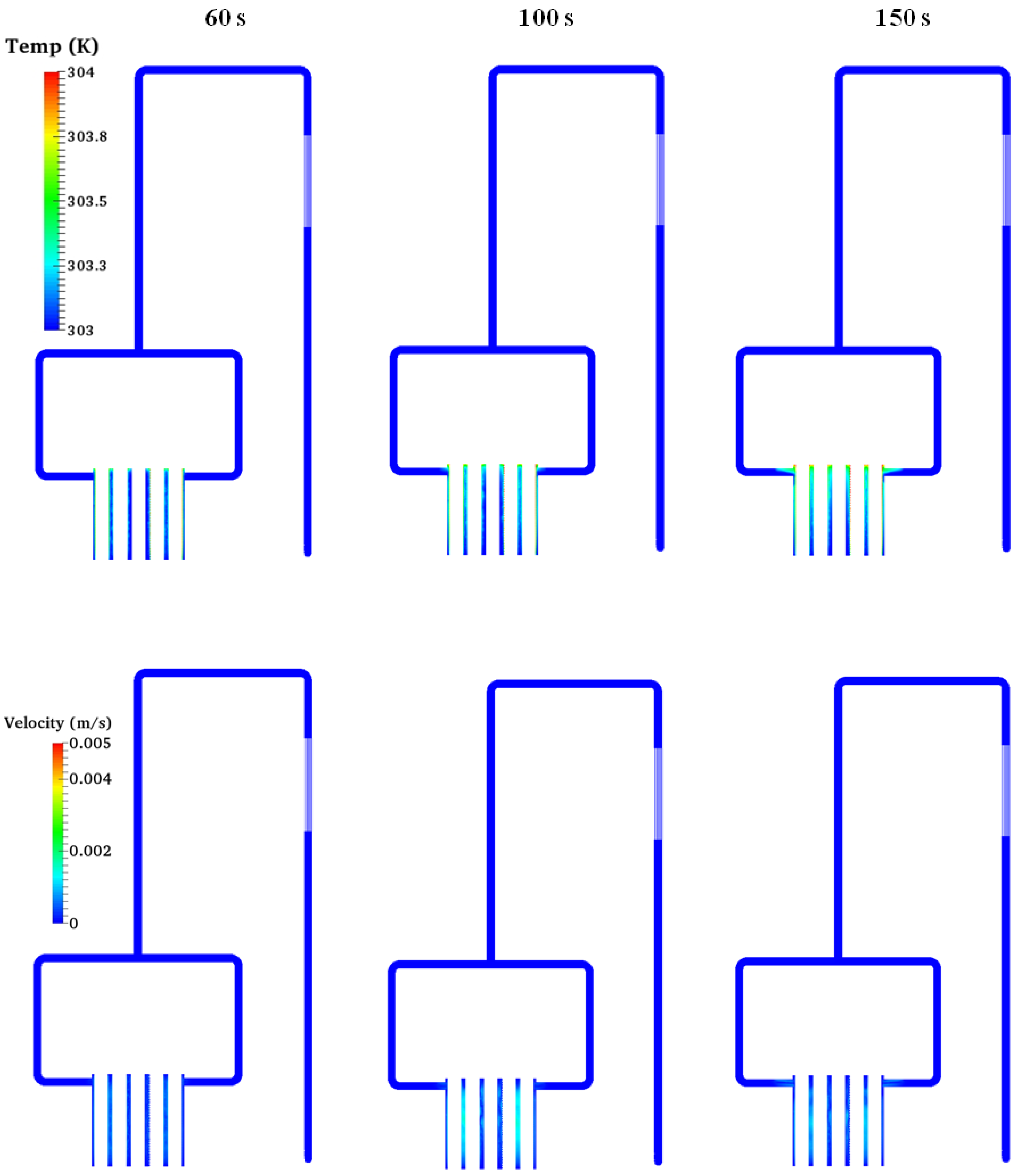
60 s
100 s
150 s
Temp (K)
304
303.8
303.5
303.3
303
Velocity (m/s)
0.005
0.004
0.002
0

Figure 7.8 (A)

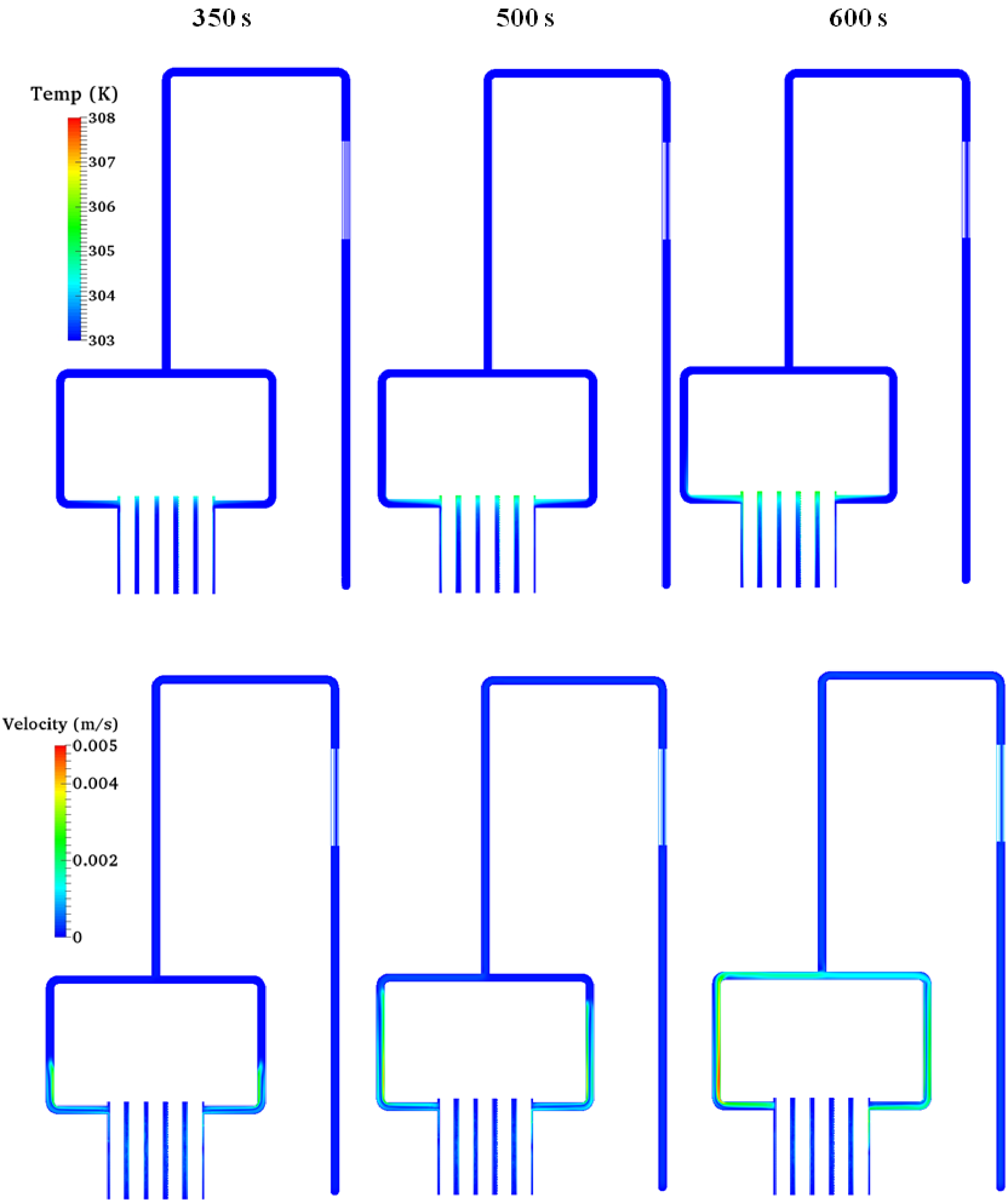
350 s
500 s
600 s
Temp (K)
308
307
306
305
304
303
Velocity (m/s)
0.005
0.004
0.002
0

Figure 7.8 (B)

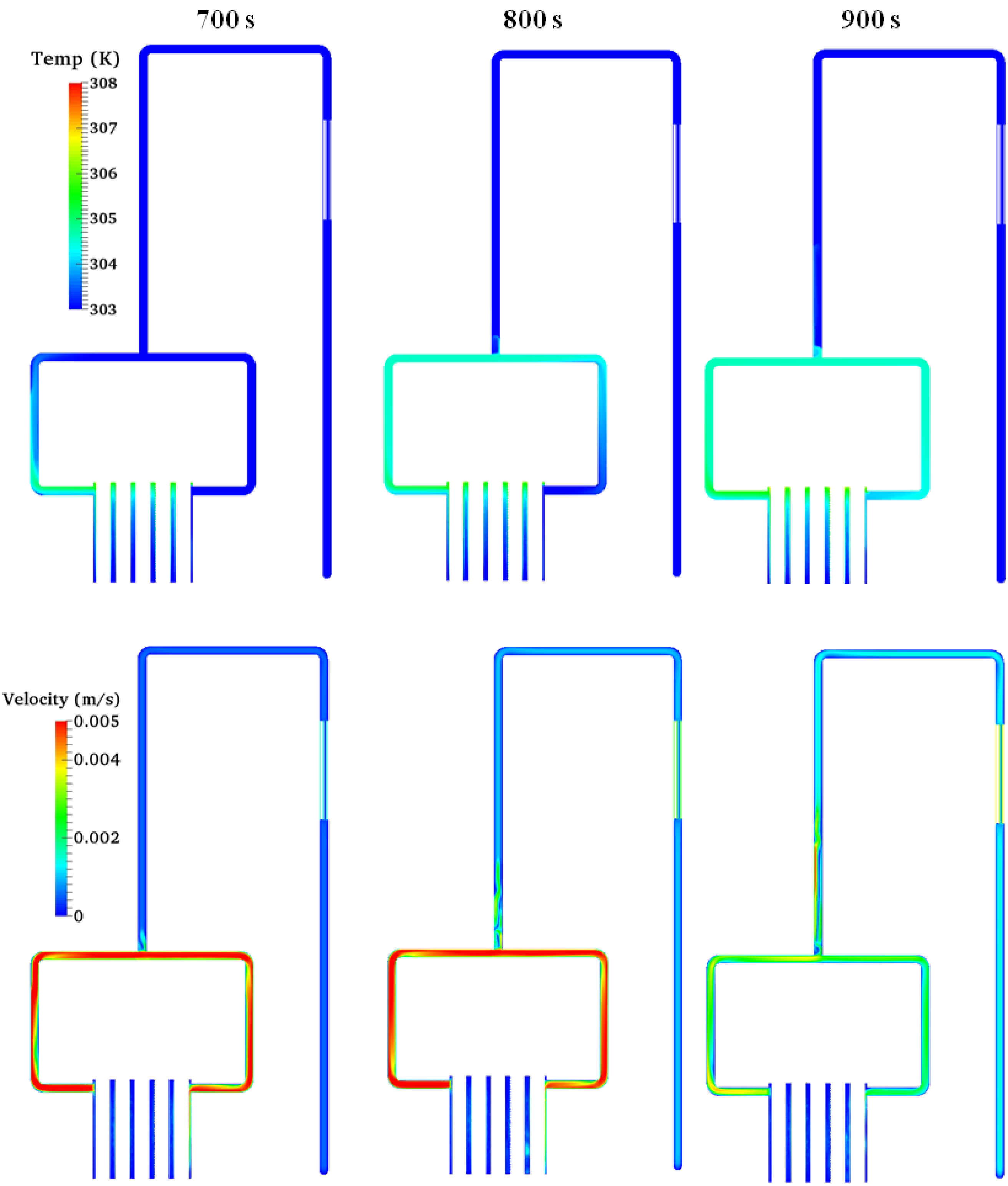
700 s
800 s
900 s
Temp (K)
308
307
306
305
304
303
Velocity (m/s)
0.005
0.004
0.002
0

Figure 7.8 (C)

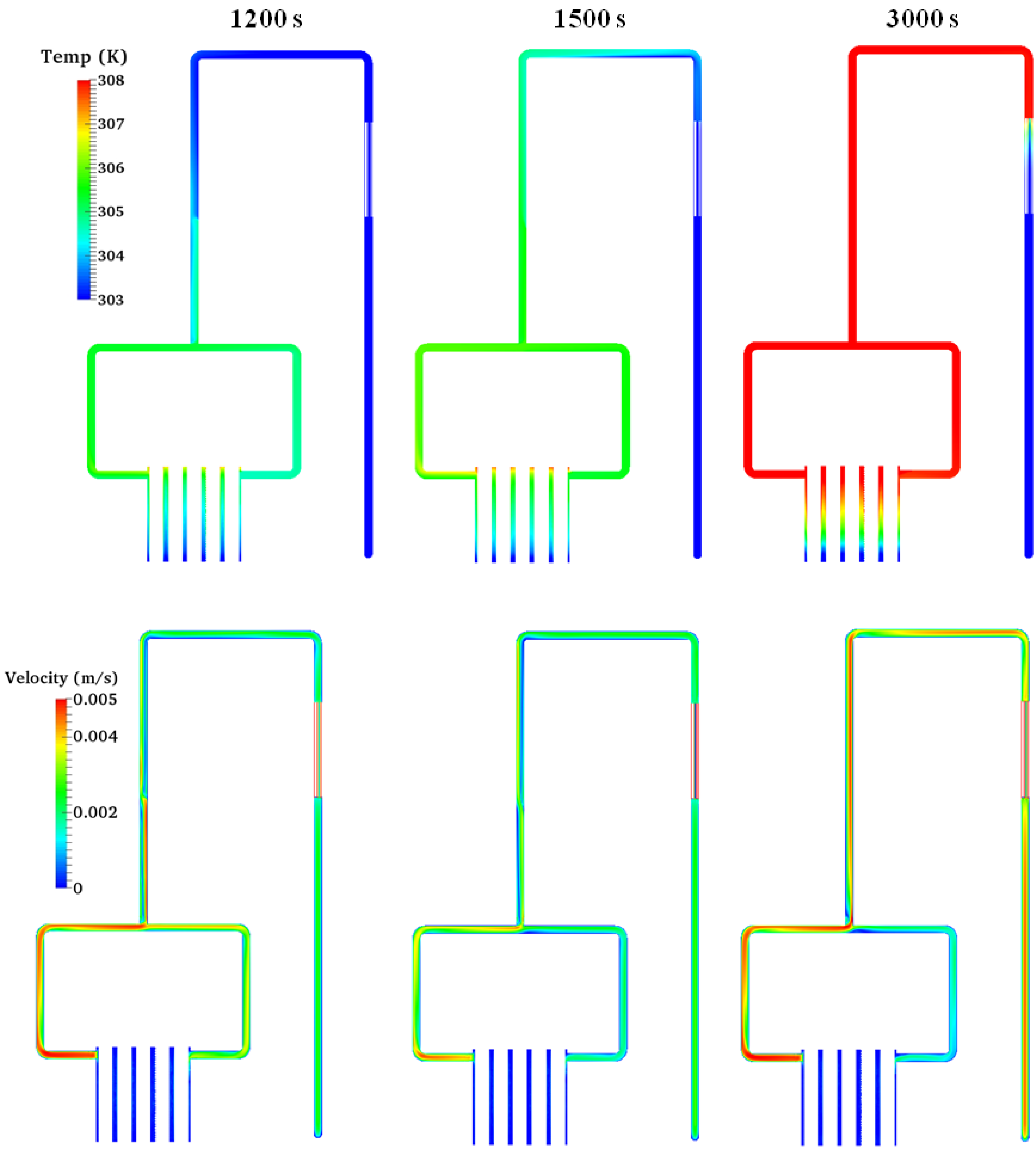

(D)

Figure 7.8: (A-D) Time varying temperature and velocity contours on a plane passing through the Calandria and heat exchanger tubes for 500 W power input.

7.4.2 Time dependent simulations

Time dependent simulation for the primary loop at an input heater power of 500 W was carried out. The cooler surface was kept at constant temperature of 303 K and the fluid was taken to be at rest at time t = 0 s. The simulation was executed for a physical time of 3000 s. The temperature and velocity contour evolution with time is shown in Fig. 7.8.

It was observed that at 60 s, the temperature in the Calandria vessel close to the tube walls rises, causing the hot fluid to rise due to buoyancy. This hot fluid reaches the top of the Calandria, turns at the top surface and recirculates within the Calandria. This sets up a natural convection system within the Calandria vessel only.

At time 100 s, the hot fluid starts flowing out of the Calandria vessel through the two horizontal outlets, and the velocity of fluid inside Calandria also increases. Near the outlets, the hot fluid is immediately replaced by the nearby cold fluid in the outlet pipes. Hence, there is a small region of backward flow near the outlets.

At 150 s, the temperature increases further, the velocity inside the Calandria starts to drop and the flow coming out of the outlets increases.

At 350 s, the temperatures within the Calandria continue to rise and more hot fluid keeps flowing out of the outlets. Simultaneously the flow inside Calandria reduces. Around 500 s, the high velocity region in the outlet pipes reach the elbows and turn upwards. It is observed that the left outlet flow becomes slightly dominant than the right outlet flow. in reaching the top bend. This difference in flow causes the dominant flow to push back the upward flow in the right outlet. Thus at 600 s, a circulating flow is established between the two outlet arms. The flow comes out of the left and returns back inside the Calandria through the right outlet. This can be seen in greater detail in the velocity vector plots in Fig. 7.9.

Despite the geometry being exactly symmetrical, this phenomenon is caused because of the slightest difference in the tetrahedral meshing at the junction of the outlets to the Calandria, which causes the establishment of a slightest height difference between the two outlets. However this height difference is sufficient to establish a natural circulation loop. It is interesting to note that practically in the actual experimental facility; the two outlets from the

Calandria is bound to have this fine height difference, because of the manufacturing tolerances of the equipments and the pipelines. Hence this phenomenon can be expected in the actual experiments also.

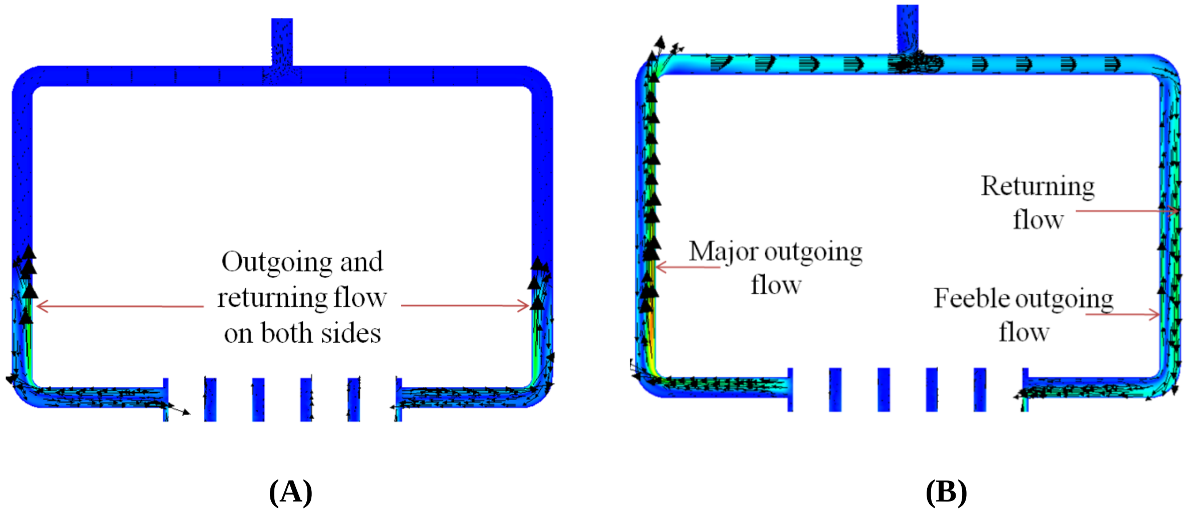

Figure 7.9: Velocity vectors on the outlets for time dependent CFD simulation at heater power input of 500 W (A) 350 s and (B) 600 s.

Through 700 s to 900 s, it is observed that the major stream causes the hot fluid to be flowing out of the right outlet and into the left. Simultaneously, the velocity in the loop formed between the two outlets increases. At 700 s, part of the stream is seen to be branched out into upper hot leg, which is connected to the heat exchanger tubes. By 900 s, the major flow breaks and is now getting diverted mainly towards the heat exchanger, i.e. the temperature difference between the hot lighter fluid in the Calandria (also the outlets) and the cold dense fluid in the cold leg is sufficiently high to generate flows to overcome the resistance to flow in the entire loop. This leads to the flow circulating through the entire loop.

From 1200 s onwards, the hot fluid keeps on rising into the hot leg towards the Calandria. Furthermore, the temperature of the entire loop now keeps on increasing in magnitude. However the stratified temperature contour in the Calandria continues. It is observed that the backward flow through the right outlet coming back into the Calandria also start to decrease with time. Thus eventually, the flow goes upwards in this outlet also.

Thus, the fluid behavior inside the loop can thus be broken into two types of flows: First, the recirculation flows formed within the Calandria vessel due to the buoyancy and second, a gross flow in the loop as a natural circulation loop.

Table 7.3. Comparison of pseudo steady temperature between experimental data and CFD simulations at various locations in the PMCTF.

Temperature (K)	Total input for heater (W)							
	500 W		1000 W		1500 W		2000 W	
	Expt	CFD	Expt	CFD	Expt	CFD	Expt	CFD
Calandria Outlet	308.2	310.2	315.2	316.0	319.7	321.8	323.6	326.8
Calandria Inlet	306.4	305.3	310.1	309.9	313.1	312.8	316.4	315.7
Shell inlet	302.3	305.1	302.8	308.7	302.6	310.9	303.7	313.6
Shell outlet	303.4	-	307.3	-	308.8	-	310.9	-

7.4.3. Comparison with experimental data

The comparison between the CFD predictions and the experimental measurements of the temperatures at the inlet and outlet of the Calandria for the different heater input is summarized in Table 7.3, which shows a fairly close agreement (within ±6%). For lower heater power inputs the agreement is better than at higher powers. For “the four hours 500 W power step up” experiment, the temperature and power at the end of every four hour was given as input conditions to steady state simulations. The steady state results for these give details of temperature and flow distributions throughout the system, especially Calandria vessel. The steady state results are listed in Table 7.3.

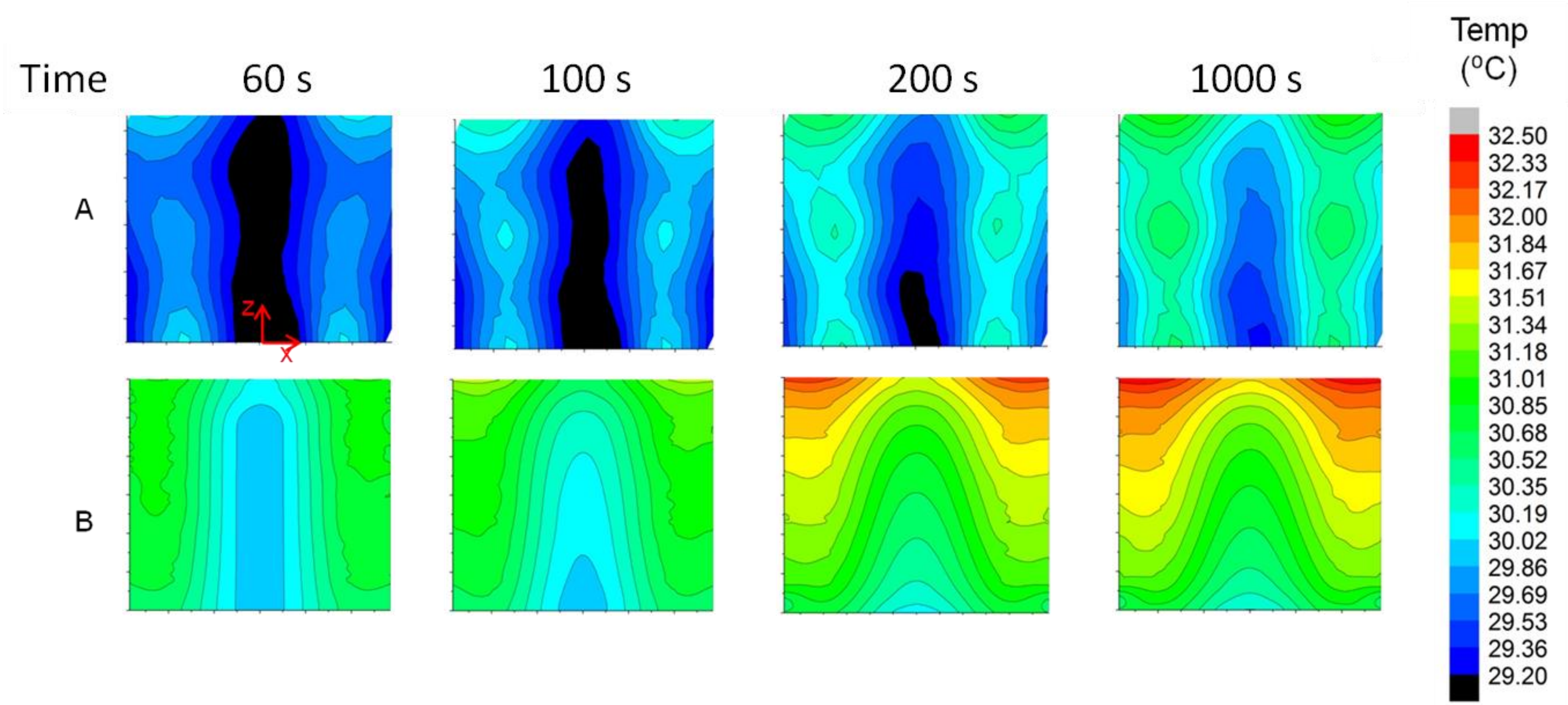

Figure 7.10: Comparison of temperature (ºC) contours on a plane passing through the Calandria and its inlets for (A) experimental data and (B) CFD for 60 s to 1000 s, at heater power of 500 W.

Fig. 7.10 compares the simulated with the experimental time dependent temperature contours on a vertical plane through the Calandria passing through the inlets. At 60 s, the temperature contours are very similar. The central tube shows a cold fluid region, whereas the outer tubes show a relatively high temperature region. Also, there is a high temperature stratified region at the top. From 200 s onwards, the CFD results show distinct stratified region being formed, whereas in the experimental contours this stratification is not yet as prominent. At all times, both the experimental and CFD contours show cold zones at the bottom corners. This is where the inlet opens into the Calandria. Thus, a relatively cooler fluid is observed. At 600 s the CFD show beginning of stratified contour, however in the experiments the contours are still developing. Thus the transient phenomena are moving faster in the CFD simulation. The possible reason for this could come from not simulating the heat lost to the solid boundaries (such as the Calandria and tubes walls). During the initial transients in the experiments, heat is lost from the fluid system in terms of heating up of solid walls (Calandria tube and shell walls, pipe walls, heat exchanger walls etc.). Thus when these losses are assumed to be negligible in the CFD simulations, the results show deviation from experimental contours. Finally, it was observed that the temperature values inside the Calandria were predicted to be slightly higher as compared to the experimental value.

7.5. Closure

Experiments at different power and time durations were carried out in the scaled model of Passive Moderator Cooling Facility (PMCS). The temperature and flow distribution inside the various components of the PMCS loop was understood through these experiments. The effect of change in the power input, on these distributions was also observed. A comparison between the performance of the CFD code with experimental data was done. The following conclusions can be made:

1. The steady state CFD simulations are in good agreement (within ±6%) with the experimental data (the experimental error is ± 0.6 ºC), with regard to the gross behavior of the system, i.e. the inlet and outlet temperature of the Calandria.
2. CFD predictions show that the temperatures inside the Calandria are stratified. The hot leg and the cold leg have a uniform temperature.
3. Starting from rest in a coupled natural circulation loop, majority of the flow recirculates within the Calandria and only after a certain time period flow was initiated in the entire loop.
4. The CFD model predicts that even at the steady state the gross flow in the loop is unable to disrupt the stratification inside the Calandria. This phenomenon is also captured in the experimental observations.
5. For the transient CFD simulations, the temperatures increased faster as compared to that in the experiments. This could possibly because of the adiabatic wall assumption in the CFD simulations and also not simulating the heat lost to the solid boundaries (such as the Calandria and tubes walls).

CHAPTER 8:

THERMAL HYDRAULICS STUDIES INSIDE THE CALANDRIA IN THE PASSIVE MODERATOR COOLING SYSTEM OF AHWR

8.1 Introduction

The objective of this study is to assess the capability of the PMCS to remove heat generated in the moderator during a SBO condition. In order to simulate this a full reactor scale time dependent simulation of the SBO condition is performed using the 1D system code RELAP5/MOD3.2. However as previously described the 1D code is unable to capture the details of the flow and temperature patterns inside the Calandria. Thus the previously validated CFD code must be used to simulate the Calandria and locate possible flow details such as, hotspots, dead zones and stratification.

The CFD code under consideration has been assessed to simulate the natural convection phenomena in the pilot scale of the PMCTF. However, as evident from the work in the previous chapters a full scale CFD simulation of the entire PMCS of the AHWR requires a very large mesh, huge computing power and long time to converge the simulation. In order to minimise the computational efforts and time required, a pseudo transient simulation was performed. In this method, a reactor scale simulation of the PMCS was performed using the 1D RELAP5/MOD3.2 code. Next, ‘snapshots’ of boundary conditions (i.e. the power, inlet mass flow and temperature) at various time instants throughout the prolonged SBO transience were obtained from the 1D simulation. These time snaps were then simulated for the

Calandria using the CFD code. This gives the 3D temperature and flow inside the Calandria of AHWR under PMCS operating conditions.

8.2 RELAP5 Simulation of PMCS

As discussed briefly in section 3.3, a 1D RELAP5/MOD3.2 simulation was carried out for the initial assessment of the PMCS of AHWR during a prolonged SBO. The results indicate that the systems remain within the defined safety limits for more than 9 days. Here the further details are discussed.

Table 8.1: Initial Operating Conditions for Various Systems of the Reactor.

System	Pressure	Temperature	Power
MHTS	70 bar	Core Inlet = 260 ºC Core Outlet = 285 ºC	920 MW (Full Power)
Moderator (PMCS)	1 bar	Calandria Inlet = 65 ºC Calandria outlet = 70 ºC	
V1 Volume	1.0056 bar	285 ºC	
V2 Volume	1.0046172 bar	40 ºC	
Advanced Accumulator (ECCS)	55 bar	40 ºC	
GDWP (ECCS)	4 bar	40 ºC	
Passive Valve	Start opening at 76.5 bar and fully opens at 79.5 bar of MHTS		
Active Valve	Opens at 79.5 bar of MHTS or 30 minutes after SBO (due to loss of pneumatic supply)		

8.2.1 RELAP- simulation of PMCS: Modelling of the system

Various systems of the reactor viz MHTS, ICS, ECCS, PCCS, and Primary Containment volumes, i.e. V1 and V2 along with the PMCS are integrally simulated with the system code RELAP5/MOD3.2. V1 volume encloses the MHTS, thus during normal operation of the reactor, V1 is at a higher temperature of 285 ºC, whereas, V2 is at a lower temperature of 40

°C [Fig. 8.1 (A)]. Initially, steady state is obtained for MHTS and the containment volumes V1, V2 and ECCS are initialized as per the initial conditions in Table 8.1.

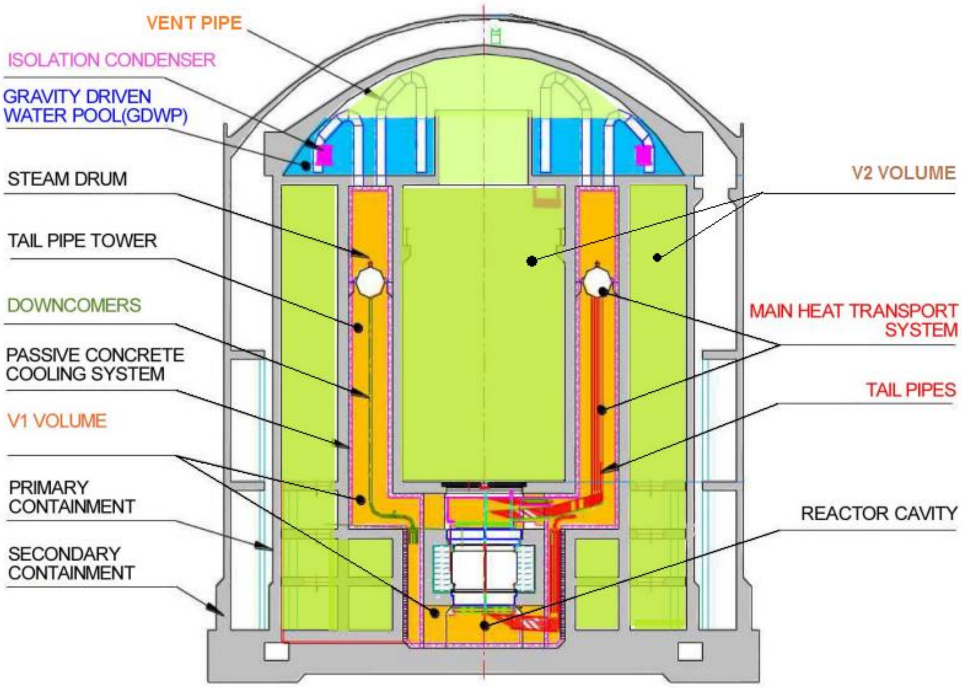

(A)

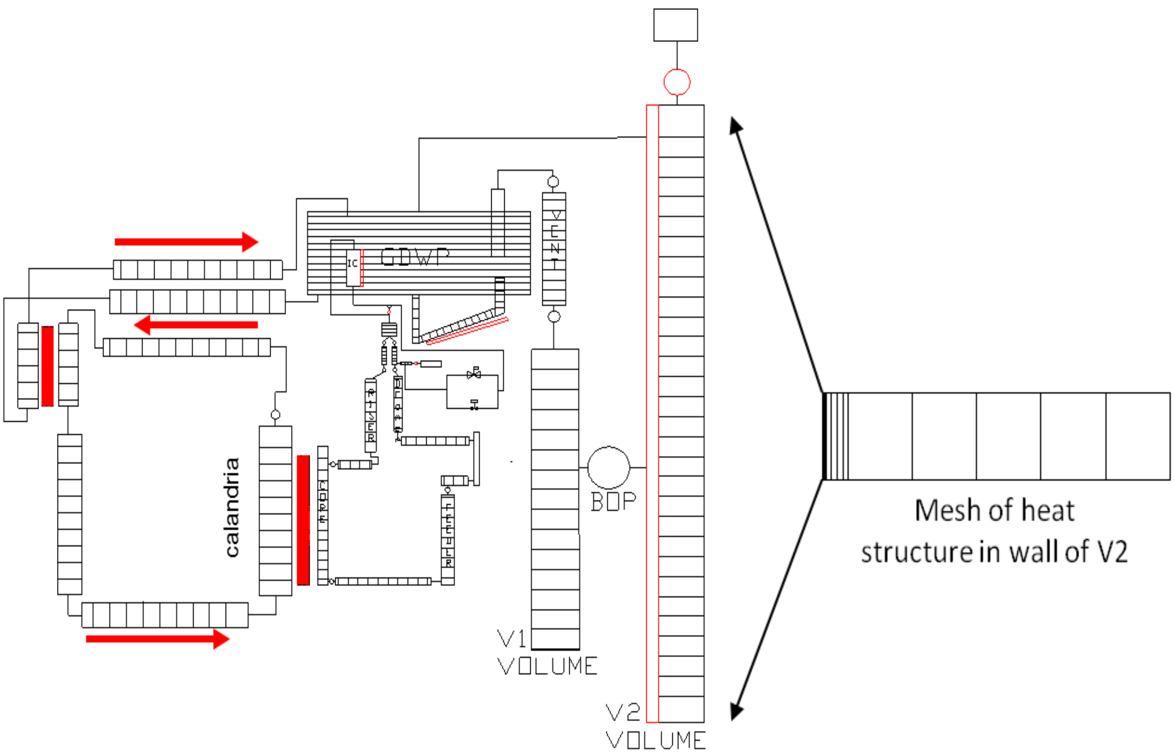

(B)

Figure 8.1: (A) Schematic of AHWR reactor cross sectional view showing volumes V1 (orange) and V2 (green) (B) RELAP5 nodalisation of AHWR passive systems and heat structure nodalisation in Volume V2 concrete wall.

Figure 8.1(B) shows the RELAP5 nodalisation of the various systems of the reactor. All the channels in the MHTS are grouped as a single equivalent channel having the total flow area and heat transfer area, generating the full power. This channel is connected to a single equivalent feeder of the 452 feeders of the reactor and a single equivalent tail pipe of the 452 tail pipes of the reactor. The four steam drums are combined into an equivalent steam drum. Similarly all the down comers are modelled as an equivalent down comer which is connected between the header and steam drum. All the tubes in the ICS are combined into an equivalent tube connected between the headers of the ICS. Five axial nodes are taken for IC tubes, which are associated with heat structure.

The GDWP is connected to the containment volume V2 since the GDWP is situated at the top of the containment. The two containment volumes are initially isolated from each other and filled with air at the normal operating condition as shown in Table 8.1. The containment volume V1 is modelled without heat absorbing capacity, while volume V2 is modelled with heat absorbing capacity. In the event of a prolonged SBO, the steam generated due to boiling in GDWP and also via vent pipe from volume V1; is expected to enter the volume V2 [Fig. 8.1 (A)]. Since the walls of this volume V2 are present at low temperature of 40 °C, thus this steam will condense on the concrete walls. In order to estimate the heat transfer to the containment wall during condensation, the heat structure associated with the wall of containment volume V2 is modelled by dividing it into 21 mesh points. The first 5 mesh points are 5 mm wide and the next 5 mesh points are 10 mm wide. This is followed by 5 mesh points of 25 mm width and 6 mesh points of 322.5 mm [Fig. 8.1 (B)]. Since concrete has poor thermal conductivity and high heat capacity, the nodalisation considered in the radial direction gives a more accurate prediction of condensation on the V2 volume wall than considering an lumped one, so to account for the realistic rate of heat transfer relatively fine nodalisation is taken. This nodalisation is similar to the meshing in CFD simulation. Here, close to the hydraulic volume of V2 (from where heat is transferred to the wall), the meshing is fine in order to capture the gradients accurately and far away the mesh is kept coarser as the gradients are less severe and hence can be resolved easily.

All the Calandria tubes are lumped in a representative one and heat transfer area of all the tubes are provided for heat removal calculations. Radiation mode of heat transfer is considered between the MHTS pressure tube and Calandria tubes. Calandria tubes are connected to the moderator thermally, moderator is considered inside the Calandria vessel. All the Calandria tubes are lumped in a representative one and heat transfer area of all the tubes are provided for heat removal calculations in heat structure model of RELAP5. Calandria tubes are connected to the moderator thermally (as a heat structure). Total 24 axial nodes are considered for the Calandria tubes as well as for the Calandria vessel. The outlets to the Calandria were clubbed together into one outlet connected to the outlet header. Similar treatment was given to the inlets. The intermediate heat exchanger shell and tubes are again lumped in a single representative shell and tube. The number of nodes given to the heat exchanger is 24. The shell side of the heat exchanger is connected thermally to the tube side by heat structure defined in the input file.

8.2.2 Scenario considered

A prolonged SBO condition has been considered for analyzing the decay heat removal capability of the reactor. When the simulation starts the system is assumed at a condition of rest. The power is first increased slowly to the normal operating power (920 MW) and kept constant for 7500 s. After this the SBO is initiated (which is considered as time t = 0 s). With initiation of the SBO the reactor is shut down (trips). The turbine is tripped which causes closure of Condensate Isolation Emergency Stop Valve (CIESV) and the feed water supply line is also isolated at the same time due to unavailability of feed pumps. Closure of CIESV isolates the turbine from MHTS, this stops the flow of steam from the steam drum to the turbine. Thus, the MHTS becomes boxed up, which causes the pressure of the MHTS to start rising.

When the pressure of the MHTS reaches the set point of the passive valve of the Isolation Condenser (IC), i.e. 76.5 bar, it opens and the ICS becomes operational. Due to unavailability of the power supply, the pneumatic pressure is lost after 30 minutes, which causes the active valve in the ICS to remain continuously open. If the pressure of the MHTS falls below 50 bar, ECCS injection from accumulators starts and continues until the level in the accumulators falls below 75 cm which is a low level isolation of accumulator. If the MHTS pressure falls below 3 bar then injection from GDWP may start injecting water into the core.

The PMCS system is plugged in from the time SBO is initiated. The heat from the MHTS is modelled to be transferred to the moderator by radiation mode of heat transfer. The moderator temperature is initially at 67.5 ºC. The heat transferred from MHTS causes the moderator temperature to rise and due to buoyancy the natural circulation loop is established. Similarly, on the heat exchanger shell side the water from GDWP cools down the tube side water, and forms a natural circulation loop. This system shall maintain the temperature of the moderator below boiling temperatures, till the time cooling water is available in GDWP.

8.2.3. Results and Discussion

For the first 1500 s of numerical simulation, the power input to the MHT is slowly increased from zero to normal steady state operation power of 920 MW. From 1500 s till 9000 s, this 920 MW is kept constant in order to bring the whole system to a steady state. Uptill 9000 s, the IC is not connected to the MHTS, i.e. the steam from the MHT does not enter the IC. At 9000 s, a SBO occurs.

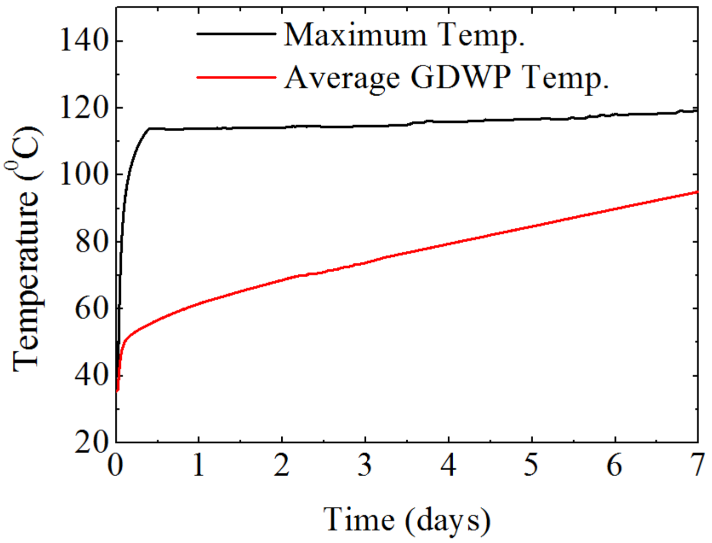

Figure 8.2: Variation of GDWP Water Temperature.

Thus the IC is connected and the hot MHT coolant enters the GDWP, resulting in an upsurge of the GDWP temperature (Fig. 8.2). Also at this instant the decay heat is very high. In the later period there is a continuous steady flow of steam to the IC and also the decay heat generated also decreases. Thus a smooth continuous increase in GDWP temperature is observed. Later when the graphs were plot 9000 s was subtracted from the timeline in order to bring the SBO initiation at time t= 0 s.

Figure 8.3 shows the mass flow rate in the primary and secondary loop of the moderator circuit. It can be observed from this figure that mass flow rates are high during the initial period and decreases subsequently as decay power decreases. After 2.5 days, the moderator and the shell side of the heat exchanger mass flow rates stabilize at 10 kg/s and 21 kg/s, respectively. However, the temperature of the moderator entering the Calandria vessel as well as leaving the Calandria vessel (Figure 8.4 and 8.5) increases with time as the sink (GDWP) temperature rises.

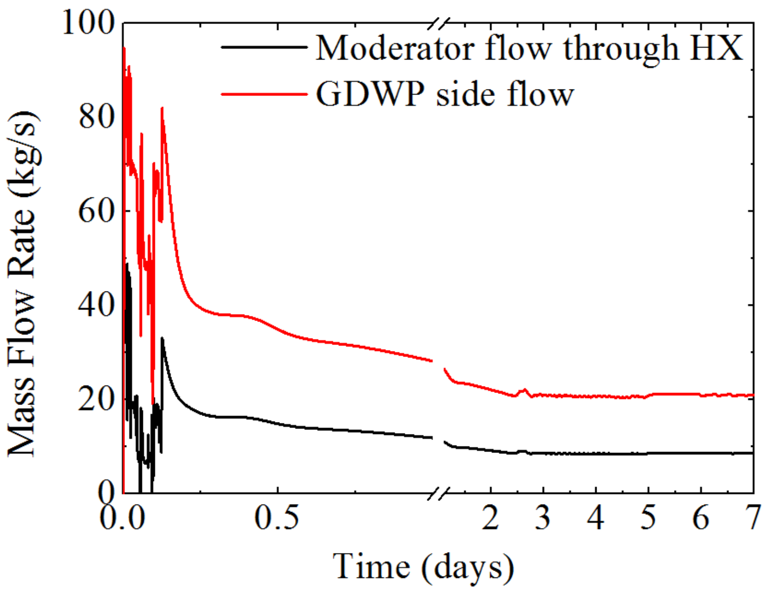

Figure 8.3: Variation of Moderator and GDWP side coolant mass flow rates.

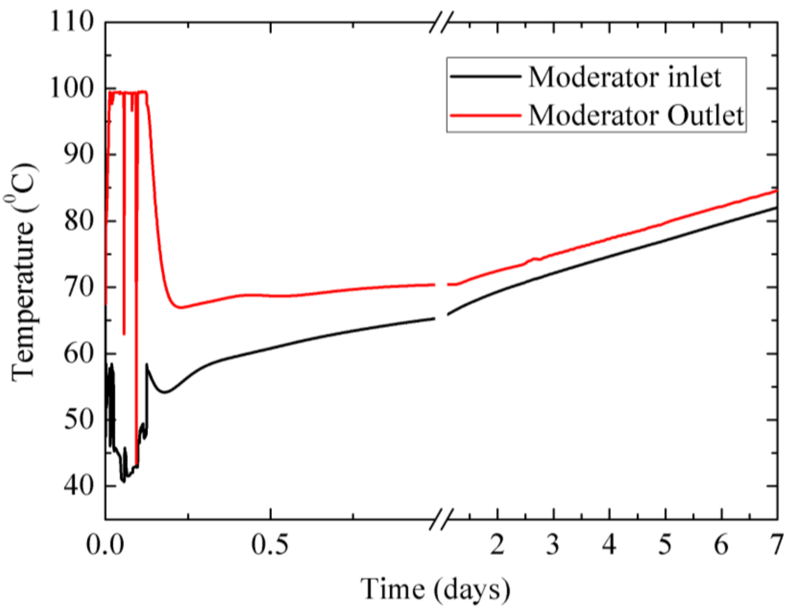

Figure 8.4: Variation of Moderator Temperature at the inlet and outlet of the Calandria.

In Figure 8.4, for time t < 0.2 days, it is observed that the temperature at the inlet and outlet of the Calandria fluctuates. This is because the flow in the fluid in the PMCS was considered to be at rest at the beginning and with the power input (i.e. SBO initiation) at time t = 0, the system flow is getting developed under transient behaviour. After 2.5 days, the temperature difference between the inlet and outlet is maintained at an almost constant value of 3°C.

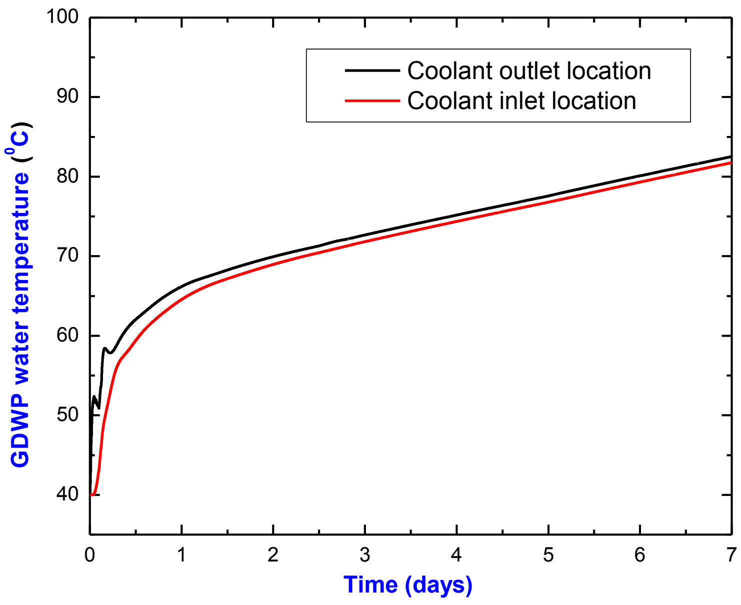

Figure 8.5: Variation of GDWP side coolant temperature (shell side temperature).

In the current study it is assumed that when SBO occurs, the moderator fluid is at rest. When SBO starts, a sudden input of heat flux is given to the moderator which initiates the buoyant flows in the PMCS. The flow is highly unstable, fluctuating and the temperatures reach close 100 °C. However, in reality the PMCS system alongwith the forced moderator cooling system is always online and operating during normal operation of the reactor. So 2 MW heat is always being removed by the PMCS heat exchanger and there is a steady flow in this system. Furthermore, there are flywheels connected to the pumps of the forced moderator cooling system. Consequently in the event of a SBO, the flow inside Calandria will not start from absolute zero and also the flywheels will prevent the flow from dying out fast. Thus in reality during the initial transient phase heat load, the moderator flow velocities are capable of removing the steady state maximum heat load of 2 MW.

Figure 8.6 shows the heat balance between the moderator primary and secondary side of the heat exchanger. It is observed that in the initial transience, the heat load to the moderator and that to the heat exchanger are not equal. After t = 0.5 days, these heat loads equalize, i.e. the heat deposited in the moderator is entirely transferred through the heat exchanger to the GDWP. Finally, after 2 days the moderator heat load is small due to the reduction of the MHTS temperature and decay heat.

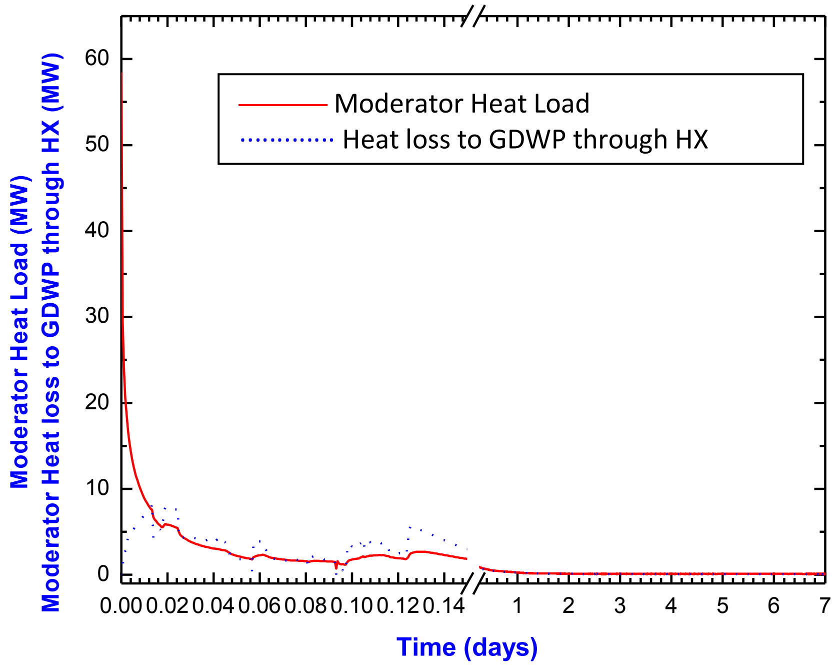

Figure 8.6: Heat balance between moderator primary and secondary side.

Even after around 7 days, boiling is not found to occur in the GDWP. It is observed that there is still more than 7500 m^3 of water in the GDWP even after 7 days of the accident. During this time period the temperature in the moderator remains below the boiling conditions. The analysis led to the conclusion that the concept works. Furthermore, the system is able to maintain the moderator temperature below boiling conditions for a time period of 7 days without any operator intervention.

8.3 CFD Simulation of Calandria in PMCS

8.3.1 Geometrical Details

The Calandria vessel in consideration is a vertical cylindrical tank with inner diameter of shell being 6.9 m and height 5.3 m. There are 513 Calandria tubes (fuel channels) in this tank whose outer diameter is 0.168 m and are arranged in a square pitch layout (pitch = 0.225 m). Inside the Calandria tubes, the primary coolant flows inside another concentric tube (namely the pressure tube) separated from the Calandria tube by an air gap. There are 16 inlets and 16 outlets located near the bottom and top of the Calandria, respectively. Since there is a symmetry in the geometry, only 1/8th section (45° sector) of the geometry is simulated (Fig. 8.7).

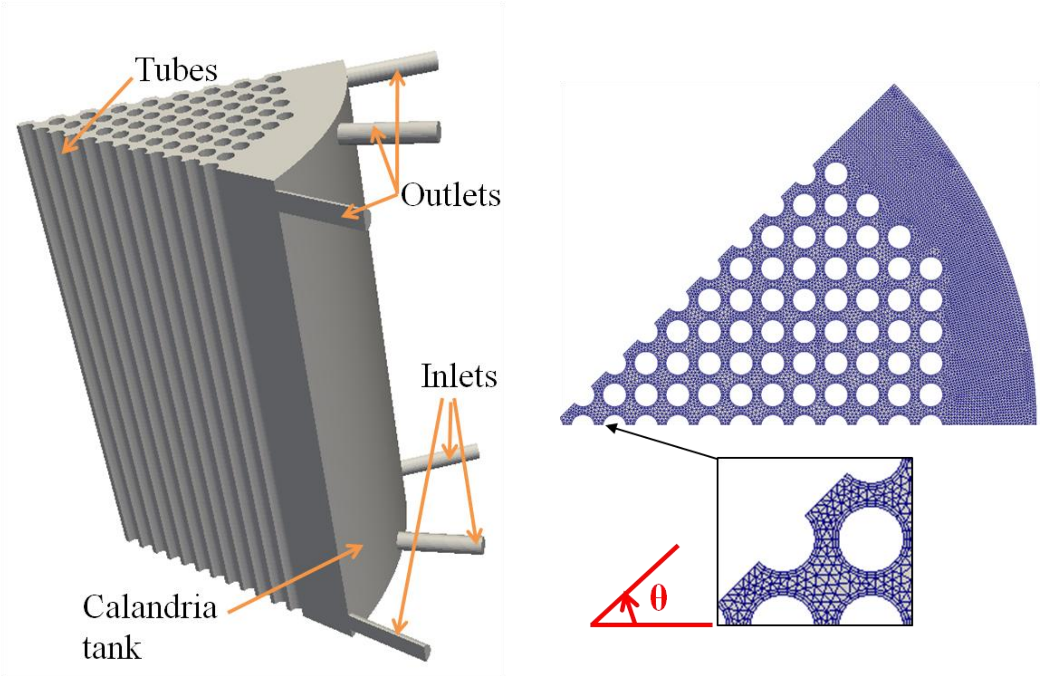

(A) **(B)**

Figure 8.7: (A) Geometry of Calandria simulated and (B) top view of the meshed geometry.

8.3.2 Numerical Modelling

8.3.2.1 Governing equations

The computational work is carried out on the opensource solver OpenFoam 2.2.0 which is a three-dimensional CFD tool, based on the finite volume method. The single phase, steady state, Reynolds averaged Navier-Stokes equations of motion and the equation of energy are solved for an incompressible Newtonian fluid. The equations are described in section 6.2. The Ra number for the given heat input (2 MW) is 1.2×10^{15} inside the control volume. This lies in the turbulent regime (Ra $>10^9$), thus we select k-ε turbulence model to capture turbulence phenomena.

8.3.2.2 Solution methodology

The solver used in OpenFOAM is buoyantBoussinesqSimpleFoam, which solves fluid flow and heat transfer under Boussinesq approximation. The upwind scheme is used for discretisation which is sensitive to the direction of flow and it is first order accurate. The diffusion terms are discretized using central differencing scheme which is second order accurate. SIMPLE (Semi-Implicit Method for Pressure Linked Equations) algorithm was selected for pressure-velocity coupling with relaxation factors of 0.3 for pressure and 0.7 for momentum. All the solutions were considered fully converged when sum of scaled residuals were below 10^{-4}. Before stopping the calculations, relative variations of key physical variables, such as flow velocities and temperature were imposed to be lower than 10^{-4}m/s and 0.1K, respectively. All the computations were carried out in a parallel manner on a cluster using 32 processors.

8.3.2.3 Grid independence

In presence of natural circulation, higher gradient of velocity and temperature are present close to heat source region. Therefore, it is important to provide a fine mesh close to the heat source and then increase the mesh size away from it. Accordingly, the mesh is finer near the fuel channels, and coarser in between them and towards the Calandria vessel wall. The mesh is a mix prismatic and tetrahedral unstructured mesh containing 5,100,000 cells (Fig. 8.7 B). This mesh was generated using commercial meshing software, Hypermesh.

The grid independence was investigated for three grid sizes for the case of mass flow of 32 kg/s [considered as the average case amongst the steady state flux of 2 MW (Section 8.3.3.1)]: (1) 1.7 million; (2) 5.1 million and (3) 10.3 million cells. The temperature along the height of the Calandria at a radial location (Fig.8.8 A) for different grid sizes is shown in Fig. 8.2 B. The results of mesh size of 5.1 and 10.3 million are nearly the same (within 0.5ºC).

Thus we use the grid of 5.1 million for further studies. The y^+ values near the walls vary between 32 to 90 for various grid sizes, for flow rate of 32 kg/s.

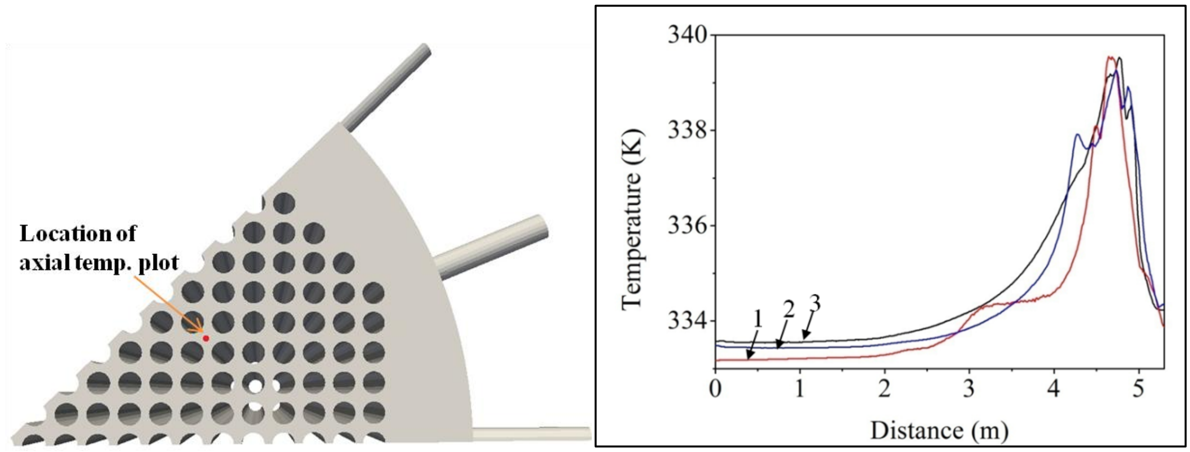

(A) (B)

Figure 8.8: (A) Radial location for temperature plot along the axis of the Calandria from bottom to top and (B) grid independence studies for grid size (1) 1.7 million; (2) 5.1 million and (3) 10.3 million.

8.3.3 Event Scenario Considered

It is considered that a prolonged station blackout event occurs in the reactor. In such an event, the reactor is safely shut down. The turbine is tripped and isolated from the MHTS. Simultaneously, the feed water line is also isolated due to unavailability of the feed water supply line. Thus, the MHTS is boxed up, which cause rise in the pressure of MHTS. At a set point of 76.5 bar, the passive valve to the isolation condenser gets opened and the Passive Decay Heat Removal System (PDHRS) start removing heat from the MHTS continuously. Thus, cooling of the reactor core is maintained. During this entire process, the MHTS is at a temperature higher than moderator resulting heat transfer by radiation across the gap between Pressure tube and the Calandria tube walls. The PMCS is designed to remove this heat from the moderator for at least 7 days without operator intervention.

8.3.3.1 Steady State simulation of Calandria

During a SBO condition, at t = 0 s, the MHTS is present at 558 K and the moderator is at 333 K, which results in a 2 MW heat deposition in the moderator by radiation heat transfer across the pressure tube Calandria tube gap. Thereafter, the decay heat reduces and the PDHRS starts to work. This lowers the temperature of the MHTS and consequently less heat is transferred to the moderator.

Hence, the PMCS system must be able to remove this maximum heat load of 2 MW, while preventing local boiling of moderator. Keeping this as a design criteria for PMCS, 3D simulations is performed at various input mass flow rates keeping the power constant at 2 MW. The results give temperature and flow fields inside the Calandria. The objective is to determine the minimum mass flow rate required to maintain the temperature of the moderator inside the Calandria vessel below boiling conditions.

In the present study, the walls of the Calandria vessel were considered as adiabatic walls with no slip boundary condition. Furthermore, no-slip boundary condition was applied on the fuel channel surfaces. A constant heat flux boundary condition was applied on the surface of the fuel channels, with total heat input of 2 MW to the moderator. Outlets are at atmospheric pressure and inlets are given constant mass flow varying from 10 kg/s, 20 kg/s, 32 kg/s and 50 kg/s at 333 K. In the previously performed 1D simulation of the system, the initial transient phase of the PMCS showed major fluctuations in the system between 10 to 50 kg/s. Thus, we take four different mass flow rates in this range to study the 3D temperature and flow distribution inside Calandria vessel.

8.3.3.2 Pseudo-transient simulation of Calandria in a Station Blackout Condition

Kumar et al. (2013) performed transient 1D simulation using RELAP5/MOD3.2, for the reactor in an SBO condition for a period of 7 days. This simulation included all the reactor safety systems (for instance, the Main Heat Transport System, the Passive Decay Heat Removal System and the Passive Moderator Cooling System) along with the Pressure tubes, the Calandria tubes and the moderator in the Calandria. The decay heat curve of the reactor was given as a heat input boundary condition to the fuel inside the Calandria tubes. Due to radiation heat transfer across the Calandria tube and pressure tube gap, moderator temperature rises and this heat deposited in the moderator was estimated by the code. The rise in temperature resulted in natural circulation flows in the PMCS, and the mass flow rate in the Calandria also was estimated by the code. Thus, at any given instant we have input power, temperature and flow conditions to the moderator.

We consider six cases spread over the span of 7 days since SBO (listed in Table 8.2), after which the heat input to the moderator remains constant. The fuel channel was given a uniform heat flux calculated from the total heat input to the moderator alongwith a no-slip boundary condition. The tank wall was given adiabatic no slip boundary condition. The outlet was maintained at constant atmospheric pressure, whereas the inlet was given a constant temperature and mass flow input according to the Table 8.2.

Table 8.2: Boundary conditions for pseudo steady simulations during an SBO condition.

Case No.	Time from beginning of SBO (days)	Heat input to moderator (MW)	Inlet mass flow rate (kg/s)	Initial temperature of moderator (K)
Case 1	0.5	0.49	14.83	333.78
Case 2	1	0.25	11.82	338.29
Case 3	2	0.12	10.2	343.00
Case 4	3	0.1	8.6	345.14
Case 5	4	0.094	8.47	347.66
Case 6	6	0.092	8.52	353.54

8.3.4 Results and discussion

8.3.4.1 Steady state simulation of Calandria

Table 8.3 gives the steady state maximum temperature and the average temperature of moderator in the entire volume of the Calandria for the different mass flow rates considered. It is observed that the maximum temperature for the inlet mass flow rate of 10 kg/s is 375.45 K, which is above the boiling point of the heavy water (~374 K). It must be noted that although the CFD code is not capable of capturing the two-phase behavior; however, the main concern is that the moderator should not reach boiling temperatures. On the other hand, it is also observed that average temperature in the Calandria for all mass flow rates is below the boiling conditions. This indicates that there is local boiling at certain locations inside Calandria where the temperature is above 374 K.

Table 8.3: Steady state maximum and average moderator temperature in Calandria.

Mass flow rate (kg/s)	Maximum temperature (K)	Average temperature (K)
10	375.45	339.99
20	368.24	338.86
32	362.08	337.63
50	361.31	337.25

For any heat exchanger, the fluid entering the shell side from inlet absorbs heat from the hot tubes (fuel channels in Calandria) and then flow towards the outlet. In this process, the temperature of the fluid rises as going out of the outlet. Thus for Calandria geometry being similar to that of the shell side of a shell and tube heat exchanger, a plane at z/L_{Tank}= 0.9, i.e. at the top and close to the outlet is considered to observe for hotspots in the temperature contours.

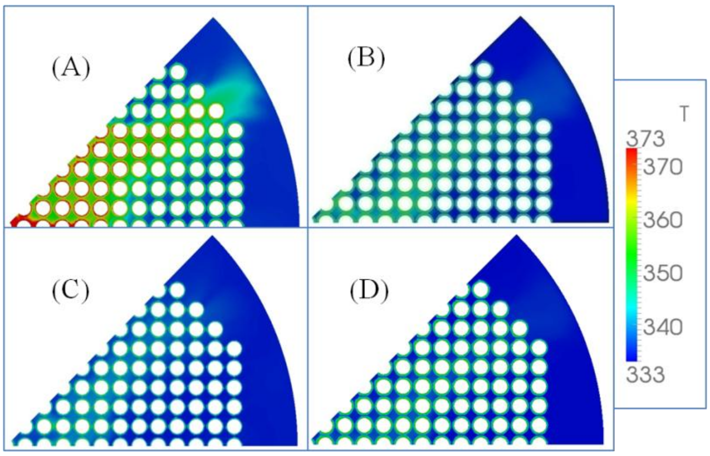

Figure 8.9: Temperature distribution on a plane z/L_{Tank}=0.9 for inlet mass flow rate of (A) 10 kg/s, (B) 20 kg/s, (C) 32 kg/s and (D) 50 kg/s.

The temperature distribution on a plane perpendicular to *z* axis (vertical axis) for different mass flow rates at steady state in the Calandria are shown in Fig. 8.9 A-D. It is observed that, at mass flow of 10 kg/s, the temperatures at the center of the fuel channels reach temperatures close to boiling. However, the temperatures for mass flow rates greater than 20 kg/s are below boiling conditions.

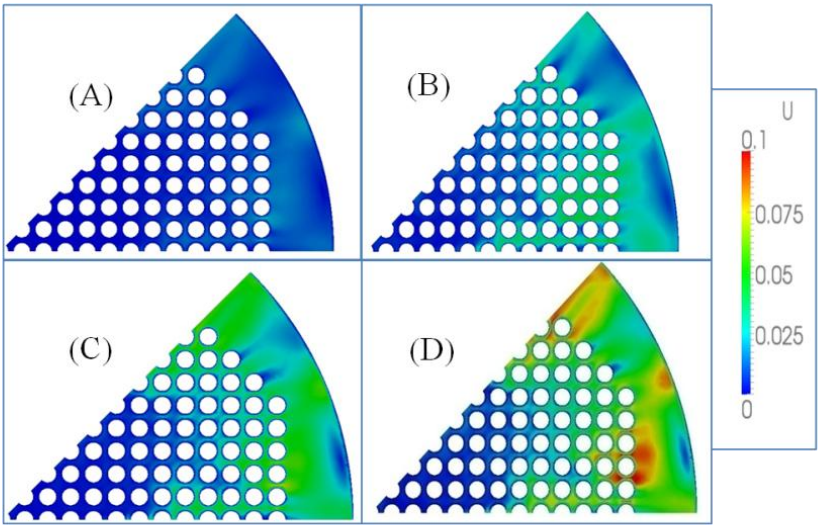

Figure 8.10: Velocity distribution on a plane z/L_{Tank}=0.9 for inlet mass flow rate of (A) 10 kg/s, (B) 20 kg/s, (C) 32 kg/s and (D) 50 kg/s.

The velocity contours in the plane z/L_{Tank}=0.9 also concrete this observation (Fig. 8.10). It is observed that the velocities are higher in the outer periphery of fuel matrix and the open region between fuel channels and shell wall. Thus, the flow is unable to penetrate through to the center of the tight fuel channel lattice. Hence, there is lower cooling in the central region of fuel channels. However, above mass flow rates 20 kg/s the fluid velocities are sufficient to ensure cooling of the moderator.

Along the radial direction, it is observed that for all the mass flow rates, as we move from inlet towards the central fuel channel only 0.1 % of the actual fluid velocity remains. For example, for 10 kg/s mass flow, the inlet velocity dropped to a maximum of 0.6 mm/s near the central fuel channel and inlet velocity drops to 3.6 mm/s for 50 kg/s.

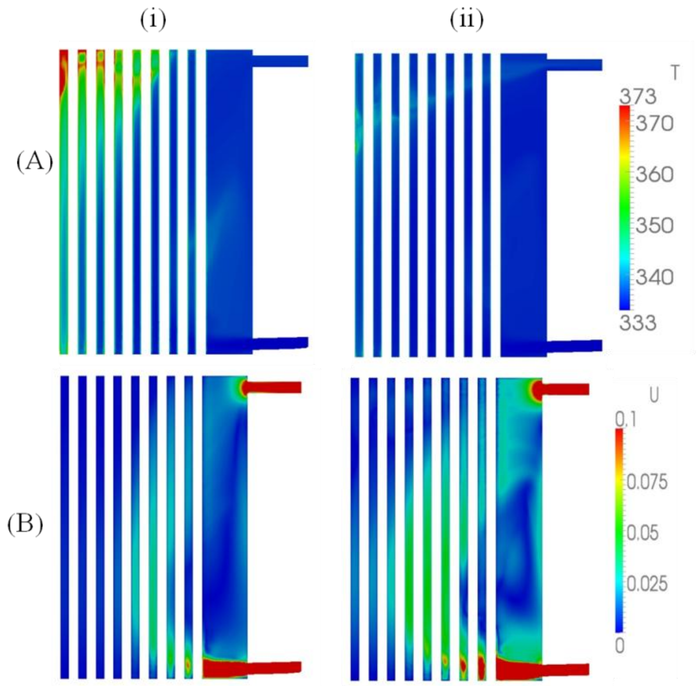

Figure 8.11: (A) Temperature and (B) Velocity contour of Calandria on a plane at θ=45° for mass flow rate = (i) 10 kg/s and (ii) 20 kg/s.

In Fig. 8.11, the steady state velocity and temperature contours on a vertical plane (θ=45°), parallel to the fuel channels is shown for the two mass flow rates, 10 kg/s and 20 kg/s. For mass flow rate 10 kg/s, the fluid flow is unable to penetrate through entire of the fuel channels towards the central region. The main flow is diverted from the outer layers of channels towards the outlet, before it reaches the top of the Calandria. Hence, there is a dead zone near the top part at the center. This results in accumulation of hot fluid in this top region. On the other hand, for mass flow rate higher than 20 kg/s, the fluid is able to carry away heat from the top central region.

Fig. 8.12 shows the velocity vectors on two vertical planes parallel to the fuel channels as shown in Fig. 8.12 D. Here the color scale depicts the magnitude of velocity in Fig. 8.12 A, whereas the scale depicts the temperature scale in Fig. 8.12 B and C. Fig. 8.12 A show the velocity vector at mass flow 10 kg/s on the plane ξ. It is observed that two distinct recirculation zones are formed: one large zone going up through the fuel channels and coming down near the Calandria walls; and a second smaller one at the top of the central fuel channel. Velocity vectors on the plane *ξ'* (Fig. 8.12 D), are shown in Fig. 8.12 B for a mass flow rate of 10 kg/s. This clearly shows the dead zone at the top, which keeps the hot fluid recirculating within itself and is cut off from the main flow inside the Calandria. This results in high temperature fluid zone. Fig. 8.12 C shows the velocity vector for mass flow 20 kg/s on the plane *ξ'*. It is observed that although a smaller recirculation zone is formed, the inlet mass flow is high enough so that a part of the flow from the bigger recirculation zone entrails in this recirculating region. This entrainment brings cooler fluid into the recirculating region and hence reduces the temperature in this region.

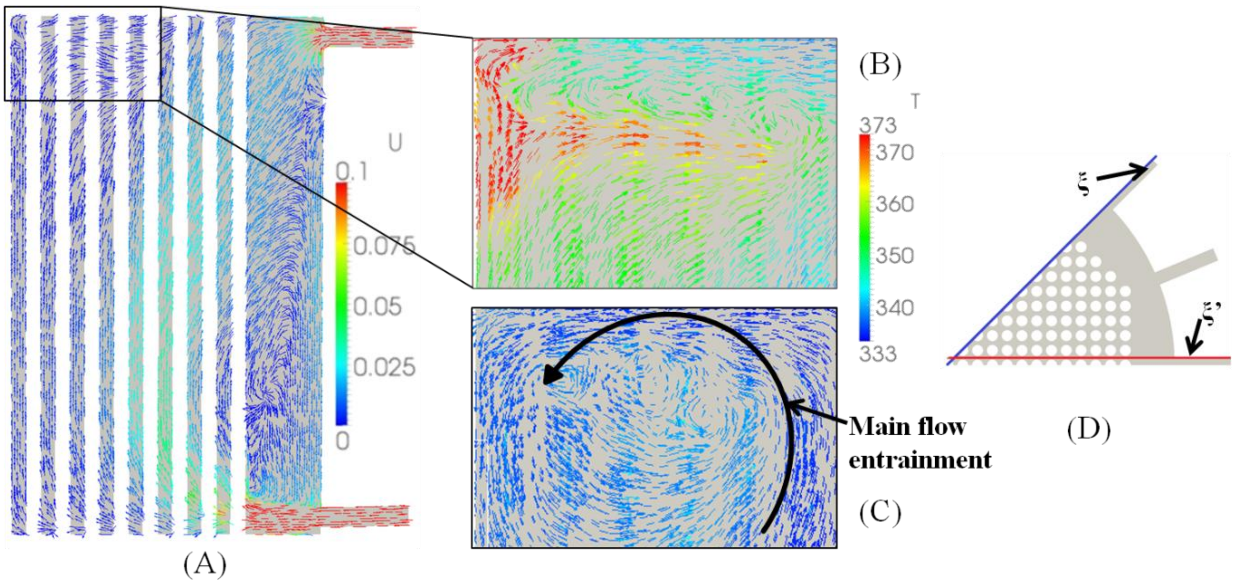

Figure 8.12: Velocity vectors (A) on a plane ξ for mass flow rate 10 kg/s; on a plane ξ' (B) 10 kg/s and (C) 20 kg/s (D) the planes ξ and ξ'.

The temperature and velocity distribution at various axial and radial planes are shown in Fig. 8.13. The flow is asymmetrical in nature as we go along the axial as well as radial direction. This is because of the asymmetric placement of the fuel channels with respect to the shell, which gives rise to highest temperatures in the locality of fuel channels at a plane $\theta = 22.5°$(plane passing through the central inlet and outlet in Fig. 8.13).

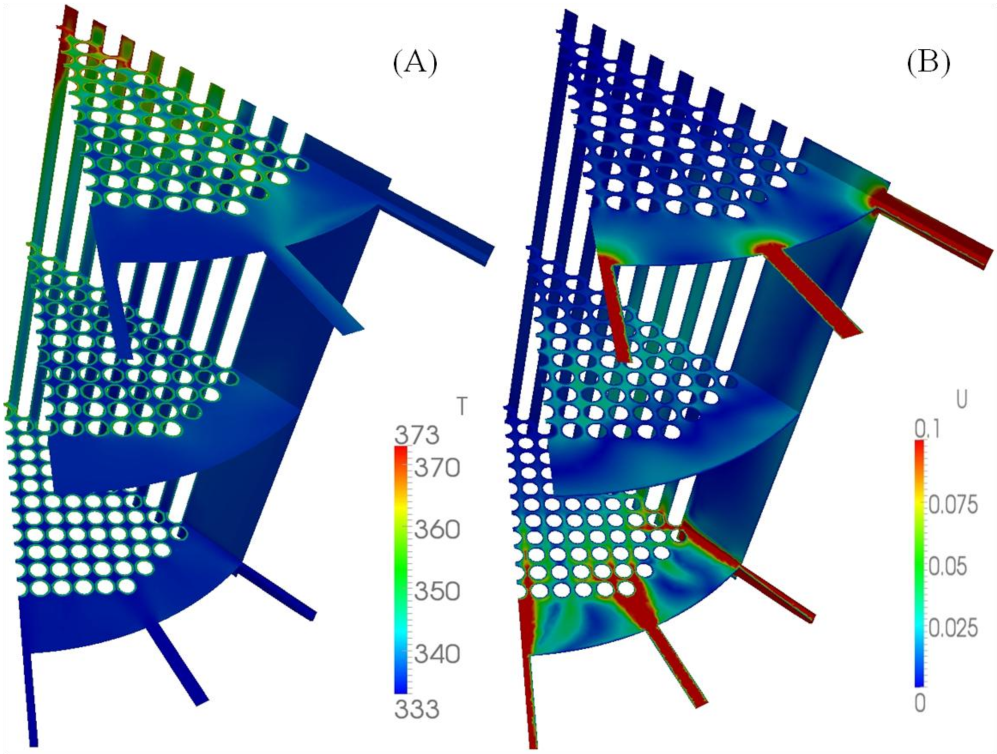

Figure 8.13: (A) Temperature and (B) Velocity distribution on planes θ=45°, z/L_{Tank}= 0.0377 (inlet plane), z/L_{Tank}= 0.5 (mid plane) and z/L_{Tank}= 0.962 (outlet plane).

8.3.4.2 Pseudo-transient simulation of Calandria in a Station Blackout Condition

The temperature contours at different time instants and different axial planes are shown in Fig 8.14. It is observed that for all the cases there is a visible overall stratification in the Calandria. This indicated that the flow is buoyancy dominated for all the time of SBO operation. Furthermore, the temperatures are higher in the center of the fuel matrix close to the top, whereas the region near the wall is at much lower temperature. This is because the flow is not able to penetrate the fuel channels efficiently, in order to carry away heat from them.

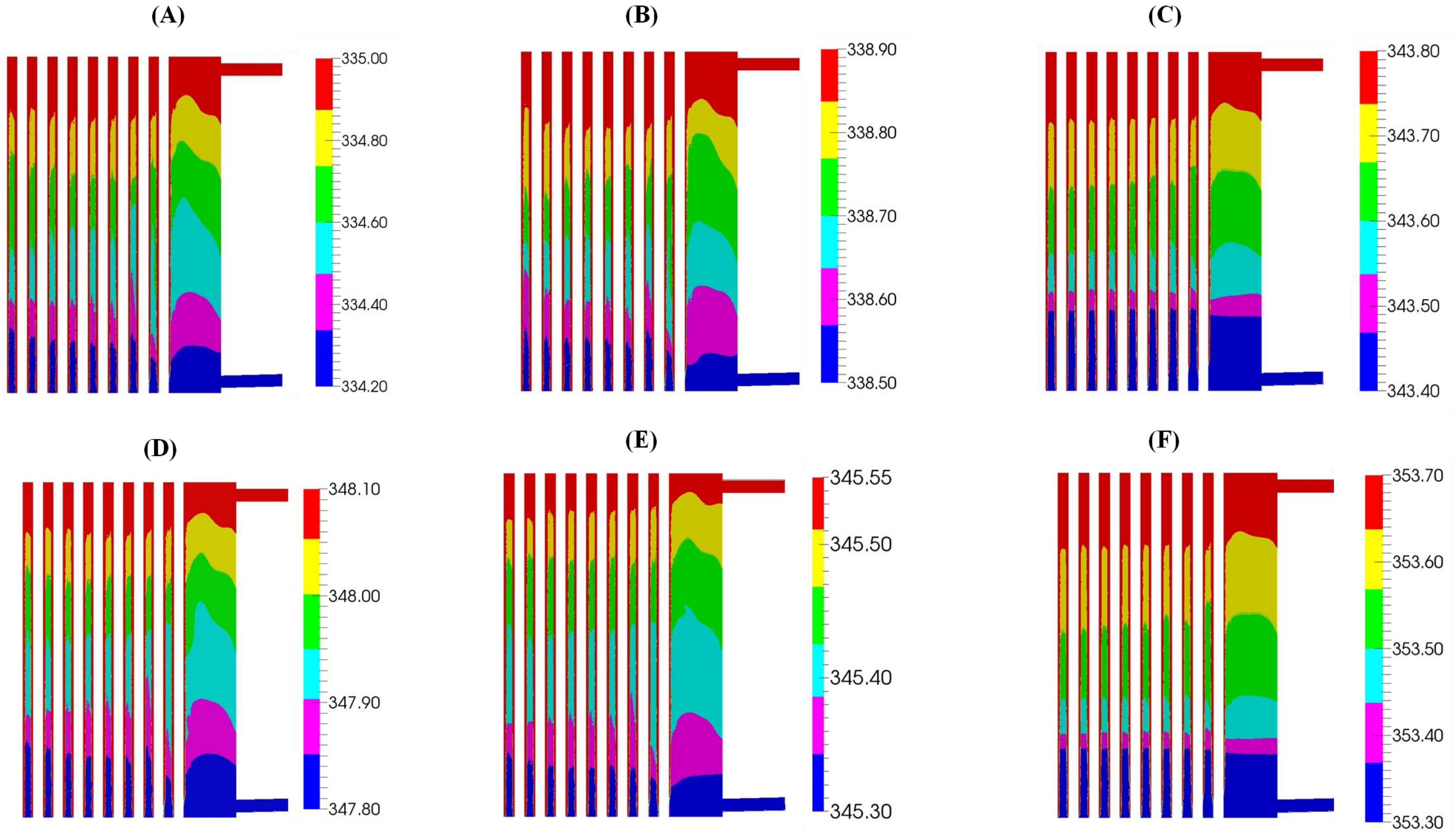

Figure 8.14: Temperature contour of Calandria on a plane at θ=45° for (A) Case 1 (B) Case 2 (C) Case 3 (D) Case 4 (E) Case 5 and (F) Case 6.

With increasing time (Fig. 8.14), the difference between maximum temperature (Table 8.4) and the inlet temperature reduces in the Calandria. This is due to reduction in heat load with time (due to reduction in radioactive decay of fuel). This higher temperature difference in the initial period, results in a greater density difference, and a higher buoyant force, thus resulting in higher velocities. It should be noted that the inlet temperature increases due to the increase in cooling water temperature, i.e. the temperature of the GDWP.

Table 8.4: Maximum temperature inside Calandria from pseudo steady simulations during an SBO.

Case No.	Time from beginning of SBO (days)	Maximum temperature (K)
Case 1	0.5	337.57
Case 2	1	340.73
Case 3	2	344.71
Case 4	3	346.41
Case 5	4	348.89
Case 6	6	354.44

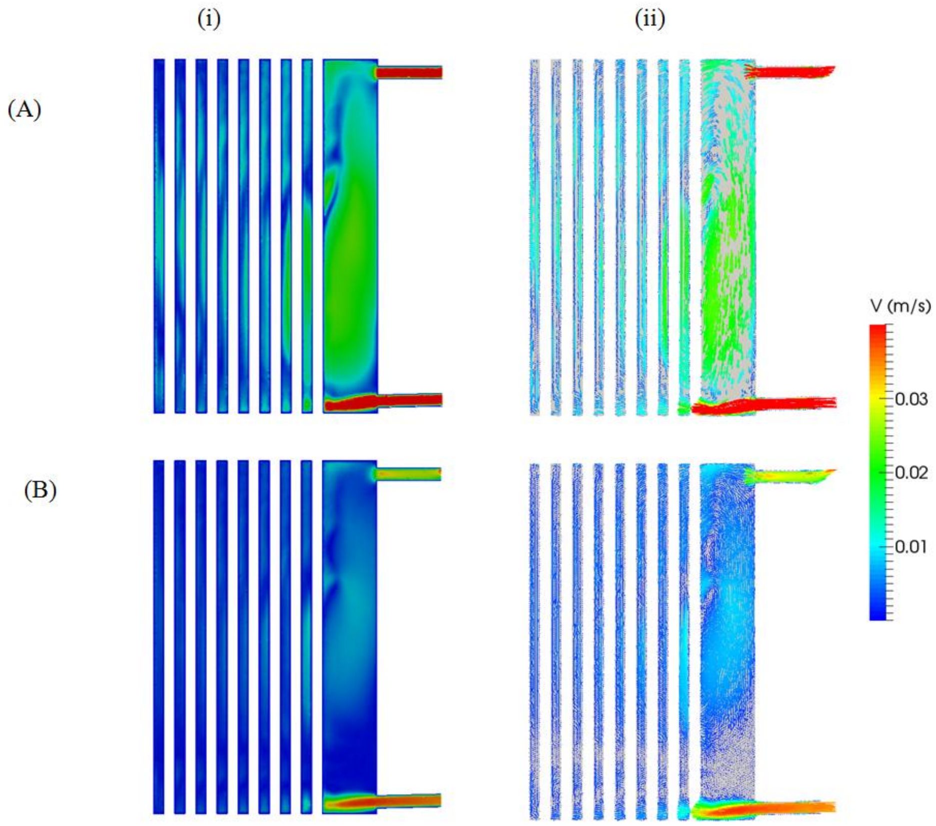

Figure 8.15: (i) Velocity contours and (ii) velocity vectors on a plane θ=45° for (A) Case 1 and (B) Case 6.

Fig. 8.15 shows the velocity contour and velocity vector plots at t =12 h from SBO and t = 6 days. The flow after entering the fuel channel region goes upward, and exits from the outlets at the top. However, part of this flow comes downward along the Calandria tank wall, setting a natural circulation system within the Calandria vessel. Moreover, the overall flows decrease for Case 6 comparing to Case 1. The high flow region between the fuel matrix and the Calandria wall reduces in size. The overall flow circulation region also shrinks down. This is due to the lower inlet velocities and also due to the fact that the buoyant natural circulation force is also low due to lower temperature difference.

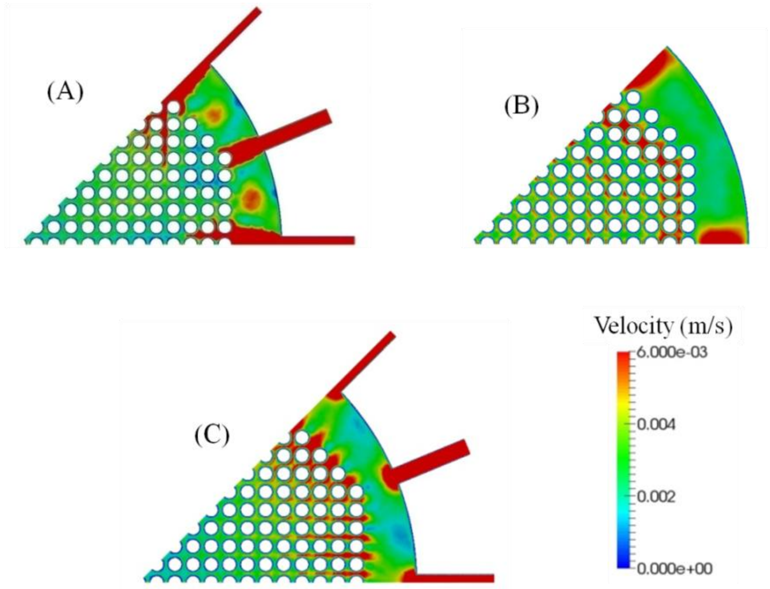

Figure 8.16: Velocity contour on a plane perpendicular to z axis at z/L_{Tank} = (A) 0.0377 (inlet plane) (B) 0.5 (mid plane) (C) 0.962 (outlet plane) for Case 6.

Fig. 8.16 shows the velocity contours on the inlet, mid and the outlet planes for the case 6. As discussed in the steady state cases (Section 8.3.4.1), the flow immediately after impinging on the fuel matrix moves in an upward direction. Thus, the center of the fuel channel region receives very low flow. At the mid plane (Fig. 8.16 B), it is observed that the higher flow is in the outer periphery of the fuel matrix, which is the upward coming flow after impingement. On the outlet plane, the velocities are more or less uniform, except at the periphery of the fuel channel matrix. This is due to buoyancy which makes hot fluid rise upward and at the top (near the outlets) these buoyant flows are most developed.

8.4 Closure

The main objective of this work was to investigate the temperature and flow distribution inside a complex three-dimensional structure of the Calandria vessel and to test the performance of the PMCS. It was observed that the majority of the incoming flow on impinging on the fuel channels is diverted outwards with low penetration into the fuel channel matrix. Furthermore, large fraction of this flow is recirculated within the Calandria vessel (upward flow in the tube bank and downward along the Calandria walls). Furthermore, near the top of the central region of the fuel channels the region is flow devoid, which results in small localized recirculation cells in this zone. This results in accumulation of hot fluid in this region. In addition, the temperature and velocity distribution is three dimensional and not symmetric in the Calandria. For the SBO condition, there is an overall stratification in the Calandria vessel. The temperature differences across Calandria are higher initially than later, this result in higher density difference and hence higher buoyant driving forces and velocities. Following are the important conclusions:

1. Hotspots occurred in the central region of the fuel channels at $z/L_{Tank} = 0.9$.
2. Mass flow above 20 kg/s would prevent boiling in moderator for a SBO condition.
3. During the SBO transient, the temperatures inside the Calandria are below the boiling conditions for continuous 7 days operation without any external interventions.
4. As compared to the PMCTF, in PMCS the tube bank lattice is quite tight. Hence the gross flow is not able to penetrate as easily as in the former geometry.

These simulations bring forth the fact that although system codes can give results for overall mass flow and temperatures, it is crucial to look closely into the three dimensional temperature and flow distributions in order to ensure safety of the system.

CHAPTER 9:

CONCLUSIONS AND RECOMMENDATIONS FOR FUTURE WORK

In the present work, an experimental and numerical investigation of the Passive Moderator Cooling System of the Advanced Heavy Water Reactor is carried out. A scaled facility was designed and built. The numerical simulations were performed on 1D thermal hydraulic code RELAP5/MOD3.2 and a 3D CFD code OpenFOAM 2.2.0. The transient behaviour of a coupled natural circulation loop was studied through various experiments. The numerical code RELAP5/MOD3.2 was used to simulate the experimental conditions, in order to validate the code. Next, the CFD model was first validated for a number of natural circulation and multidimensional flow systems. The validated model was then used to simulate the experimental setup. Finally, inputs from 1D reactor scale simulations were used to simulate the Calandria 3D flows and temperature distribution under passive moderator cooling conditions.

The main conclusions from the present study could be summarized as follows:

- A scaled experimental facility was designed and built for Passive Moderator Cooling System. During the power start up, the temperature contours inside the Calandria vessel show transient behavior initially. However, after 6 h, the temperature contours indicated that the Calandria temperature remains stratified throughout the experiment.
- From the power step up experiments, a flow initiation phenomenon in multidimensional coupled natural circulation loop was understood.

- When power is increased the temperature difference across the Calandria increases and hence the flow in the loop also increases.
- The RELAP model show increase in Calandria and heat exchanger temperatures much earlier than the experiments. It is unable to capture the transients accurately for this PMCTF system.
- The steady state CFD simulations are in good agreement with the experimental data (within ± 6%), with regard to the gross behavior of the system, i.e. the inlet and outlet temperature of the Calandria.
- CFD predictions show that the temperatures inside the Calandria are stratified. Whereas, the hot leg and the cold leg have a uniform temperature. The CFD model predicts that even at the steady state the gross flow in the loop is unable to disrupt the stratification inside the Calandria.
- From the time dependent studies it was observed that starting from condition of rest, the majority of the natural convective flow generated, tends to recirculate within the Calandria. The flow recirculates within this structure and after a certain time period flows in the entire loop.
- The 3D CFD model is used in a unique pseudo-transient approach to simulate the reactor scale moderator during an SBO. The results show that the temperatures in the Calandria are below boiling conditions at all times. The 3D CFD simulations capture the multidimensional flow inside the Calandria, which reveals that the flow tends to recirculate by going up near the hot tubes and then coming down along the walls of the Calandria.
- From the present investigations of the passive moderator cooling system, it can be concluded that the CFD simulations provide an indispensible tool to understand and

estimate the temperature and flow distribution inside a complex multidimensional system. Thus giving an insight into improving the design of the system.

There is a lot of scope to improve the current simulation methodologies by considering a conjugate heat transfer system, which will simulate both the primary and the secondary loop of this coupled natural circulation system. Such a simulation will be able to predict the temperatures without the requirement of inputs from the experimental conditions. Also, the effect of heat loss to the ambience and heating of the structural elements can be included. Such a detailed study requires the computational ability to handle the simulation domains of the order of millimetres as well as meters.

A systematic sensitivity study of the various parameters in the loop can be carried out in order to obtain the optimised design of the system. The parameters can be the elevation between the Calandria and the heat exchanger, the piping diameter, the heat exchanger dimensions etc.

Finally, the experimental facility can be upgraded to include a flow visualisation system in the Calandria vessel and the outlets, in order to observe the flow and temperature distribution. The flow pattern obtained will aid in validating the flow distributions predicted by the CFD codes.

Since the Calandria vessel is an extremely critical equipment that houses all the fuel and safety rods and also contains all the fission reaction, any changes in the design of the Calandria vessel is not preferred. However, both the stratification and lack of penetration of flow to the center of the lattice of the Calandria tubes can be resolved by increasing the flow in the Calandria vessel; i.e. increase in flow of the primary loop. This feat can be accomplished by increasing the elevation of the heat exchanger, or in other words, by increasing the natural circulation driving force.

References

Afrianto, H., Tanshen, M., Munkhbayar, B., Suryo, U., Chung, H., Jeong, H., 2014. A numerical investigation on lng flow and heat transfer characteristic in heat exchanger. International Journal of Heat and Mass Transfer 68, 110-118.

Aicher, T., Kim, W., 1998. Experimental investigation of the influence of the cross flow in the nozzle region on the shell-side heat transfer in double-pipe heat exchangers. International Communication in Heat and Mass Transfer 25(1), 43-58.

Ambrosini, W., Ferreri, J.C., 1998. The effect of truncation error on numerical prediction of stability boundaries in a natural circulation single phase loop. Nucl. Eng. Des. 183, 53–76.

Ambrosini, W., Ferreri, J.C., 2003. Prediction of stability of one-dimensional natural circulation with a low diffusion numerical scheme. Ann. Nucl. Energy 30 (15), 1505–1537.

Ambrosini, W., Ferreri, J.C., 2006. Analysis of basic phenomena in boiling channel instabilities with different flow models and numerical schemes. In: Fourteenth International Conference on Nuclear Engineering (ICONE 14), Miami, Florida, USA, July 17–20, 2006

Ambrosini, W., Forgione, N., Ferreri, J.C., Bucci, M., 2004, The effect of wall friction in single-phase natural circulation stability at the transition between laminar and turbulent flow, Annals of Nuclear Energy 31, 1833-1865.

Ambrosini. W., Ferreri, J. C., 2000, Stability analysis of single-phase thermosyphon loops by finite difference methods, Nuclear Engineering and Design, 201, 11-23.

Angelo, G., Andrade, D.A., Angelo, E., Torres, W.M., Sabundjian, G., Macedo, L.A., Silva, A.F., 2012. A numerical and three-dimensional analysis of steady state rectangular natural circulation loop. Nuclear Engineering and Design, 244, 61– 72.

Baek, W.P., Spinks, N.J., 1994. CANDU Passive heat rejection using the moderator. In: Proceedings of International Conference on New Trends in Nuclear System Thermalhydraulics, Pisa, Italy, May 30 - June 2.

Bau, H.H., Torrance, K.E., 1981. Transient and steady behaviour of an open symmetrically heated, free convection loop. Int. J. Heat Mass Transfer 24, 597–609.

Bhole, M. R., Joshi, J.B., Ramakrishna, D., 2007. Population balance modeling for bubble column operating in the homogeneous regime. AIChE J., 53, 750-756.

Bhutta, M., Hayat, N., Bashir, M., Khan, A., Ahmad, K., Khan, S., 2012. Cfd applications in various heat exchangers design: A review. Applied Thermal Engineering 32, 1-12.

Biswas, G., Eswaran, V., 2002. Turbulent flows: Fundamental Experiments and Modelling. Narosa Publishing House, New Delhi.

Carbiener, W.A., Cudnik, R.A., 1969. Similitude considerations for modeling nuclear reactor blowdowns, Trans Am. Nucl. Soc, 12, 361.

CFX-4.2: Solver Manual, CFX International, United Kingdom, 1997.

Chen, K., 1985. On the oscillatory instability of closed loop thermosyphons. J. Heat Transfer, Trans. ASME 107, 826–831.

Devia, F., Misale, M.., 2012. Analysis of the erects of heat sink temperature on single phase natural circulation loops behaviour. International Journal of Thermal Science, 59, 195-202.

Dhotre, M. T., Joshi, J. B., 2004. Cfd simulation of heat transfer in turbulent pipe flows. Ind. Eng. Chem. Res., 43, 2816-2829.

Dhotre, M., Ekambara, K.and Joshi, J. B., 2004. Cfd simulation of sparger design and height to diameter ratio on gas hold-up profiles in bubble column reactors. Exper. Therm & Fluid Sci., 28, 407-421.

Dimmick, G.R., Chatoorgoon, V., Khartabil, H.F., Duffey, R.B., 2002. Natural-convection studies for advanced CANDU reactor concepts. Nuclear Engineering Design, 215, 27-38.

Dirker, J., Meyer, J., 2004. Convection heat transfer in concentric annuli. Experimental Heat Transfer: A Journal of Thermal Energy Generation, Transport, Storage, and Conversion 17(1), 19-29.

Dirker, J., Meyer, J., 2005. Convective heat transfer coefficients in concentric annuli. Heat Transfer Engineering 26(2), 38-44.

Donhue D. A., 1949. Heat Transfer and Pressure Drop in Heat Exchangers, Industrial and Engineering Chemistry, 41, 11.

FLUENT 6 User's Guide, 2001. Volumes 1–4. Fluent Inc., Lebanon, December 2001.

Gandhi, M. S., Sathe, M. J., Joshi, J. B., Vijayan, P. K. 2011. Two phase natural convection: CFD simulations and PIV measurement. Chemical Engineering Science, 66(14), 3152-3171.

Ganguli, A. A., Sathe, M. J., Pandit, A. B., Joshi, J. B., Vijayan, P. K. 2010. Hydrodynamics and heat transfer characteristics of passive decay heat removal systems: CFD simulations and experimental measurements. Chemical Engineering Science, 65(11), 3457-3473.

Geuzaine, C., Remacle, J.F., 2009. Gmsh: a three-dimensional finite element mesh generator with built-in pre- and post-processing facilities. International Journal for Numerical Methods in Engineering, Volume 79, Issue 11, pages 1309-1331.

Gnielinski, V., 2009. Heat transfer coefficients for turbulent flow in concentric annular ducts. Heat Transfer Engineering 30(6), 431-436.

Gordon, M., Ramos, E., Sen, M., 1987. One dimensional model of a thermosyphon with known wall temperature. Int. J. Heat Fluid Flow 8, 177–181.

Greif, R., 1988. Natural circulation loops. J. Heat Transfer 110, 1243–1258.

Hanna, B. N., 1998. CATHENA: A thermalhydraulic code for CANDU analysis. Nuclear Engineering and Design, 180(2), 113-131.

Huget, R.G., Szymanski, J., Galpin, P.F., Midvidy, W. 1990. MODTURC_CLAS : An efficient code for analysis of moderator circulation in CANDU reactors. In: Proceedings of Third International Conference on Simulation Methods in Nuclear Engineering, Montreal, Canada, April 18-20.

Huget, R.G., Szymanski, J., Midvidy, W. 1989. Status of physical and numerical modelling of CANDU moderator circulation. In: Proceedings of 10th Annual Conference Canadian Nuclear Society, Ottawa, Canada, June 4-7.

Ishii, M., Kataoka, I., 1983. Similarity Analysis and Scaling Criteria for LWRs Under Single Phase and Two-Phase Natural Circulation. NUREG/CR-3267, ANL-83-32, Argonne National Laboratory.

Ishii, M., Revankar, S.T., Leonardi, T., Dowlati, R., Bertodano, M.L., Babelli, I., Wang, W., Pokharna, H., Ransom, V.H., Viskanta, R., Han, J.T., 1998. The Three-Level Scaling Approach with Application to the Purdue University Multi-Dimensional Integral Test Assembly (PUMA). Nuclear Engg. and Design, 186, 177-211.

Jeong, J.J., Yoon, H.Y., Park, I.K., Cho, H.K., 2010a. The CUPID code development and assessment strategy. Nuclear Engineering and Technology 42, 636–655.

Jeong, J.J., Yoon, H.Y., Park, I.K., Cho, H.K., Lee, H., 2010b. Development and preliminary access of a three-dimensional thermal hydraulic code, CUPID. Nuclear Engineering and Technology 42 (3), 279–296.

Joshi, J.B., 1980. Modifications in the design of gas inducing impellers. Chem.Eng. Commun., 5, 213-218.

Joshi, J.B., 1982. Gas phase dispersion in bubble columns. Chem. Eng. J., 24, 213- 216.

Joshi, J.B., 2002. Reduction of empiricism through flow visualization and computational fluid dynamics. Chem. Eng. Technol. 25. 321-328.

Joshi, J.B., Ranade, V. V., 2003. Computational fluid dynamics for designing process equipment: Expectations, current status and path forward. Ind. Eng. Chem. Res., 42, 1115-1128.

Joshi, J.B., Sharma, M., 1977. Mass transfer and hydrodynamic characteristics of gas inducing type of agitated contactors. Can. J. Chem. Eng., 55, 683-695.

Joshi, J.B., Sharma, M., 1978. Liquid phase back-mixing in sparged contactors. Can. J. Chem. Eng., 56, 116-119.

Joshi, J.B., Sharma, M., Shah, Y., Singh, C., Ally, M., Klinzing, G., 1980. Heat transfer in multiphase contactors. Chem. Eng. Commun., 6, 257-271.

Khartabil, H. F., Spink, N. J., 1995. An Experimental Study of a Flashing-driven CANDU Moderator Cooling System. In: Proceedings of 16th Annual Conference of Canadian Nuclear Society, Saskatoon, Canada, June 4-7.

Kiang, R. L. 1985. Scaling criteria for nuclear reactor thermal hydraulics. Nuclear science and engineering, 89(3), 207-216.

Kim, M., Yu, Seon-Oh, Kim, Hho-Jung, 2006. Analyses on fluid flow and heat transfer inside Calandria vessel of CANDU-6 using CFD. Nuclear Engineering and Design, 236, 1155-1164.

Kim, W., Aicher, T., 1997. Experimental investigation of heat transfer in shell and tube heat exchanger without baffles. Korean Journal of Chemical Engg 14(2), 93-100.

Kim, Y. S., Bae, B. U., Park, G. C. 2007. Integral loop test and assessment of modified RELAP5/MOD3. 3 for RCS coolant inventory during a LBLOCA. Nuclear engineering and design, 237(2), 182-198.

Kim, Y. S., Bae, B. U., Park, C. H., Park, G. C., Suh, K. Y., Lee, U. C. 2005. RELAP5/MOD3. 3 analysis of coolant depletion tests after safety injection failure during a large-break loss-of-coolant accident. Nuclear engineering and design, 235(22), 2375-2390.

Kulkarni, A., Badgandi, S., Joshi, J.B., 2009. Design of ring and spider type spargers for bubble column reactor: Experimental measurements and cfd simulation of flow and weeping. Chemical Engineering Research and Design, 87 (12), Pages 1612-1630.

Kumar, M., Nayak, A. K., Jain, V., Vijayan, P. K., Vaze, K. K., 2013. Managing a prolonged station blackout condition in AHWR by passive means, Nuclear Engineering Technology, 45, 605-612.

Kumar, M., Pal, E., Nayak, A. K., Vijayan, P. K., 2015. Conceptual design of a passive moderator cooling system for a pressure tube type natural circulation boiling water cooled reactor. Nuclear Engineering and Design, 291, 261-270.

Kumaresan, T., Joshi, J.B., 2006. Effect of impeller design on the flow pattern and mixing in stirred tanks. Chem. Eng. J., 115, 173-193

Launder, B.E., Sharma, B.I., 1974. Application of the Energy-Dissipation Model of Turbulence to the Calculation of Flow Near a Spinning Disc. Letters in Heat and Mass Transfer 1(2), 131-138.

Lee, J.R., Park, S.G., Yoon, H.Y., Kim, H.T., Jeong, J. J., 2013. Numerical study for CANDU moderator temperature prediction by using the two-phase flow analysis code, CUPID. Annals of Nuclear Energy 59, 139-148.

Mathpati, C., Joshi, J.B., 2007. Insight into theories of heat and mass transfer at the solid-fluid interface using direct numerical simulation and large eddy simulation. Industrial and Engineering Chemistry Research 46, 8525-8557.

Menter, F. R. 1993, Zonal Two Equation k-ω Turbulence Models for Aerodynamic Flows, AIAA Paper 93-2906

Menter, F., 1994. Two equation eddy viscosity turbulence models for engineering applications. AIAA J. 32(8), 37-40.

Minocha, N., Joshi, J.B., Nayak, A.K., Vijayan, P. K., 2015. Numerical investigation of three-dimensional natural circulation phenomenon in passive safety systems for decay heat removal in large pools. Int. Jour. of Heat and Mass Trans., 81, 659-680.

Misale, M., Garibaldi, P., Passos, J.C., Ghisi de Bitencourt, G., 2007. Experiments in a single-phase natural circulation mini-loop. Experimental Thermal and Fluid Science, 31, 1111-1120.

Murthy, B., Ghadge, R., Joshi, J.B., 2007b. Cfd simulations of gas-liquid-solid stirred reactor: Prediction of critical impeller speed for solid suspension. Chem. Eng. Sci., 62, 7184-7195.

Murthy, B., Joshi, J.B., 2008. Assessment of standard k-ε, rsm and les turbulence models in a baffled stirred vessel agitated by various impeller designs. Chem. Eng. Sci., 63, 5468-5495.

Nahavandi, A. N., Castellana, F. S., Moradkhanian, E. N. 1979. Scaling laws for modeling nuclear reactor systems. Nuclear Science and Engineering, 72(1), 75-83.

Nayak, A.K., Vijayan, P.K., Saha, D., Venkat Raj, V., 1995. Mathematical modelling of the stability characteristics of a natural circulation loop. Mathematical and Computer Modelling 22 (9), 77–87.

Nere, N. K., Patwardhan, A.W., Joshi, J.B., 2003. Liquid phase mixing in stirred vessels: Turbulent flow regime. Ind. Eng. Chem. Res., 42, 2661-2698.

Ozden, E., Tari, I., 2010. Shell side cfd analysis of small shell and tube heat exchanger. Energy Conversion and Management, 51, 1004-1014.

Pal, E., Kumar, I., Joshi, J. B., Maheshwari, N. K., 2016. CFD simulations of shell-side flow in a shell-and-tube type heat exchanger with and without baffles. Chemical Engineering Science, Accepted for publication. Jan 2015.

Park, H. S., Euh, D. J., Choi, K. Y., Kwon, T. S., & Baek, W. P. 2007. An assessment of a LBLOCA similarity for a reduced-height integral effect test loop design for PWRs. Annals of Nuclear Energy, 34(11), 931-937.

Passive Safety Systems and Natural Circulation in Water Cooled Nuclear Power Plants. 2009. IAEA-TECDOC-1624, 1-2.

Patwardhan, A.W., Joshi, J. B., 1999. Design of gas inducing reactors. Ind. Eng. Chem. Research, 37, 49-80.

Pilkhwal, D.S., Ambrosini, W., Forgione, N., Vijayan, P.K., Saha, D., Ferreri, J.C., 2007. Analysis of the unstable behaviour of a single-phase natural circulation loop with one-dimensional and computational fluid-dynamic models. Annals of Nuclear Energy, 34, 339–355.

Pope, S. B., 2000. Turbulent flows. Cambridge University Press, Cambridge.

Prithiviraj, M., Andrews, M., 1998a. Three-dimensional numerical simulation of shell-and-tube heat exchangers. part i: Heat transfer. International Journal of Computation and Methodology 33(8), 799-816.

Prithiviraj, M., Andrews, M., 1998b. Three-dimensional numerical simulation of shell-and-tube heat exchangers. part ii: Foundation and fluid mechanics. Int. J. Comp & Methodology 33(8), 817-828.

Prithiviraj, M., Andrews, M., 1999. Comparison of a three-dimensional numerical model with existing methods for prediction of flow in shell-and-tube heat exchangers. Heat Transfer Engineering 20(2), 15-19.

Ranade, V., Bourne, J., Joshi, J.B., 1991. Fluid mechanics and blending in agitated tanks. Chem. Eng. Sci., 46, 1883-1893.

Ranade, V., Joshi, J.B., 1989. Flow generated by pitched bladed turbine part I: Experimental. Chem. Eng. Commun., 81, 197-224.

Ranade, V., Joshi, J.B., 1990a. Flow generated by a disc turbine I: Experimental. Trans. Instn. Chem. Engrs. (U.K.).-A: Chem. Eng. Res. Des., 68, 19-33.

Ranade, V., Joshi, J.B., 1990b. Flow generated by a disc turbine II: Mathematical model. Trans. Intsn. Chem. Engrs. (U.K.).-A: Chem. Eng. Res. Des., 68, 34-50.

Ranade, V., Joshi, J.B., Marathe, A., 1989. Flow generated by pitched bladed turbine part II: Mathematical modelling and comparison with experimental data. Chem. Eng. Commun., 81, 225-248.

Ranade, V., Mishra, V., Saraph, V., Deshpande, G., Joshi, J.B., 1992. Comparison of axial flow impellers using lda. Ind. Eng. Chem.Res., 31, 2370-2379.

Ravi, S.D., Rajan, N.K.S., Kulkarni, P.S., 2008. Computational and Experimental Studies of Fluid Flow and Heat Transfer in a Calandria Based Reactor. In: Proceedings of Symposium on CFD Division of the Aeronautical Society of India (AeSI), NAL, Bangalore, India, August 11-12.

Rewatkar, V., Joshi, J.B., 1991. Role of sparger design in mechanically agitated gas-liquid reactors -ii: Liquid phase mixing. Chem. Eng. Techno., 14, 386-393.

Sahu, A. K., Kumar, P., Patwardhan, A. W., Joshi, J. B., 1999. Cfd modeling and mixing in stirred tanks. Chem. Eng. Sci., 54, 2285-2293.

Sarchami, A., Ashgriz, N., Kwee, M., 2013. Temperature fluctuations inside the CANDU reactor Moderator Test Facility (MTF). Annals of Nuclear Energy, 60, 157-162.

Seo H., Kim H.T., Cha, J.E., Bang, I.C. 2014. Measurements and visualization of velocity profiles in a scaled CANDU6 moderator tank using particle image velocimetry. Annals of Nuclear Energy, 45, 361-372.

Sharma, M., Vijayan, P.K., Nayak, A.K., Saha, D., Sinha, R.K., 2002. Numerical study of stability behaviour of single-phase natural circulation in a rectangular loop. In: Proceedings of the Fifth ISHMT – ASME Heat and Mass Transfer Conference and Sixteenth National Heat and Mass Transfer Conference, Kolkata, India. January 6–8, 2002.

Short, B. E., 1943. Heat Transfer and Pressure Drop in Heat Exchangers, Univ. Texas Publ., 4324, 1-5.

Sieder, E., Tate, G., 1936. Heat transfer and pressure drop of liquids in tubes. Ind. Eng. Chem. 28, 1429-35.

Sinha, R.K., Kakodkar, A., 2003. The road map for a future Indian nuclear energy system. In: International Conference on Innovative Technologies for Nuclear Fuel Cycles and Nuclear Power, Vienna, 23–26 June.

Sinha, R.K., Kakodkar, A., 2006. Design and development of the AHWR—the Indian thorium fuelled innovative nuclear reactor. Nucl. Engg. and Des. 236, 683-700.

Sinha, R.K., Kushwaha, H.S., Agarwal, R.G., Saha, D., Dhawan, M.L., Vyas, H.P., Rupani, B.B., 2000. Design and development of AHWR—the Indian thorium fuelled innovative nuclear reactor, INSAC-2000. In: Annual Conference of Indian Nuclear Society, Mumbai, 1–2 June.

Tabib, M. V., Joshi, J. B., 2008. Analysis of dominant flow structures and their flow dynamics in industrially relevant equipment using proper orthogonal decomposition. Chem. Eng. Sci., 63, 3695-3715.

Thakre, S. S., Joshi, J.B., 1999. Cfd simulation of flow in bubble column reactors importance of drag force formulation. Chem. Eng. Sci., 54, 5055-5060.

Thakre, S., Joshi, J.B., 2002. Momentum, mass and heat transfer in single phase turbulent flow. Reviews in Chem. Engg. 18, 83-293.

The Relap5 Development Team, “RELAP5/Mod3.2 Code Manual”, NUREG/CR-5535 Report, vols. 1-5, Idaho National Engineering Laboratory, August 1995.

Umar, E., Subki, M. H., Vecchiarlli, J., 1999 Analysis of Passive Moderator Cooling System of CANDU-6A Reactor at Emergency Condition. AECL Report.

Umar, E., Vecchiarelli, J., 2000. Parametric Study of Moderator Heat Exchanger for CANDU 6 Advanced Reactor. Indonesian Journal of Nuclear Science and Technology, 1(1), 83-98.

Uzzan, M., Leinen, K., Labuza, T., 2004. Temperature profiles within a double-pipe heat exchanger with countercurrent turbulent flow of Newtonian fluids: derivation, validation, and application to food processing. Journal of Food Science 69(8), 433-440.

Van Zyl, W., Dirker, J., Meyer, J., 2013. Single-phase convective heat transfer and pressure drop coefficients in concentric annuli. Heat Transfer Engineering 34(13), 1112-1123.

Vijayan, P.K., 2002. Experimental observations on the general trends of the steady state and stability behaviour of single-phase natural circulation loops. Nucl. Eng. Des. 215, 139–152.

Vijayan, P.K., Austregesilo, H., 1994. Scaling laws for single-phase natural circulation loops. Nucl. Eng. Des. 152, 331–347.

Vijayan, P.K., Austregesilo, H., Teschendorff, V., 1995. Simulation of the unstable oscillatory behavior of single-phase natural circulation with repetitive flow reversals in a rectangular loop using the computer code ATHLET. Nucl. Eng. Des. 155, 623–641.

Vijayan, P.K., Bhojwani, V.K., Bade, M.H., Sharma, M., Nayak, A.K., Saha, D., Sinha, R.K., 2001. Investigations on the effect of heater and cooler orientation on the steady state, transient and stability behaviour of single-phase natural circulation in a rectangular loop. Bhabha Atomic Research Centre, Report BARC/2001/E/034.

Vijayan, P.K., Sharma, M., Saha, D., 2007. Steady state and stability characteristics of single-phase natural circulation in a rectangular loop with different heater and cooler orientations. Exp. Therm. Fluid Sci. 31, 925–945.

Wang, J.Y., Chuang, T.J., Ferng, Y.M., 2013. CFD investigating flow and heat transfer characteristics in a natural circulation loop. Annals of Nuclear Energy, 58, 65–71.

Wang, Q., Chen, Q., Chen, G., Zeng, M., 2009. Numerical investigation on combined multiple shell-pass shell-and-tube heat exchanger with continuous helical baffles. International Journal of Heat and Mass Transfer 52, 1214-1222.

Welander, P., 1967. On the oscillatory instability of a differentially heated fluid loop. J. Fluid Mech. 29 (1), 17–30.

Yang, S. K., 2009. Scaling methodology for a passive moderator cooling system. Transactions of the American Nuclear Society 101, 917-918.

Yoon, C., Park, J.H. 2008. Development of a CFD model for the CANDU-6 moderator analysis using a coupled solver. Annals of Nuclear Energy, 35, 1041-1049.

Yoon, C., Rhee, B.W., Bo, W., Kim, H.T., Park, J., Min, B.J. 2006. Moderator analysis of wolsong units 2/3/4 for the 35% reactor inlet header break with a loss of emergency core cooling injection. Journal of Nuclear Science and Technology, 43, 505-513.

Yoon, C., Rhee, B.W., Min, B.J. 2004. Development and validation of the 3-D computational fluid dynamics model for CANDU-6 moderator temperature predictions. Nuclear Technology 148,259-267.

Zeng, W., Zhang, Z., 2012. Problems involved in the shell-side performance of a longitudinal-flow shell-and-tube heat exchanger with decrease in l/d and its solutions. International Journal of Low-Carbon Technologies 7, 310-317.

Zvirin, Y., 1981. A review of natural circulation loops in PWR and other systems. Nucl. Eng. Des. 67, 203–225.

List of Publications arising from the thesis

Journal

1. "Conceptual design of a passive moderator cooling system for a pressure tube type natural circulation boiling water cooled reactor.", Kumar M., Pal E., Nayak A. K., Vijayan P. K., *Nuclear Engineering and Design*, **2015**, *291*, 261-270.

2. "CFD simulations of moderator flow inside Calandria of the Passive Moderator Cooling System of an advanced reactor.", Pal E., Joshi J. B., Kumar M., Nayak A. K., Vijayan P. K., *Nuclear Engineering and Design*, **2015**, *292*, 193-203.

3. "CFD simulations of shell-side flow in a shell-and-tube type heat exchanger with and without baffles.", Pal E., Kumar I., Joshi J. B., Maheshwari N. K., *Chemical Engineering Science*, **2016**, 143, 314-340.

4. "Experimental and CFD Simulations of Fluid Flow and Temperature Distribution in a Natural Circulation Driven Passive Moderator Cooling System of an Advanced Nuclear Reactor." Pal, E., Kumar, M., Nayak, A.K., Joshi, J.B., *Chemical Engineering Science,* **2016**, 155, 45-64.

Conferences

1. "CFD Simulation of Natural Convection in a Passive Moderator Cooling System of an Advanced Nuclear Reactor.", Pal E., Joshi J. B., Nayak A. K., Vijayan P. K., *International Congress on Advances in Nuclear Power Plants 2015.* May 03-06, 2015. Nice (France).

2. "CFD Analysis of flow and temperature distribution inside the Calandria of natural circulation, vertical pressure tube type advanced nuclear reactor.", Pal E., Joshi J. B., Nayak A. K., Vijayan P. K., *Fluid Mechanics and Fluid Power-2014.* December'2014. Kanpur, India.

3. "Experimental and Numerical Investigation of Natural Circulation phenomena in a Rectangular Natural Circulation Loop-II.", Pal E., Joshi J. B., Nayak A. K., Vijayan P. K., *Fluid Mechanics and Fluid Power-2014.* December'2014. Kanpur, India.

4. "CFD Analysis of flow and temperature distribution inside the Calandria of Advanced Heavy Water Reactor.", Pal E., Joshi J. B., Nayak A. K., Vijayan P. K., *New Horizons in Nuclear Thermal Hydraulics and Safety.* January'2014. Mumbai, India.

5. "Experimental and Numerical Investigation of Natural Circulation phenomena in a Rectangular Natural Circulation Loop-I.", Pal E., Joshi J. B., Nayak A. K., Vijayan P. K., *New Horizons in Nuclear Thermal Hydraulics and Safety.* January'2014. Mumbai, India.